INVESTIGATIONS INTO THE TROPOSPHERIC CYCLE OF COS:

ATMOSPHERIC DISTRIBUTION, AIR-SEA AND AIR-VEGETATION EXCHANGES

Dissertation

zur Erlangung des Doktorgrades

der Naturwissenschaften

vorgelegt beim Fachbereich
Geowissenschaften / Geographie
der Johann Wolfgang Goethe-Universität
in Frankfurt am Main

von

Xiaobin Xu

aus Jiangsu, China

Frankfurt am Main, 2001

(D F 1)

vom Fachbereich Geowissenschaften / Geographie der Johann Wolfgang Goethe-Universität als Dissertation angenommen.

Contents

Abstract

This work is a study on the tropospheric cycle of carbonyl sulfide (COS). It focuses on (1) the contribution of open oceans to atmospheric COS, (2) the role of terrestrial vegetation in the budget and variability of atmospheric COS, and (3) the variability of atmospheric COS in time and space.

COS was measured in surface seawater and in marine air during two Atlantic cruises between 30°S and 50°N. Strong temporal and geographic variations in the concentration of seawater COS were observed. These variations can be explained by the variability of parameters which are related to the production and loss of COS in seawater (e.g., solar radiation, seawater temperature, precursor concentrations). The concentration of dissolved COS showed pronounced diurnal cycles, with a maximum in the early afternoon and a minimum in the early morning. Seawater was supersaturated with COS with respect to the atmosphere during the sunlit period and regularly undersaturated during periods with no or little sunlight, even in the warm seasons and in productive regions. This indicates that the open ocean can on the same day act as both a source and a sink for COS, even in tropical regions during summer. Field evidence shows that CH_3SH is one of the key precursors of seawater COS and its concentration in seawater can be used as an indicator of the precursor level. Based on the COS data and various parameters, an empirical model has been developed for estimating the concentration of seawater COS from satellite measurements. The global open ocean is estimated to be a small source of 0.10 Tg COS yr^{-1}.

For measurements of the air-vegetation exchange of COS and CS_2, a REA (<u>R</u>elaxed <u>E</u>ddy <u>A</u>ccumulation) sampler was developed, tested, and validated. Exchange fluxes of COS and CS_2 between the atmosphere and a tall spruce forest were measured for the first time from a tower using the REA technique. Both deposition and emission of COS and CS_2 were observed, with deposition occurring mostly during the daytime and emission during the dark period. The average fluxes for COS and CS_2 are -93±11.7 pmol m^{-2} s^{-1} and -18±7.6 pmol m^{-2} s^{-1}, respectively, suggesting that the forest acts as a net sink for both gases. The fluxes of both gases were correlated to the fluxes of photo-

I

synthetically active radiation, H_2O and CO_2, suggesting that the air-plant exchange of COS and CS_2 is controlled by the stomata. Global terrestrial vegetation is estimated to take up 2.3±0.5 Tg COS yr^{-1} and 0.54±0.35 Tg CS_2 yr^{-1}, based on the uptake ratios COS/CO_2 and CS_2/CO_2, and on the terrestrial net primary production.

Long-term measurements of atmospheric COS made at the Taunus Observatory between 1993 and 1999 have been evaluated. Results show that the mixing ratio of atmospheric COS has a seasonal variation with maxima and minima in the late winter and the late summer, respectively. The seasonality is most probably a result of the COS uptake by terrestrial vegetation. The background signal of atmospheric COS shows an average peak-to-peak amplitude of 99.2 ppt. Based on this amplitude, the global vegetation sink is estimated to be 1.9±0.3 Tg COS yr^{-1}, which agrees well with the vegetation sink obtained on the basis of the REA measurements of COS fluxes. This result suggests that the vegetation sink of COS may have been significantly underestimated in some budget estimates.

Measurements of COS in the marine atmosphere showed average mixing ratios of 474±33 and 502±38 pptv for the two cruises. The COS level in marine air was higher in the equatorial and tropical regions than in the subtropical and temperate regions. No significant interhemispheric gradient was observed during the two cruises. Atmospheric COS at the Taunus Observatory showed an average mixing ratio of 422.5±91.8 ppt and a secular trend of 4.9±0.9 ppt yr^{-1}.

Chapter 1

Introduction

1.1   Atmospheric COS and Stratospheric Aerosol

Anthropogenic and natural sources release a variety of sulfur compounds (such as COS, CS_2, DMS, SO_2, H_2S, CH_3SH, etc) into the atmosphere. Among these trace gases, COS is the most abundant and ubiquitous one. Measurements show that COS has a tropospheric mixing ratio of about 500 ± 100 pptv (e.g. *Torres et al.*, 1980; *Mihalopoulos et al.*, 1991; *Bandy et al.*, 1992), corresponding to an atmospheric burden of about 5.2 Tg (*Chin and Davis*, 1995), which is about 15 times that of SO_2 (*Andreae and Crutzen*, 1997). In the troposphere, COS is chemically inert. Estimates suggest a tropospheric lifetime of COS of about 2-7 years (*Johnson*, 1981; *Khalil and Rasmussen*, 1984; *Chin and Davis*, 1995; *Griffith et al.*, 1998). The relatively long lifetime allows COS to be well mixed within the troposphere and even transported into the stratosphere.

In the stratosphere, COS is mainly decomposed photochemically by the following reactions:

$$COS + h\nu(< 388 \ nm) \rightarrow CO + S \tag{1.1}$$

$$COS + O(^3P) \rightarrow CO + SO \tag{1.2}$$

$$COS + OH \rightarrow CO_2 + HS. \tag{1.3}$$

The resulting species S, SO and HS are subsequently oxidized to eventually form H_2SO_4, which then condenses to form aerosol particles. All available measurements of stratospheric COS have shown a steep decrease of the COS mixing ratio above the tropopause (*Inn et al.*, 1979, 1981; *Louisnard et al.*,

Table 1.1: Modeled sulfate production from COS photooxidation in the strato-
sphere.

Reference	Flux, Tg S yr^{-1}
Crutzen (1976)	0.12 (0.05)[a]
Sze and Ko (1979)	0.10
Turco et al. (1980)	0.15
Chin and Davis (1995)	0.03
Weisenstein et al. (1997)	0.049
Kjellström (1998)	0.013

[a]The original value (0.05) was obtained on the basis of a boundary condition of 200 ppt
COS at the tropopause. Chin and Davis (1995) modified this value to 0.12 by changing
the boundary condition to 475 ppt COS.

1983; Leifer, 1989; Engel and Schmidt, 1994; Kourtidis et al., 1995) , indi-
cating the effective destruction of COS by these reactions.

The role of atmospheric COS in stratospheric aerosol was first studied
by Crutzen (1976). Based on his model results, Crutzen (1976) proposed
that photodissociation of stratospheric COS may contribute significantly to
the Junge layer, i.e., the nonvolcanic background sulfate layer in the strato-
sphere. This idea is supported by early modeling studies (Sze and Ko, 1979;
Turco et al., 1980), but has been challenged by more recent modeling re-
sults (Chin and Davis, 1995; Weisenstein et al., 1997; Kjellström, 1998). As
shown in Table 1.1, there is a substantial discrepancy in the modeled sul-
fate production from COS photodissociation in the stratosphere between the
earlier and the more recent models. Chin and Davis (1995) attribute this
discrepancy to the differences in the vertical distribution of atmospheric COS
and in the photodissociation rate for COS, used in the models. Based on the
correlation of stratospheric COS to simultaneously observed tracers (CFCl$_3$
and CF$_2$Cl$_2$) and the lifetimes of these tracers, Engel and Schmidt (1994)
obtained a stratospheric sink of 0.047-0.112 Tg COS yr^{-1} (or 0.025-0.06 Tg
S yr^{-1}), which lies between the early and recent model estimates. The sulfur
flux required to sustain the stratospheric background aerosol layer has been
estimated by various authors. The estimated values are listed in Table 1.2.
They range from 0.043 Tg S yr^{-1} to 0.17 Tg S yr^{-1}. The large differences
between the estimates make it more difficult to assess the role of COS in
stratospheric background aerosol.

Stratospheric aerosol plays an important role in the Earth's radiation
budget, as well as providing a surface for heterogeneous reactions that may
enhance chemical ozone destruction (Toon and Pollack, 1982; Lacis et al.,

Table 1.2: Estimates of the sulfur flux required to sustain the stratospheric background aerosol layer.

Reference	Method	Flux, Tg S yr^{-1}
Lazrus and Gandrud (1974)	profile and transport rate	0.07
Crutzen (1976)	total mass, lifetime (2 yr)	0.043
Hofmann et al. (1976)	deduced from observation	0.17
Turco et al. (1982)	model calculation	0.16
Servant (1986)	total mass, lifetime (1.2 yr)	0.13
Hofmann (1991)	total mass, lifetime (1 yr)	0.063

1992; *Hartmann*, 1994; *Rodriguez et al.*, 1991; *Grainier and Brasseur*, 1992; *Solomon et al.*, 1993). The variability of stratospheric aerosol has drawn considerable attention over the last three decades. One of the main concerns is the potential increase in the background level of stratospheric aerosol as a consequence of possible increases in its sources, such as COS, CS_2, SO_2, etc. Aircraft measurements between 51°S and 75°N from 1971 to 1981 indicated that the stratospheric background sulfate level increased at a rate of 6-8% per year (*Sedlacek et al.*, 1983). Based on data from balloon soundings over Laramie, Wyoming (41°N), *Hofmann* (1990) reported an increase of 5±2% per year in the stratospheric background sulfate aerosol mass during the period from 1979 to 1989. Both *Sedlacek et al.* (1983) and *Hofmann* (1990) speculated that a possible increase in anthropogenic emission of COS might be responsible for the observed elevation of the stratospheric background aerosol loading. However, this idea contradicts the fact that no significant long-term trend of atmospheric COS is observed (*Mihalopoulos et al.*, 1991; *Bandy et al.*, 1992; *Rinsland et al.*, 1996). In view of the absence of any secular trend in the COS level and an increase of 5% per year in jet fuel consumption, *Hofmann* (1991) subsequently attributed the observed increase in the stratospheric background sulfate level to the increase in aircraft sulfur emissions. However, a model investigation by *Bekki and Pyle* (1992) shows that the rise in air traffic is largely insufficient to account for the trend in stratospheric background aerosol, reported by *Hofmann* (1990), although aircraft sulfur emissions may be a significant source of sulfate below 20 km. Another model study by *Gettelman* (1998) shows that aircraft sulfur emissions contribute at most 7% to stratospheric background aerosol. Model results of *Golombek and Prinn* (1993) suggest that COS photodissociation and the upward transport of SO_2 from the troposphere are equally important sources of stratospheric background aerosol. COS photodissociation is more important above 20 km, whereas the transport of SO_2 is more important between 12 km and 20 km. Calculations using a 2D-model including H_2S, CS_2,

DMS, COS, and SO_2, suggest that the stratospheric aerosol mass may be strongly influenced by deep convection in the troposphere, which transports sulfate precursors into the upper troposphere and leads to elevated levels of SO_2 there (*Weisenstein et al.*, 1997). However, there are many uncertainties associated with the model. Data from lidar measurements of stratospheric aerosol over Mauna Loa Observation show that by the end of 1996, 5.5 years after the Pinatubo eruption, stratospheric aerosol had decayed to its lowest level in the period from 1980 to 1996 (*Barnes and Hofmann*, 1997). An increase in the stratospheric background aerosol level was not observed at the site. A convincing explanation to the early observed increases in the stratospheric background aerosol loading is lacking.

Even though there is no current consensus as to how significantly atmospheric COS as a sulfur provider contributes to stratospheric background aerosol, there is no doubt that atmospheric COS is one of the important sources of stratospheric background aerosol.

1.2 Spatial and Temporal Variability of Atmospheric COS

Hanst et al. (1975) made the first measurement of atmospheric COS and reported a mixing ratio of about 0.2 ppb of atmospheric COS, with an uncertainty of at least 50%. Measurements at various locations and altitudes over continents and oceans show a mean mixing ratio of atmospheric COS of about 500 pptv, ranging between 410 pptv and 610 pptv (*Sandalls and Penkett*, 1977; *Maroulis et al.*, 1977; *Torres et al.*, 1980; *Ferek and Andreae*, 1984; *Carroll*, 1985; *Johnson and Harrison*, 1986; *Bingemer et al.*, 1990; *Mihalopoulos et al.*, 1991; *Bandy et al.*, 1992; *Staubes-Diederich*, 1992; *Staubes and Georgii*, 1993; *Johnson and Bates*, 1993; *Johnson et al.*, 1993; *Weiss et al.*, 1995; *Thornton et al.*, 1996; *Talbot et al.*, 1996). Although the variation in the COS level in the boundary layer is larger than that in the free troposphere, the mean mixing ratio of atmospheric COS shows almost no vertical gradient in the troposphere (*Chin and Davis*, 1995). Some ship-based or airborne measurements of tropospheric COS show substantial hemispheric differences of atmospheric COS, with an Interhemispheric Ratio (IHR=M_{NH}/M_{SH}) between 1.10 and 1.25 (*Bingemer et al.*, 1990; *Staubes-Diederich*, 1992; *Johnson et al.*, 1993) while some other measurements found only small or no N-S gradient (*Torres et al.*, 1980; *Staubes-Diederich*, 1992; *Weiss et al.*, 1995; *Thornton et al.*, 1996). A comparison of measurements of total column COS in both hemispheres shows a north/south interhemi-

spheric ratio in the range of 1.1-1.2 (*Griffith et al.*, 1998). It is not clear whether the COS excess observed in the Northern Hemisphere is caused by anthropogenic sources or by seasonal fluctuations of COS sources (such as the oceans) or sinks (such as vegetation).

Previous in-situ measurements at Amsterdam Island did not show any significant seasonality of atmospheric COS (*Mihalopoulos et al.*, 1991). However, measurements of the COS total column abundance by ground-based solar infrared absorption spectroscopy displayed a seasonal variation in total column COS, with a summer maximum and a winter minimum (*Rinsland et al.*, 1992; *Griffith et al.*, 1998). The reported peak-to-peak amplitudes lay in the range 6-18%, about 2-6% of which were attributed to the seasonal variation of the tropopause height and the remainder to seasonal fluctuations in the COS mixing ratio in the troposphere. Analyses of long-term data showed no significant secular trend of atmospheric COS (*Bandy et al.*, 1992; *Mihalopoulos et al.*, 1991; *Griffith et al.*, 1998), indicating a balance between the total source and the total sink.

1.3 Sources, Sinks and Budget of Atmospheric COS

Although numerous studies have been conducted to identify and quantify the sources and sinks of atmospheric COS, our knowledge about these sources and sinks is still too poor to allow a reliable estimate of the global COS budget. So far, very different results have been obtained from measurements using various techniques and methods. There are large discrepancies between the results. Some of the results are even contradictory. These problems have been caused by the wide variability of the sources and sinks and by drawbacks in the techniques and methods applied in previous studies.

1.3.1 Sources

Table 1.3 shows a summary of various estimates of individual COS source strengths. The sources are divided into natural, mixed (i.e., both natural and anthropogenic), anthropogenic, and chemical types.

COS is mainly produced in the biosphere. Organosulfur compounds are formed during the assimilatory sulfate reduction. The oxidation of some of these compounds, such as thiol (-SH) groups, may lead to COS production. COS produced in this way may be partially emitted into the atmosphere through air-sea and atmosphere-biosphere gas exchanges.

Table 1.3: Global COS source estimates from different authors.

Source	Estimate, Tg COS yr^{-1}	Reference
Natural:		
Ocean	0.6±0.2	*Rasmussen et al.* (1982)
	0.87	*Ferek and Andreae* (1983)
	0.60(0.2-0.9)	*Khalil and Rasmussen* (1984)
	0.64	*Andreae* (1986)
	0.25(0.2-0.4)	*Johnson and Harrison* (1986)
	0.43(0.30-0.60)	*Mihalopoulos et al.* (1992)
	0.77	*Andreae and Ferek* (1992)
	0.32(0.16-0.64)	*Chin and Davis* (1993)
	0.25	*Erickson and Eaton* (1993)
	0.15	*Ulshöfer and Andreae* (1998)
	0.30±0.18	*Watts* (2000)
Soil	0.40(0.2-0.6)[a]	*Khalil and Rasmussen* (1984)
	0.27(0.14-0.52)[a]	*Chin and Davis* (1993)
	0.02±0.01[b]	*Watts* (2000)
Volcano	0.02	*Cadle* (1980)
	0.02(0.01-0.05)	*Khalil and Rasmussen* (1984)
	0.006-0.09	*Belviso et al.* (1986)
	0.02(0.006-0.09)	*Chin and Davis* (1993)
Mixed:[c]		
Biomass burning	0.45	*Crutzen et al.* (1979)
	0.14(0.04-0.26)	*Chin and Davis* (1993)
	0.13(0.06-0.21)	*Nguyen et al.* (1995)
Anthropogenic:		
Tire wear	0.08±0.01	*Pos and Berresheim* (1993)
Aluminium production	0.08±0.02	*Harnisch et al.* (1995a)
Others[d]	0.14(0.05-0.45)	*Khalil and Rasmussen* (1984)
	0.042(0.027-0.059)	*Chin and Davis* (1993)
Chemical:		
CS$_2$ conversion[e]	0.6(0-2)	*Khalil and Rasmussen* (1984)
	0.34(0.17-0.61)	*Chin and Davis* (1993)
DMS conversion	0.10-0.28	*Barnes et al.* (1994)
Precipitation	0.13±0.06	*Watts* (2000)

[a]These estimates are derived from measurements which are believed to be wrong (see Text).

[b]Only anoxic soils are considered to be a COS source.

[c]Fires are initiated by both natural and human activities.

[d]Including coal combustion, chemical production, sulfur recovery, etc.

[e]Since 60% of atmospheric CS$_2$ are released by anthropogenic sources, the oxidation of CS$_2$ is an indirect anthropogenic source.

The ocean was originally believed to be the largest single source of atmospheric COS (*Khalil and Rasmussen*, 1984; *Chin and Davis*, 1993). The global marine COS source was first estimated as 0.4-0.9 Tg yr^{-1} (*Rasmussen et al.*, 1982; *Ferek and Andreae*, 1983; *Khalil and Rasmussen*, 1984; *Andreae*, 1986; *Andreae and Ferek*, 1992; *Mihalopoulos et al.*, 1992), based on data showing that the surface waters of practically all ocean regions studied were supersaturated with COS, with respect to the atmosphere. However, this data base for global extrapolation was biased towards conditions suiting high COS production, i.e., low latitudes, warmer seasons and productive areas. Measurements of seawater COS in the equatorial and northern Pacific Ocean showed lower COS saturation ratios than in the productive regions, leading to an estimate of 0.25 Tg COS yr^{-1} (*Johnson and Harrison*, 1986). Taking into consideration the seasonal and regional variations in the saturation ratio of COS in seawater, *Chin and Davis* (1993) estimated the ocean source to be 0.32 Tg COS yr^{-1} by reducing the estimate of *Andreae* (1986) by a factor of 2. A comparison between the mean primary productivity values and the mean COS concentrations for different biogeographic regions shows a high degree of correlation (*Andreae and Ferek*, 1992). Based on this finding and the satellite chlorophyll data from CZCS (C̲oastal Z̲one C̲olor S̲canner), *Erickson and Eaton* (1993) obtained a global ocean source of 0.25 Tg COS yr^{-1}, using the general circulation models. The recent discovery of large scale uptake of COS by the open ocean during winter (*Weiss et al.*, 1995; *Ulshöfer et al.*, 1995) and the improvement of models for the marine cycle of COS have led to a substantial downward revision of global and regional estimates of the COS air-sea flux. It has been suggested by *Weiss et al.* (1995) that the open ocean is a weak sink for COS. Considering this open ocean sink, the total marine emission of COS to the atmosphere was estimated by *Ulshöfer and Andreae* (1998) to be 0.15 Tg COS yr^{-1}. In a more recent review *Watts* (2000) estimated the sources of the open and coastal oceans to be 0.10±0.15 Tg COS yr^{-1} and 0.20±0.10 Tg COS yr^{-1}, respectively, giving a global ocean contribution of 0.30±0.18 Tg COS yr^{-1}.

Surface soil is one of the major reservoirs of organosulfur compounds (*Freney and Williams*, 1983). Microbial processes in the soil can produce COS. COS is also consumed by some biological processes and chemical reactions in the soils. Therefore, soils can act both as a source and as a sink for COS.

Earlier measurements of the COS exchange between soils and the atmosphere almost exclusively showed an emission of COS into the atmosphere (*Aneja et al.*, 1979; *Adams et al.*, 1981; *Steudler and Peterson*, 1985; *Goldan et al.*, 1987; *Lamb et al.*, 1987; *Melillo and Steudler*, 1989; *Staubes et al.*, 1989; *Hines and Morrison*, 1992). On the basis of these measurements, a

global soil source of 0.2-0.6 Tg COS yr^{-1} was estimated by *Khalil and Rasmussen* (1984) and *Chin and Davis* (1993). However, this value may be an overestimate, or even completely wrong, because of the experimental errors in these earlier measurements. The use of a sulfur-free gas to sweep the soil flux chamber used in these measurements introduced artificial gradients of COS between the soil and chamber air, resulting in artificial emission fluxes. In fact, a comparison study demonstrated that soils emitted COS if sulfur-free air was used as a sweep gas and took up COS if ambient air was used (*Castro and Galloway*, 1991). More recent studies avoided this artifact by using dynamic chambers swept with ambient air, or static chambers. All results from these studies show uptake of COS by various soils (*Fried et al.*, 1993; *De Mello and Hines*, 1994; *Kuhn et al.*, 1999; *Simmons et al.*, 1999). The nocturnal removal of COS from the surface layer, observed by *Kesselmeier et al.* (1993) in Cameroon, provides another piece of field evidence for COS uptake by soils. In view of these findings, *Andreae and Crutzen* (1997) proposed considering soils as a global COS sink instead of as a global source. Taking only the soil types oxic and anoxic into account, *Watts* (2000) recently estimated that the global anoxic soil is a source of 0.02 Tg COS yr^{-1} and the global oxic soil is a sink of 0.9 Tg COS yr^{-1}, with an uncertainty of about 85%. A more reliable estimate of the soil contribution appears to be impossible on the basis of the data which is presently available. Recent laboratory studies of mechanisms and parameters controlling the COS air-soil exchange revealed that in addition to the soil type, the COS mixing ratio, temperature, soil water content, etc., are also important in the exchange of COS between soils and the atmosphere (*Lehmann and Conrad*, 1996; *Kesselmeier et al.*, 1999; *Conrad and Meuser*, 2000). This will be very useful for future field studies and for global estimates of the COS budget.

Another natural source of atmospheric COS is volcanic emission. This source is estimated between 0.01 and 0.09 Tg COS yr^{-1} (*Cadle*, 1980; *Khalil and Rasmussen*, 1984; *Belviso et al.*, 1986; *Chin and Davis*, 1993). Although there is a large uncertainty in this estimate, volcanoes appear to make only a minor global contribution to atmospheric COS.

Biomass burning, caused mainly by human activities, also releases COS into the atmosphere. Elevated COS levels of up to tens of ppb were observed in the plumes of natural and human-induced fires, with net emission ratios $\Delta COS / \Delta CO_2$ varying from 1.2×10^{-6} to 61×10^{-6} (*Crutzen et al.*, 1979, 1985; *Bingemer et al.*, 1992; *Nguyen et al.*, 1990, 1995). The global emission of COS from biomass burning was first estimated by *Crutzen et al.* (1979) to be 0.45 Tg COS yr^{-1}. On the basis of the average emission ratio $\Delta COS / \Delta CO_2$ from several field measurements (*Crutzen et al.*, 1979, 1985; *Nguyen et al.*, 1990; *Bingemer et al.*, 1992) and the average amount of carbon released from

different burning sources as given by *Andreae* (1991), *Chin and Davis* (1993) obtained a biomass burning source of 0.14 Tg COS yr^{-1}. Arguing that COS is mainly released during the smoldering phase, as is CO, *Nguyen et al.* (1995) estimated the emission of COS from biomass burning on the basis of the emission ratio ΔCOS/ΔCO and of the CO emission flux from biomass burning, given by *Crutzen and Andreae* (1990), and obtained a biomass burning source of 0.13 Tg COS yr^{-1}. Although biomass burning is only a small source of global atmospheric COS, this source may have a significant impact on the atmospheric COS level in certain seasons and regions, due to its strong seasonal and geographical variability (*Andreae*, 1991).

COS may be emitted by some direct anthropogenic sources other than biomass burning, such as coal combustion, chemical industry, sulfur recovery and automobile exhausts. Earlier estimates of these source showed a small total contribution of about 0.04-0.14 Tg COS yr^{-1} (*Khalil and Rasmussen*, 1984; *Chin and Davis*, 1993). Recently, two other anthropogenic COS sources, i.e., automotive tire wear and aluminum production, have been identified by *Pos and Berresheim* (1993) and *Harnisch et al.* (1995b,a), respectively. The global COS emission by automotive tire wear was estimated to be roughly 0.08 Tg COS yr^{-1} (*Pos and Berresheim*, 1993), which is one order of magnitude higher than the emission of automobile exhausts (*Fried et al.*, 1992). Aluminum production may release 0.08$\pm$0.02 Tg COS annually into the atmosphere (*Harnisch et al.*, 1995a). At present, both sources make only small contributions to atmospheric COS, however, considering their potential increases, they may become more important in the future.

Besides direct release by natural and anthropogenic sources, COS may be produced by atmospheric chemical reactions. The oxidation of atmospheric CS$_2$ was estimated to be one of the major sources of atmospheric COS, with a global source strength of 0.6 Tg COS yr^{-1} (*Khalil and Rasmussen*, 1984). From laboratory studies, *Chin* (1992) found a conversion factor of 0.81 for COS from CS$_2$. Based on this factor and the global CS$_2$ source strength of 0.54 Tg yr^{-1}, *Chin and Davis* (1993) revised this COS source to 0.34 Tg COS yr^{-1}. Since nearly 60% of the atmospheric CS$_2$ is considered to be emitted by anthropogenic sources (the manufacture of regenerated cellulose rayon and cellophane, CCl$_4$ production, etc.), the oxidation of CS$_2$ is thus a major indirect anthropogenic source of COS (*Chin and Davis*, 1993). Another chemical source of atmospheric COS, the oxidation of DMS, was recently identified by *Barnes et al.* (1994). Their laboratory studies showed that COS is produced during the photochemical oxidation of DMS under conditions of low NO$_x$, with a COS formation yield of 0.7 $\pm$ 0.2 %. Due to the large global DMS source (15-40 Tg S yr^{-1}), this small COS yield can lead to a production of 0.10-0.28 Tg COS yr^{-1}, hence it is a non-negligible source of atmospheric

COS (*Barnes et al.*, 1994). In addition to gaseous conversions, COS also seems to be produced in precipitation. COS supersaturation in precipitation has been reported by *Belviso et al.* (1987) and *Watts* (2000). The observed supersaturation cannot be explained by COS scavenging from the atmosphere or by the oxidation of CS_2 in the precipitation. *Watts* (2000) supposed organic matter (including sulfur containing amino acids) in the precipitation as precursors and estimated a global precipitation source of 0.13 ± 0.06 Tg COS yr^{-1}.

1.3.2 Sinks

COS sinks can be roughly divided into two types, i.e., photochemical and biospheric sinks. Estimates of the strength of individual sinks are listed in *Table 1.4*.

COS is removed from the atmosphere through photochemical decomposition, and through deposition to terrestrial ecosystems. Photolysis of COS occurs mainly in the stratosphere. *Khalil and Rasmussen* (1984) estimated a photolysis sink of 0.1 Tg COS yr^{-1} based on a model calculation of *Crutzen* (1976). According to the estimates of *Chin and Davis* (1993), photolysis of atmospheric COS destroys only 0.03 Tg COS yr^{-1}. Other photochemical sinks of COS are the reactions with OH and O radicals. *Khalil and Rasmussen* (1984) estimated that the reaction of COS with OH may remove 0.8 Tg COS yr^{-1}. A much smaller value for this sink (0.13 Tg COS yr^{-1}) was obtained by *Chin and Davis* (1993) based on new data for the reaction rate and for the OH mixing ratio. The loss of COS due to reaction with O radical represents only a minor sink ($\leq$0.03 Tg COS yr^{-1}), as estimated by *Khalil and Rasmussen* (1984) and *Chin and Davis* (1993). The photochemical reactions remove only a small fraction of the COS emitted into the atmosphere. The remainder is believed to be taken up by terrestrial ecosystems. Since no significant trend in the mixing ratio of atmospheric COS has been observed, a balance between the sources and the sinks of atmospheric COS is to be expected.

As discussed above, soils appear to be one of the important sinks of atmospheric COS. The estimate of *Watts* (2000) shows that the global oxic soil may remove 0.92 ± 0.78 Tg COS yr^{-1}. This estimate needs to be confirmed by further studies.

The uptake of COS by vegetation has been recognized as a major COS sink (*Brown and Bell*, 1986; *Goldan et al.*, 1988; *Chin and Davis*, 1993). Earlier studies demonstrated the ability of plants to take up COS (*Kluczewski et al.*, 1983, 1985; *Taylor et al.*, 1983). Based on the deposition velocities reported by *Kluczewski et al.* (1983, 1985), the estimated mean leaf area index,

Table 1.4: Global COS sink estimates from different authors.

Sink	Estimate, Tg COS yr^{-1}	Reference
Photolysis	0.1($\leq$0.2)	*Khalil and Rasmussen* (1984)
	0.029(0.020-0.040)	*Chin and Davis* (1993)
Reaction with OH	0.8(0.1-1.5)	*Khalil and Rasmussen* (1984)
	0.13(0.02-0.80)	*Chin and Davis* (1993)
Reaction with O	0.03	*Khalil and Rasmussen* (1984)
	0.015(0.009-0.026)	*Chin and Davis* (1993)
Oxic soil	0.92$\pm$0.78	*Watts* (2000)
Vegetation uptake	2-5	*Brown and Bell* (1986)
	0.2-0.6	*Goldan et al.* (1988)
	0.86-1.0	*Kesselmeier and Merk* (1993)
	0.43(0.16-1.0)	*Chin and Davis* (1993)
	1-3.4	*Hofmann* (1993)
	0.56$\pm$0.10	*Watts* (2000)

and the productive land area, *Brown and Bell* (1986) obtained a preliminary estimate of the vegetation sink of 2-5 Tg COS yr^{-1}. Seasonal changes in the vegetation area and the deposition velocity were not considered in this estimate. *Goldan et al.* (1988) studied the uptake of COS by some agricultural plants under laboratory controlled conditions and showed that the major uptake pathway is through open stomata, as it is in the case of the uptake of CO_2. This similarity led the authors to estimate an annual plant sink of 0.2-0.6 Tg COS through the global primary productivity of terrestrial plants. Assuming that the uptake ratio COS/CO_2 is equal to the ratio of the atmospheric concentrations [COS]/[CO_2], *Kesselmeier and Merk* (1993) derived a vegetation sink of 0.86-1.0 Tg COS yr^{-1}. Applying the assumption of *Kesselmeier and Merk* (1993), and taking into consideration the dependence of the uptake of COS on the terrestrial ecosystem type, *Chin and Davis* (1993) obtained a global vegetation sink of 0.43 Tg COS yr^{-1}. Cuvette studies by *Hofmann* (1993) showed that plants prefer COS to CO_2. Based on the uptake ratio COS/CO_2 from his studies, *Hofmann* (1993) estimated that the vegetation sink might be between 1 Tg COS yr^{-1} and 3.4 Tg COS yr^{-1}.

Mechanistic studies (*Protoschill-Krebs and Kesselmeier*, 1992; *Protoschill-Krebs et al.*, 1995, 1996) have shown that all enzymes involved in CO_2 assimilation can metabolize COS, and that the key enzyme is carbonic anhydrase (CA), which catalyzes the hydrolysis of COS to CO_2 and H_2S. These findings, however, are not always supported by field measurements. While some in-situ measurements (*Mihalopoulos et al.*, 1989; *Hofmann et al.*, 1992; *Bartell et al.*, 1993) demonstrated COS deposition, other measurements showed ei-

ther no evidence of deposition (*Berresheim and Vulcan*, 1992) or the existence of both deposition and emission (*Kesselmeier et al.*, 1993; *Hofmann*, 1993; *Huber*, 1994). The disagreement between the measurements indicates on the one hand the complexity of the COS exchange between the atmosphere and the soil/plant systems, while on the other hand it probably also shows the deficiencies of the techniques used to determine the COS flux.

In addition to the uptake by soils and plants, COS can also be consumed by some other biological communities, i.e., algae and lichens, as shown by recent studies (*Gries et al.*, 1994; *Protoschill-Krebs et al.*, 1995; *Kuhn and Kesselmeier*, 1996; *Kuhn*, 1997; *Blezinger et al.*, 2000; *Kuhn et al.*, 2000). In both cases, the ubiquitous enzyme CA is involved in the uptake processes. Marine algae appear to be of minor importance for the COS cycle (*Blezinger et al.*, 2000). At present, there is no estimate of the effect of lichen as a sink of COS on the global scale.

1.3.3   Budget

Due to the variety of sources and sinks of atmospheric COS and the large uncertainties in quantifying the individual sources and sinks, it has been difficult to obtain a reliable global budget for atmospheric COS. Nevertheless, budget estimates have been made in several papers, as shown in *Table 1.5*. The first budget estimate by *Khalil and Rasmussen* (1984) showed a total global source of 2 Tg COS yr^{-1}. At that time, all the known sinks could together only remove 0.9 Tg COS yr^{-1} from the atmosphere, and the remainder was termed the "missing sink" (*Brown and Bell*, 1986). Based on new data including the vegetation sink of COS, *Chin and Davis* (1993) reestimated COS sources and sinks and obtained a total source of 1.14 Tg COS yr^{-1} and a total sink of 0.58 Tg COS yr^{-1}, again indicating a substantial imbalance between COS sources and sinks. This is inconsistent with the fact that there is no significant trend for atmospheric COS (*Mihalopoulos et al.*, 1991; *Bandy et al.*, 1992). In view of the finding of COS uptake by some open ocean regions in winter, and by soils, *Andreae and Crutzen* (1997) proposed a downward revision of the ocean source to 0.15 Tg COS yr^{-1} and considered soils as a sink for 0.3 Tg COS yr^{-1}. These changes have led to an approximately balanced budget of atmospheric COS. In a more recent review, *Watts* (2000) reported a total source of 1.31 $\pm$ 0.25 Tg COS yr^{-1} and a total sink of 1.66 $\pm$ 0.79 Tg COS yr^{-1}. The major revision undertaken by this author is the soil contribution. According to his estimate, the soil is the largest global sink of atmospheric COS with a net uptake of 0.90 Tg COS yr^{-1} and an uncertainty of about 85%.

The above revisions have led to substantial changes in estimates of the

Table 1.5: Global total COS source and sink estimated by different authors.

Reference	Total source Tg COS yr^{-1}	Total sink Tg COS yr^{-1}
Khalil and Rasmussen (1984)	2($\leq$5)	0.9(0.1-1.5)
Chin and Davis (1993)	1.14(0.55-2.19)	0.58(0.19-1.77)
Andreae and Crutzen (1997)	0.72	0.9
Watts (2000)	1.31$\pm$0.25	1.66$\pm$0.79

global COS budget as well as in the distribution of the COS sources and sinks between the Northern and Southern Hemispheres. They need to be confirmed by further studies on air-sea and air-soil exchange. At present, it is hardly possible to derive a better budget estimate of atmospheric COS from the still sparse and partially very uncertain databases. Obviously, more reliable measurements of COS exchanges between the atmosphere and the ocean, as well as the terrestrial ecosystems, are needed to reduce the uncertainties in the estimates of COS sources and sinks, and to check the consistency of the atmospheric COS distribution with the geographical and seasonal variations of COS sources and sinks.

1.4   The Objectives of this Work

This work has been designed to improve our understanding of the tropospheric COS cycle, especially the roles of the global open ocean and terrestrial vegetation in this cycle. The detailed objectives of this thesis were:

- To characterize the spatio-temporal variability of atmospheric COS and air-sea COS exchange using large-scale in-situ measurements on a ship in different seasons and to investigate the main parameters controlling the concentration and air-sea COS exchange.

- To develop, construct and test a micrometeorological sampler for measuring gas fluxes according to the principle of <u>R</u>elaxed <u>E</u>ddy <u>A</u>ccumulation (REA) and to use this sampler to measure COS exchange between the atmosphere and a soil/plant ecosystem.

- To evaluate the global importance of terrestrial vegetation, using data obtained by the REA method and the long-term COS measurements at a midlatitudinal observatory (the Taunus Observatory).

The oceanic measurements, the development of an empirical model for seawater COS, and the application of the air-sea flux model are presented

in *Chapter 2*. The development and validation of the REA sampler, and the measurements of COS exchange between the atmosphere and a forest ecosystem are described in *Chapter 3*. *Chapter 4* discusses the results of the long-term COS measurements at the Taunus Observatory and their implications. *Chapter 5* summarizes this work and gives some recommendations for future research. Readers who prefer German to English may read the expanded summary of this thesis in German (Zusammenfassung). Although this thesis deals mainly with atmospheric COS, some CS_2 measurements are also presented, due to the importance of CS_2 as a precursor of atmospheric COS.

Chapter 2

COS in Seawater and Marine Air and its Air-Sea Flux

2.1 Introduction

Seawater, containing 1.3×10^9 Tg S in the form of sulfate, is the second largest reservoir of sulfur next to the lithosphere (*Freney et al.*, 1983; *Chameides et al.*, 1992). A small amount of the seawater sulfate is reduced by oceanic microorganisms during assimilation to form organosulfur compounds for the purpose of nutrition. Further biochemical reactions of these organosulfur compounds produce a series of volatile reduced sulfur compounds, such as DMS, CH_3SH, COS, CS_2, H_2S, etc., with DMS being the most abundant and important one (*Andreae*, 1986).

The ocean was first speculated to be a sink for atmospheric COS due to its hydrolysis at the slightly alkaline pH of seawater (*Rowland*, 1979; *Johnson*, 1981). But most earlier measurements showed that practically all ocean regions studied were supersaturated with COS (*Rasmussen et al.*, 1982; *Ferek and Andreae*, 1983, 1984; *Turner and Liss*, 1985; *Johnson and Harrison*, 1986; *Mihalopoulos et al.*, 1992), leading to the conclusion that the global ocean is a major source of atmospheric COS (*Khalil and Rasmussen*, 1984; *Chin and Davis*, 1993). However, these earlier measurements were mostly conducted in productive (coastal and shelf) regions during warmer seasons. Later field observations in open ocean areas found a large scale undersaturation of COS in surface seawater during winter (*Ulshöfer et al.*, 1995; *Weiss et al.*, 1995), leading to a significant downward revision of the COS ocean source (*Weiss et al.*, 1995; *Ulshöfer and Andreae*, 1998).

Considerable progress has been achieved in studying the mechanisms of COS production in seawater. *Ferek and Andreae* (1984) found that the COS

15

saturation ratio in seawater had a pronounced diurnal cycle with a mid afternoon maximum, suggesting that photochemical reactions are a major source process of COS in surface seawater. Some organosulfur compounds, specially those with thiol (-SH) groups, such as glutathione (GSH), cysteine (CYS), methyl mercaptan (MeSH), 3-mercaptopropionic acid (3-MPA), etc., may act as COS precursors (*Ferek and Andreae*, 1984; *Flöck et al.*, 1997). Laboratory studies indicate that COS formation is induced by the UV part of solar radiation with the participation of natural photosensitizers (*Zepp and Andreae*, 1994). Humic acid (HA) and chromophoric dissolved organic matter (CDOM), which are ubiquitous in natural waters, especially in the coastal areas, may serve as photosensitizers (*Zepp and Andreae*, 1994; *Flöck et al.*, 1997). After absorbing UV light, they produce radicals, which attack the thiol groups to produce thiyl (RS) and sulfhydryl (HS) radicals. The latter radicals react then with some carbonyl bearing intermediates to produce COS. In view of the correlation between seawater CO and COS (*Conrad et al.*, 1982), *Flöck et al.* (1997) proposed that CO could act as a carbonyl donor. However, *Pos et al.* (1998) showed that a coupled pathway is involved in CO and COS production, and that CO is rather a product of the acyl intermediaries that react with thiyl radicals to form COS than a carbonyl donor.

Thiyl radicals may also be produced in seawater under dark conditions by some chemical processes, such as the autooxidation of thiols under the catalysis of some metallic ions (*Flöck et al.*, 1997). Radicals produced in this way may also initiate the reactions leading to the formation of COS. This can explain the observed dark production of COS in some incubation and deep seawater samples (*Radford-Knoery and Cutter*, 1993, 1994; *Flöck and Andreae*, 1996). But dark production is much slower than photoproduction, therefore, it makes only a small contribution to COS production in surface seawater (maximal 30%) and does not influence the diurnal cycle of dissolved COS (*Ulshöfer et al.*, 1996; *Flöck and Andreae*, 1996).

COS is removed from surface seawater by hydrolysis, air-sea exchange, and downward mixing, with hydrolysis being the dominant removal process (*Najjar et al.*, 1995; *Uher and Andreae*, 1997a). COS hydrolysis occurs in both acidic and alkaline media, but in an alkaline medium the hydrolysis rate is much larger than in an acidic medium (*Elliot et al.*, 1989). Since both acidic and alkaline pathways contribute to the rate constant, the rate constant (k_{hyd}) can be expressed as (*Elliot et al.*, 1989):

$$k_{hyd} = k_{acidic} + [OH^-] \times k_{alkaline}, \qquad (2.1)$$

where $[OH^-]$ is the concentration of OH^-, k_{acidic} and $k_{alkaline}$ are the rate constants for the acidic and alkaline pathways, respectively. Besides being

influenced by pH, hydrolysis is also influenced by the temperature of the medium. The hydrolysis rate increases with increasing temperature. The dependence of the rate constant on temperature can be described by the Arrhenius Expression:

$$\ln(k_{hyd}) = \ln(A) - \frac{E_a}{RT}, \tag{2.2}$$

where A is the pre-exponential factor, E_a the activity energy of the hydrolysis reaction, R the ideal gas constant, and T the temperature in Kelvin. The values of A and E_a for acidic and alkaline media have been established by *Elliot et al.* (1989) and *Radford-Knoery and Cutter* (1994) in a synthetic seawater solution and under seawater conditions, respectively. The observed decay lifetime of COS in seawater has been found to agree well with that calculated using the A and E_a values (*Weiss et al.*, 1995; *Uher and Andreae*, 1997b).

The balance between COS production from dissolved biological precursors and loss processes due to hydrolysis, downward mixing, and air-sea exchange causes geographical, seasonal, and diurnal variations in the concentration and saturation ratio of COS in seawater and in the air-sea flux. The large spatiotemporal variability of seawater COS has been one of the main problems causing the large uncertainty in estimating the global oceanic source of atmospheric COS on the basis of the available data. Knowing the factors influencing dissolved COS, it is possible to mathematically describe the variation of COS in surface seawater. *Uher and Andreae* (1997a) used a simple kinetic model to describe the observed diurnal cycle

$$\frac{d[COS](t)}{dt} = pI(t) - k_{hyd}[COS](t) - \frac{k_w}{d_{mix}}\left([COS](t) - \frac{[COS]_{air}}{H}\right), \tag{2.3}$$

where $[COS](t)$ is the concentration of dissolved COS at time t, p is the photoproduction constant, $I(t)$ is the solar UV intensity at time t, k_{hyd} is the hydrolysis rate constant, k_w is the gas exchange coefficient, d_{mix} is the depth of the mixed layer, $[COS]_{air}$ is the COS mixing ratio in the atmosphere, and H is the Henry's law constant for COS. Using this model with the appropriate constants for the processes involved, they fitted the observed diurnal profiles of COS and derived in situ photoproduction constants for the regions studied. The regional averages of these photoproduction constants were highly correlated to the observed CDOM optical properties (absorbance and fluorescence) (*Uher and Andreae*, 1997a). The close relationship between COS photoproduction and CDOM indicates the possibility of calculating COS photoproduction using ocean color data from satellites, such as SeaWiFs

(Sea-viewing Wide Field-of-view Sensor). For global applications, the local process models should be integrated into a process-based global model for estimating COS production using remote sensing data (*Andreae and Crutzen*, 1997).

To review the role of the global open oceans in the budget of atmospheric COS, atmospheric and marine COS was measured during two Atlantic cruises. The main results of the measurements are presented in this chapter. The mechanisms of COS production and decay are discussed based on the relationships between seawater COS and some of the parameters involved. An empirical model has been developed for estimating the seawater COS concentration using satellite measurements. The air-sea flux of COS along the cruise track is estimated and then extrapolated to assess the potential contribution of the global open oceans to the atmospheric COS sources or sinks.

2.2   Experiment

2.2.1   Cruises

Measurements of COS in marine air and in surface seawater were made aboard the German R/V *Polarstern* during the cruises *ANT-XV/1* (from Bremerhaven, Germany, to Cape Town, South Africa; October 15 to November 7, 1997) and *ANT-XV/5* (from Cape Town, South Africa, to Bremerhaven, Germany; May 26 to June 21, 1998). *Figure 2.1* shows the cruise tracks for the two voyages and 108-hour backward trajectories as provided by the German Weather Service (DWD) for air parcels arriving at sea level at the ship's position at 00:00 UTC each day. During both cruises the ship sailed on the open ocean most of the time and passed through the North Atlantic Current, the Canary Current, the Equatorial Counter Current, the South Equatorial Current, and the Benguela Current. The backward trajectories indicate that the sampled air masses had not passed over the continents for at least 4-5 days prior to sampling, except on October 18 and 19, 1997, when air was advected from southern Europe (Spain and France). The Intertropical Convergence Zone (ITCZ) was located around 10°N and 5°N for the two cruises, respectively.

2.2.2   Sampling of Marine Air and Seawater

Marine air was collected in 4.5 L sample bags made of Tedlar PVF film (Du Pont, 50 mm). To prevent contamination of the samples by sea spray and
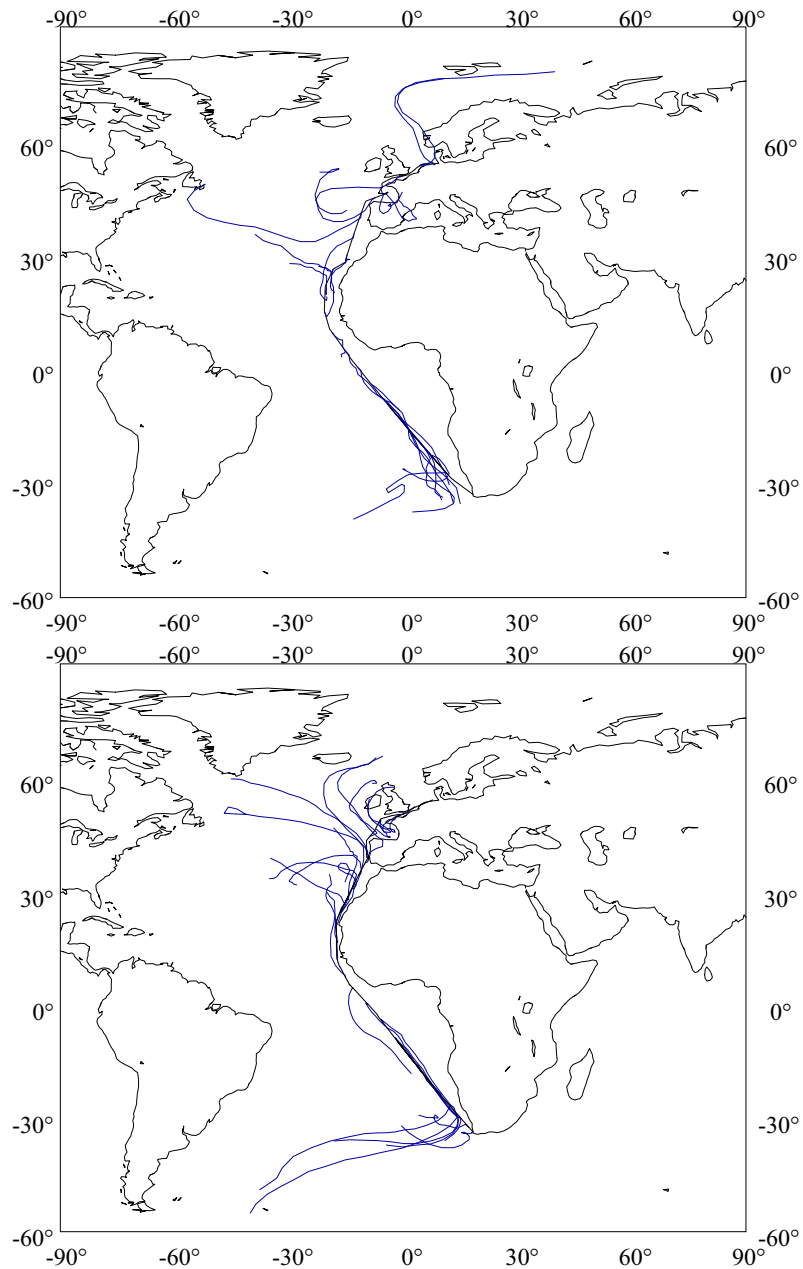
Figure 2.1: Cruise tracks and 108-hour backward air trajectories for air parcels arriving at sea level for the cruises *ANT-XV/1* (top) and *ANT-XV/5* (bottom).

emission from the ship, the air was drawn at a rate of about 2 L min^{-1} from the crow's nest ($\sim$25 m a.s.l.) to the top of the ship's bridge using a Teflon diaphragm pump (N86 KTE, KNF Neuberger). A well defined 0.2 L min^{-1} flow was used to fill the sample bag, while the remainder of the air flow from the pump was vented. The sampling interval was 15 min for a sample volume of about 3 L. After sampling, the air samples were normally analyzed within 30 min. Laboratory tests showed that samples can be stored in the bags for more than 10 hours without any significant change in the COS content.

A Weiss-type seawater equilibrator (*Figure 2.2*) from the Max Planck Institute for Chemistry (*Bange et al.*, 1996) was used to determine the saturation ratio SR (C$_{equilibrated\ air}$ / C$_{ambient\ air}$) and concentration of dissolved COS (C$_w$=C$_{eq}$/H). This instrument, made entirely of Teflon, equilibrates the headspace air ($\sim$20 L) above the surface of the sampled water with a continuous flow of 20 L min^{-1} of incoming seawater. The incoming seawater is sprayed through a nozzle into the headspace. The headspace air is circulated at 5 L min^{-1} using a Teflon pump. The equilibrator is described in detail by *Butler et al.* (1988) and *Bange et al.* (1996). Seawater was pumped from the intake in the "crossbeam-rudder-space" 5 m below surface by the ship's water pump. The residence time of sample water in the pumping system is about 2 min. In order to avoid stress or rupture of alga cells, seawater was not filtered. Comparison of the seawater temperature measured at the intake to that measured at the bow showed no significant difference, indicating a rapid exchange of seawater between the sampling location and the surroundings. The temperature of the seawater inside the equilibrator was measured using a calibrated digital thermometer. A slight warming of less than 0.7°C as compared to the seawater temperature at 5 m depth was observed. This has been taken into account in calculating the seawater COS concentrations.

2.2.3   Analysis of Sulfur Gases

Sulfur gases were measured in the air samples and in the headspace air of the seawater equilibrator using the analytical system depicted in *Figure 2.2*. Ambient air or headspace air, selected by a 3-port valve, was transferred at a rate of 60 ml min^{-1} through a silanized capillary glass loop (20 cm length, filled with 2 cm glasswool) immersed in liquid Argon (-186°C). To prevent the formation of ice in the glass loop, water vapor was removed by passing the sample through a Nafion dryer. Samples were enriched for 5-8 min. Typical sample volumes were 0.3-0.6 L. Upon switching the 8-port valve and warming the glass loop to room temperature, the trapped gases were injected into a gas chromatograph (GC, HP 5700, Hewlett Packard) equipped with a
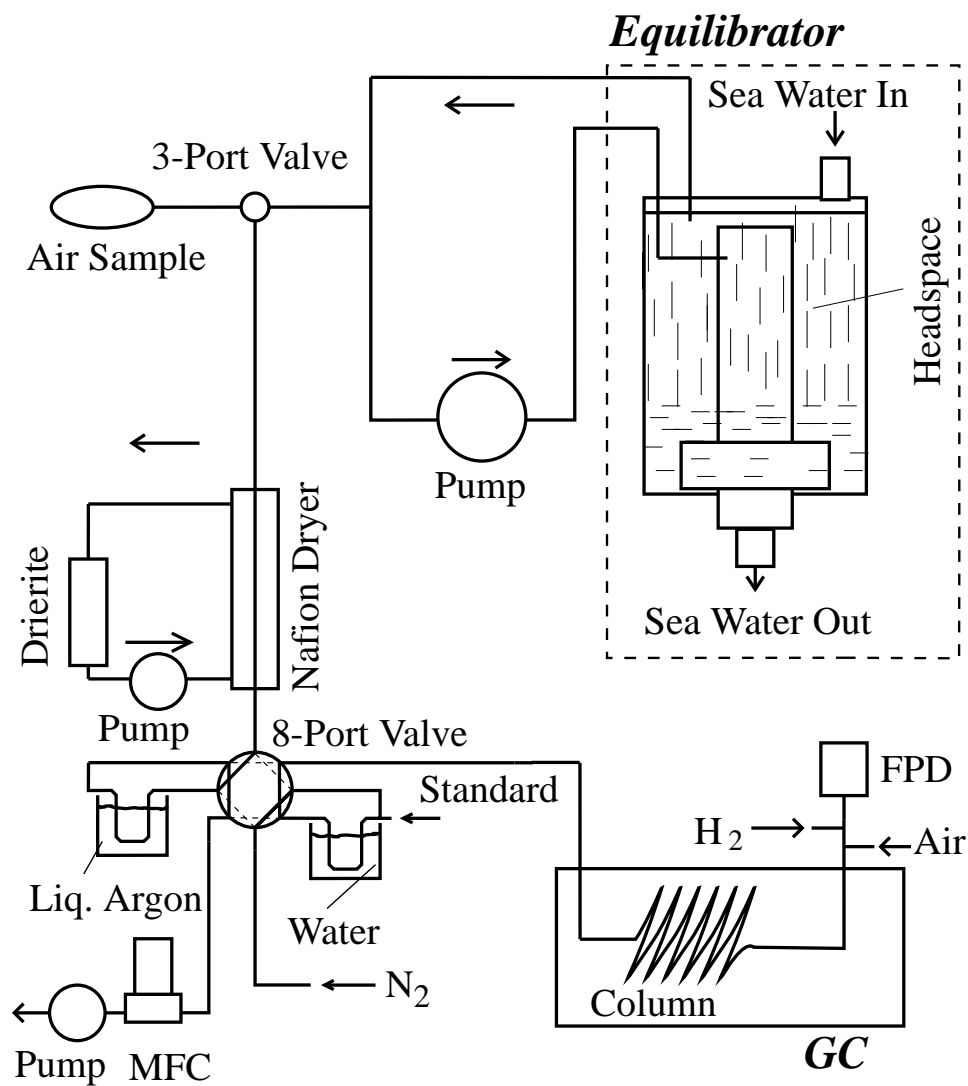
Figure 2.2: Gas chromatograph-based system for the analysis of air samples from Tedlar bags and from the headspace of a seawater equilibrator.

flame photometric detector (FPD, Tracor). The sulfur-containing gases were separated on a $5'$x$1/8''$ Teflon column packed with Carbograph 1SC (Alltech). The chromatograph was programed to stabilize the temperature at 40°C for 2 min followed by a heating phase in which the temperature was increased to 60°C at a rate of 16°C min^{-1}. The oven was then held at this temperature for 4 min. Nitrogen (99.999%, Messer Griesheim) was used as carrier gas at a flow rate of about 20 ml min^{-1}. Chromatograms were acquired and processed by an E-Lab chromatography system (OMS-Technology).

The analytical system was calibrated by the injection of a standard gas mixture into one of the glass loops, using a gas tight Teflon/glass syringe (Precision Sampling Corp.). The standard gas mixture was produced using permeation tubes (Valco VICI, Switzerland) kept at 30±0.1°C in a permeation dilution device. The permeation rates were determined by weighing the tubes about once per month with an electronic balance (Sartorius). The permeation rate of COS was 79.4±7.3 ng min^{-1} with no significant temporal trend ($>1\sigma$) over a period of 18 months. During the cruise in 1998 a CH$_3$SH permeation tube with a permeation rate of 71.3±2.5 ng min^{-1} was used for calibration. As no such tube was available during the cruise in 1997, the CH$_3$SH peaks were calibrated indirectly using the COS calibration curves and taking into consideration the different sensitivity of the system to COS and to CH$_3$SH (see *Appendix A*). Calibration of the GC was carried out on all observational days during the cruises except October 20, 1997. However, due to a leak in the permeation system which was not discovered until October 25, 1997, the calibration on the first few days of the cruise in 1997 yielded incorrect values. As a result, all samples analyzed prior to that date could only be evaluated based on the calibration curves from October 25, 1997. This could have led to a larger uncertainty for the data obtained during the first eight days of this cruise. Since the subsequent daily calibrations agreed to better than 10%, the inherent uncertainty should not be significantly larger than 10%, assuming that the GC/FPD worked stably during the entire cruise.

2.2.4   Meteorological and Oceanographical Data

Meteorological and oceanographical parameters were monitored by the ship's sensors. Wind speed and direction were measured at 37 m a.s.l. on both the port and starboard sides of the ship. Air temperature and humidity were measured at 27 m a.s.l. on the port and starboard sides of the ship. Only signals from the windward sensor were used to avoid influences from the ship. Seawater temperature and salinity were measured at the bow. The ship's position was determined by the Global Positioning System (GPS).

The ship's data used in this work are averaged over 30 min.

No in situ measurements of phytoplankton were available during either cruises. The chlorophyll *a* concentration (as a measure of the phytoplankton content) was retrieved from the SeaWiFs ocean color data provided by the Distributed Active Archive Center (DAAC) of the National Aeronautics and Space Administration (NASA) of the United States. Monthly averaged ocean color data were used for retrieving the chlorophyll *a* concentration, since data with higher time resolution, i.e., those averaged daily or over eight days, as provided by the DAAC, do not cover most of the regions studied during the two cruises. There are still a few gaps (about 10% of the total data points) in the monthly averaged data. These gaps have been filled by interpolating the data from nearby areas. The monthly mean values have a spatial resolution of 9 km, corresponding to a time interval of about 20 minutes at normal cruising speed.

2.2.5   Assessment of Errors

Permeation tubes were used for calibration in this study. The reliability of calibrating COS measurements using permeation tubes has been questioned by *Fried and Henry* (1998), who showed that COS permeation rates of relatively new tubes are significantly overestimated by gravimetric determination due to the presence of a CO_2 impurity in the tubes. The COS permeation tube used in this study was purchased several years before the beginning of the study. No temporal decrease in its permeation rate was observed, therefore, the potential systematic error caused by the CO_2 impurity in the tube is likely negligible. However, there is an uncertainty in the COS permeation rate ($\pm 9\%$). This uncertainty is the main source of the inaccuracy in the COS measurements.

Samples were cryogenically focused before being analyzed (see *Figure 2.2*). Recovery tests show that the trapping efficiency of the system is virtually 100%. During the focusing, the sample flow rate was controlled by a MFC. Sample volumes were derived from the flow rate and the focusing time determined using a stopwatch. There will be systematic errors in the sample volumes if the flow rate and/or the focusing time are inaccurately determined. The MFC has an accuracy of 0.5%, and the error in the focusing time is estimated to be less than 1%, therefore, the systematic errors in the sample volumes are estimated to be less than 2%.

The Weiss-type equilibrator, which was used for the measurements of dissolved COS, is vented to atmospheric pressure, so that a significant pressure variation inside the equilibrator is not expected. However, an influx of ambient air, caused by withdrawing samples, may introduce an error in the COS

concentration measured in the equilibrator's headspace. This error was less than 1%, as shown by simulations covering extreme conditions encountered during the measurements.

Taking into account all above error sources, the overall accuracy is estimated to be 12%.

The analytical precision for COS under the conditions in the ship's laboratory is estimated to be 3%, based on the reproducibility of the standard samples. Sample measurements involve additional random errors originating from sampling, determination of sample volumes, etc. Since the relative standard deviation of the mixing ratio of atmospheric COS during the two cruises was about 7% and 8%, respectively, the overall precision for the COS measurements made using the techniques presented in *Section 2.2.3* is better than 7%.

The precision of the supporting measurements supplied by the ship is ± 0.1°C for temperature, ± 0.1 hPa for the air pressure, ± 0.1 m s^{-1} for windspeed, $\pm 5\%$ for the relative humidity, ± 0.01‰ for salinity, and ± 0.05 W m^{-2} for the global radiation.

The accuracy of the standard algorithm for deriving chlorophyll a data from SeaWiFs measurements is estimated in *Aiken et al.* (1998) to be 35%, based on an intercomparison between the SeaWiFs chlorophyll a data and in situ measurements of chlorophyll a from the Atlantic Meridional Transect (AMT) Program during September/October, 1997.

2.3   Results and Discussion

2.3.1   Concentration and Saturation Ratio of COS in Seawater

COS concentrations in surface seawater were derived from the COS mixing ratios measured in the headspace of the equilibrator. The Henry's law constant for COS and its temperature dependence according to *Johnson and Harrison* (1986) were used in the calculation. The dimensionless Henry's law constant H is given by

$$\ln(H) = 12.722 + \frac{3496}{T}, \tag{2.4}$$

where T is the seawater temperature in Kelvin. Changes in H due to the slight warming of seawater in the equilibrator have been corrected for. The concentration and saturation ratio (SR) of COS in seawater and the global radiation data (G) are plotted in *Figure 2.3* for both cruises. As can be
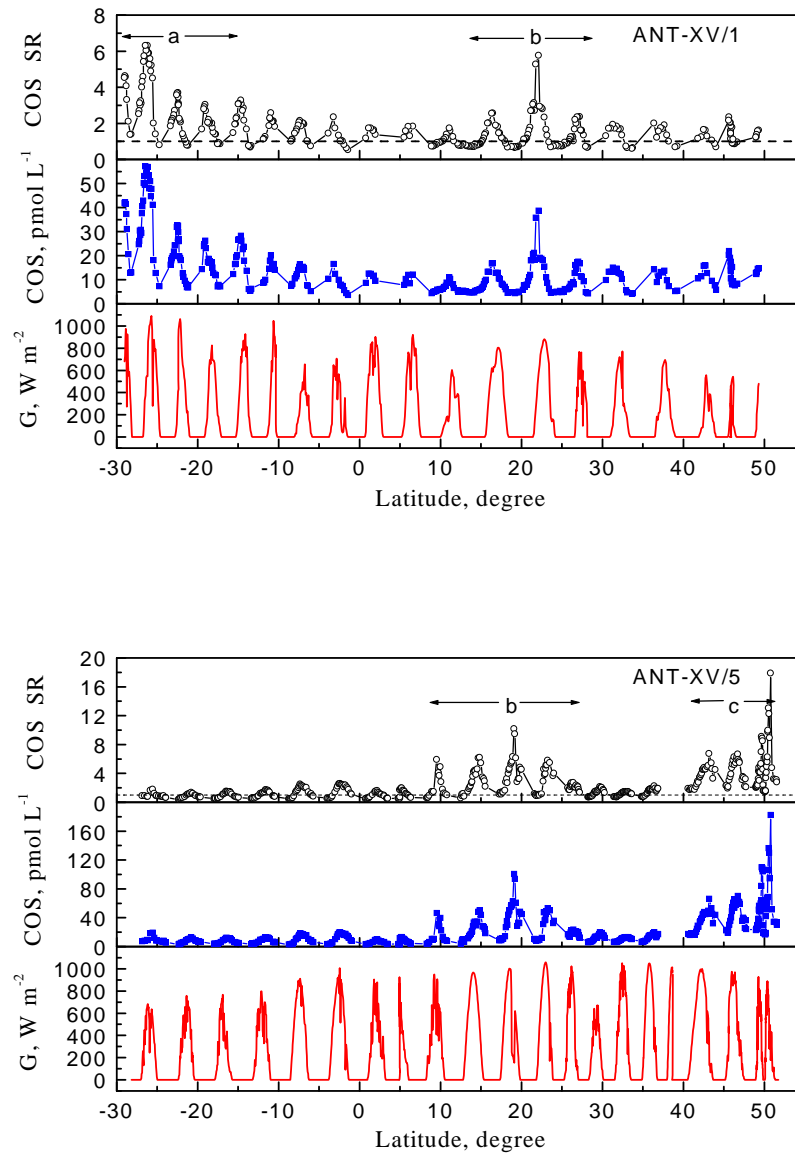
Figure 2.3: Concentration [pmol L^{-1}] and saturation ratio [SR] of COS in seawa-
ter and global radiation, G [W m^{-2}], during the cruises *ANT-XV/1*
(October 15 - November 7, 1997) and *ANT-XV/5* (May 26 - June 21,
1998). The dashed horizontal lines represent equilibrium (SR=1). The
approximate positions of the Benguela Current, the West African up-
welling area and the Northeast Atlantic region are marked by a, b and
c, respectively.

seen in the plots, the concentration and SR of seawater COS showed strong latitudinal and diurnal variation. The COS concentration ranged from 3.7 to 57.1 pmol L^{-1} during *ANT-XV/1* and from 3.0 to 182.5 pmol L^{-1} during *ANT-XV/5*. Enhanced marine levels of COS were observed in areas of high biological productivity, particularly during the warmer seasons, for example, in the Benguela Current (10°S-30°S) in November (a), in the Northeast Atlantic (40°N -50°N) in June (c) and in the West African upwelling area (10°N-30°N) (b). In other regions, the concentration of COS in seawater varied around a level of about 10 pmol L^{-1} and was about a order of magnitude lower than in the sunny eutrophic regions.

2.3.2   Diurnal Cycle of Dissolved COS

As shown in *Figure 2.3*, pronounced diurnal cycles of dissolved COS and its saturation ratio were observed each day, with afternoon maxima and early morning minima. The diurnal cycle was especially pronounced on sunny days. An important feature of the saturation ratio profile is that the saturation ratio decreased to a level of undersaturation (SR<1.0) during the late night and early morning on most observational days, i.e., surface seawater takes up COS from the atmosphere during this period of the day. COS undersaturation has been observed during winter by *Weiss et al.* (1995) in the subtropical gyres and temperate regions of the Pacific and by *Ulshöfer et al.* (1995) in the temperate North Atlantic. However, there have been no previous reports of such undersaturation as an almost regular diurnal feature of temperate and equatorial ocean waters during summer. Data presented here indicate that nocturnal COS undersaturation may occur regularly in Atlantic Ocean waters, even during the warmer seasons and in productive regions, enabling seawater to act as a sink for atmospheric COS during the late night and early morning. These measurements indicate that a further downward revision of the estimated net COS emission from the oceans may be necessary.

2.3.3   Dissolved COS and other Parameters

Correlation with Global Radiation

Figure 2.4 shows the normalized diurnal variation in the concentration of COS in seawater and in global radiation, as averaged along the cruise tracks. The diurnal cycle of dissolved COS is consistent with previous field observations (*Andreae and Ferek*, 1992; *Weiss et al.*, 1995). Dissolved COS has a minimum in the early morning, increases rapidly after sunrise, and peaks
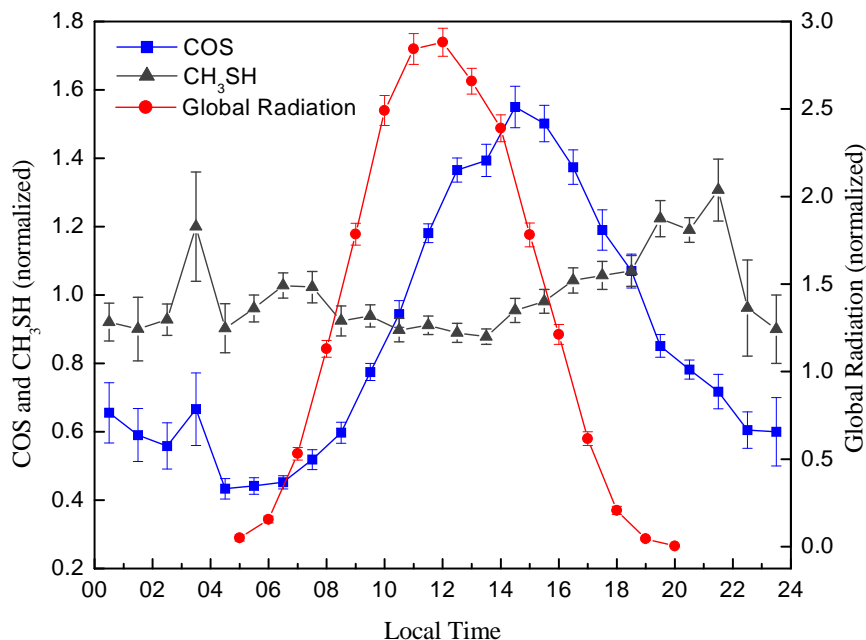
Figure 2.4: Diurnal variations in the concentration of dissolved COS and of CH$_3$SH and in global radiation during *ANT-XV/1* and *ANT-XV/5*. The individual data points are normalized to the daily mean values and then averaged over all observational days. The error bars indicate one standard error of the mean.

around 15:00 local time. The intensity of global radiation reaches its maximum at 12:00 local time. There is a time lag of about 3 hours between the peak of the normalized COS concentration and that of the intensity of global radiation. During the daytime, dissolved COS is mainly produced by photochemical reactions and is removed by hydrolysis, downward mixing, and exhalation from seawater. After sunrise, the concentration of seawater COS increases because COS is produced more rapidly than it is removed. The photoproduction rate of seawater COS approaches its maximum around noon, but the concentration of dissolved COS does not, as the production rate still exceeds the removal rate. The concentration of dissolved COS peaks about 3 hours later (i.e., at around 15:00), when the rate of production is balanced by the loss rate. Therefore the time lag observed is caused by the overall balance between the production and removal of dissolved COS. A close relationship between the net COS formation and the UV light intensity can be expected since seawater COS is believed to be dominantly produced by photochemical reactions, as expressed by the model (*Equation 2.3*). Ac-
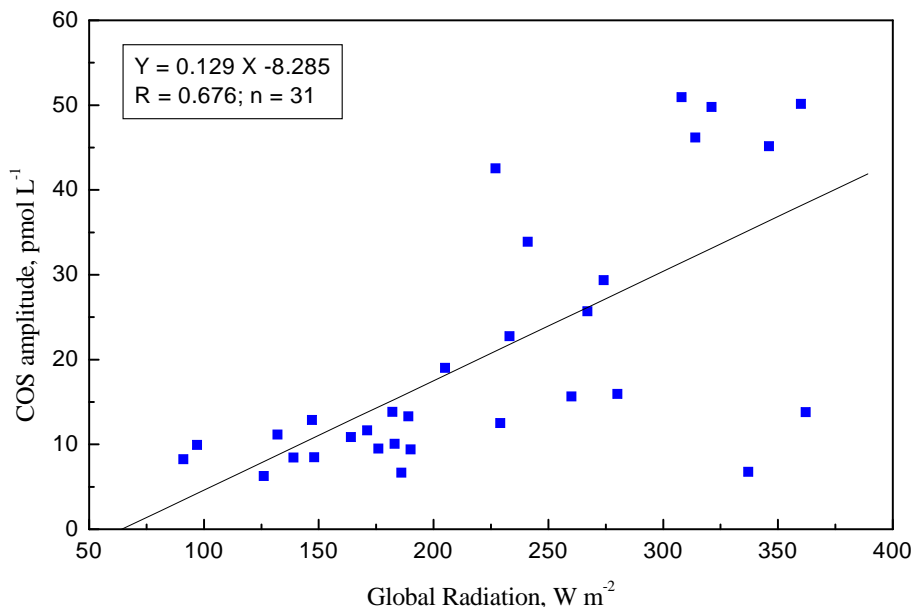
Figure 2.5: Correlation between the COS peak-to-peak amplitude and global radiation. The line shows a least square fit to the data. The regression results are shown in the box.

tually, there is a significant correlation between the diurnal peak-to-peak amplitude of dissolved COS, which presents a measure of the net production within the period from the minimum to the maximum, and the daily mean global radiation, which may be used as a proxy for incident solar radiation and UV flux (*Figure 2.5*). This result is in accordance with other laboratory and field results which support the theory of COS photoproduction (*Ferek and Andreae*, 1984; *Uher*, 1994; *Zepp and Andreae*, 1994; *Ulshöfer et al.*, 1996; *Flöck and Andreae*, 1996).

Correlation to CH$_3$SH

Besides UV radiation, the presence of COS precursors in seawater is another basic precondition for COS formation. CH$_3$SH has been proposed as a potential precursor of COS in seawater by *Ulshöfer et al.* (1996) and *Flöck and Andreae* (1996). During incubation experiments with natural seawater, they observed an inverse relationship between the concentrations of COS and CH$_3$SH . *Pos et al.* (1998) proposed a sulfur-centered radical (thiyl or sulfhydryl) as the key sulfur intermediary in COS production based on mech-

anistic studies in seawater.

In almost all chromatograms of headspace samples, a CH₃SH peak was clearly identified. The CH₃SH signal can not be an artifact from the sampling system for the following reasons: (a) no substantial changes in the concentrations of COS and CH₃SH were observed after cleaning the system, which was usually done every 2 or 3 days during the cruises; (b) the diurnal cycle of the CH₃SH signal (see *Figure 2.4*) cannot be explained by production in the sampling system since the major physical parameters in the laboratory system (temperature, radiation) underwent no diurnal cycle. A direct calibration of CH₃SH was not possible during *ANT-XV/1*, as no CH₃SH permeation tube was available. The CH₃SH peaks from this cruise were therefore calibrated indirectly, using the COS calibration curves from the same day. Because the FPD is more sensitive to COS than to CH₃SH, this nonspecific calibration was then corrected for the sensitivity difference between COS and CH₃SH. The correction factor was derived from the COS and CH₃SH calibration curves obtained during the *ANT-XV/5* cruise, when direct simultaneous calibrations were conducted for both compounds (see *Appendix A*). The Henry's law constant for CH₃SH given by *De Bruyn et al.* (1995) was used for the calculation of the seawater CH₃SH concentration. The concentration of dissolved CH₃SH was found to be 3-16 times higher than that of COS in the same water samples. The concentration of dissolved CH₃SH varied inversely to COS during daylight (*Figure 2.4*), implying that COS was produced during the same photochemical process in which CH₃SH was destroyed. The relative diurnal amplitude of CH₃SH is smaller than that of COS, suggesting longer time constants for the sources and sinks of seawater CH₃SH. After eliminating the diurnal signal in the data by averaging over 24 hours, the resulting daily means of COS and CH₃SH are correlated at a highly significant level ($R = 0.816, n = 40$) along the cruise tracks, as shown in *Figure 2.6*. The correlation between the two compounds suggests that CH₃SH is one of the key factors in the formation of COS in surface seawater. These measurements provide the first field evidence to support the idea that CH₃SH is a precursor of COS in seawater.

The small intercept (1.2) of the regression line in *Figure 2.6* is not significantly different from zero, as indicated by the 95% confidence belt of the regression line, i.e., the regression line goes practically through the origin. This phenomenon suggests that there would be no COS in seawater if there were no dissolved CH₃SH. In other words, the CH₃SH concentration may be used as an indicator for the COS production potential in seawater.

Although some other organosulfur compounds, such as GSH, 3-MPA, CYS, etc., may also act as COS precursors, as indicated by incubation experiments with synthetic seawater (*Flöck et al.*, 1997), there have as yet been
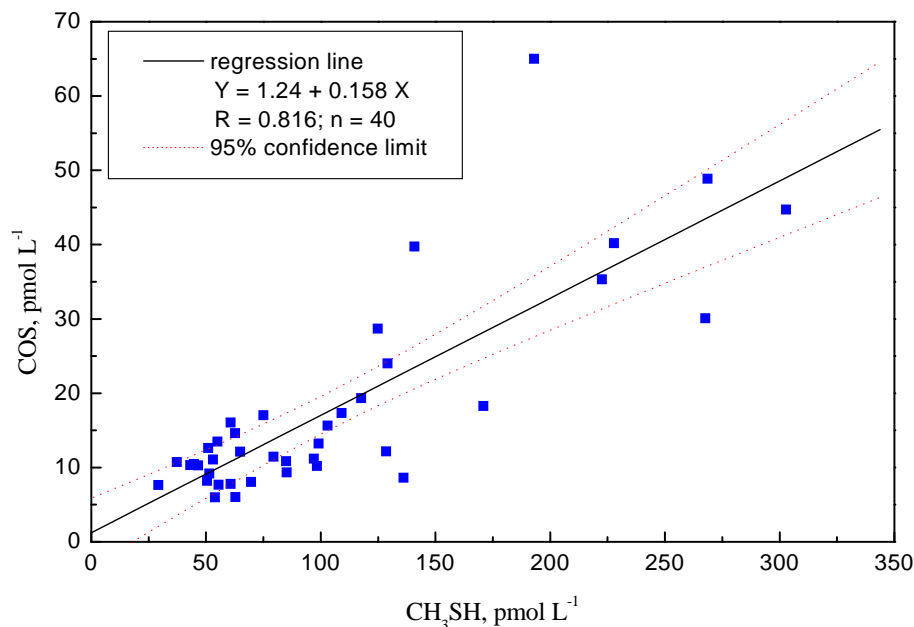
Figure 2.6: Correlation between the daily mean concentrations of COS and CH_3SH in seawater. The solid line shows a least square fit to the data. The dotted lines represent the 95% confidence belt.

no reports on the relationship between these compounds and COS in natural seawater. Future attempts to clarify this relationship would be worthwhile and would help improve our understanding of the formation mechanism of COS in seawater.

Correlation to the COS hydrolysis lifetime

In addition to being produced photochemically, COS can also be produced in the dark. However, dark production normally only contributes a small amount ($<30\%$) to COS formation and does not influence the COS diurnal cycle (*Ulshöfer et al.*, 1996; *Flöck and Andreae*, 1996). Hydrolysis is the dominant sink of COS in seawater, causing the concentration of dissolved COS to decay to its nocturnal minimum.

The hydrolysis rate constant can be calculated either using theoretical equations or from experiment data. When the ship passed through the West African upwelling area on the days from October 23 to October 26, 1997, very profound diurnal variations in seawater COS occurred due to the high intensity of solar radiation and the high concentrations of COS precursors
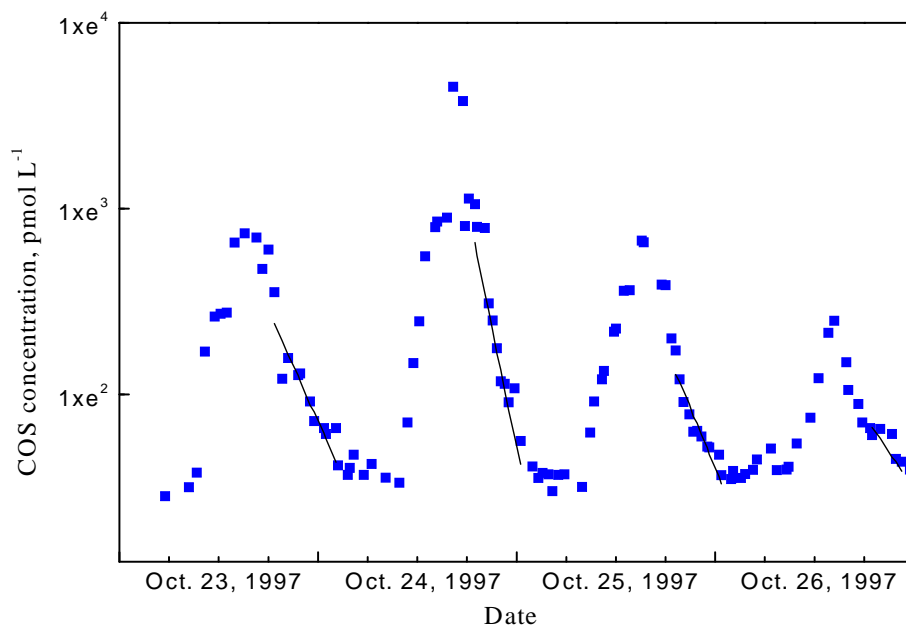
Figure 2.7: Diurnal profiles of dissolved COS between October 23 and October 26, 1997. The lines show exponential fits to the nighttime decay of COS. Hydrolysis lifetimes were derived from the slopes of the fitted lines.

in the upwelling water. The diurnal profiles of seawater COS on these days (*Figure 2.7*) were better determined by more frequent measurement of dissolved COS. These diurnal profiles allow a better quantification of the hydrolysis rate constant for COS. An average hydrolysis lifetime of 9.8 hours with a range between 4.8 and 15.5 hours was obtained by neglecting the dark production and applying an exponential fit to the nighttime decay of COS from the nights of October 23 to 26, 1997. This hydrolysis lifetime compares well to theoretic values of 4.0 to 13.4 hours calculated using the models of *Elliot et al.* (1989) and *Radford-Knoery and Cutter* (1994), implying that hydrolysis plays a major role in the removal of seawater COS. Furthermore, hydrolysis also seems to be one of the key factors controlling the large-scale geographical distribution of seawater COS. *Figure 2.8* shows the correlation between the daily means of the COS concentration and the hydrolysis lifetime of COS in seawater. The correlation is significant at the 99% confidence level. Since each data point in the figure represents both a temporal and a spatial average, the observed correlation suggests that hydrolysis exerts a major influence on the level of dissolved COS. Further factors are the UV
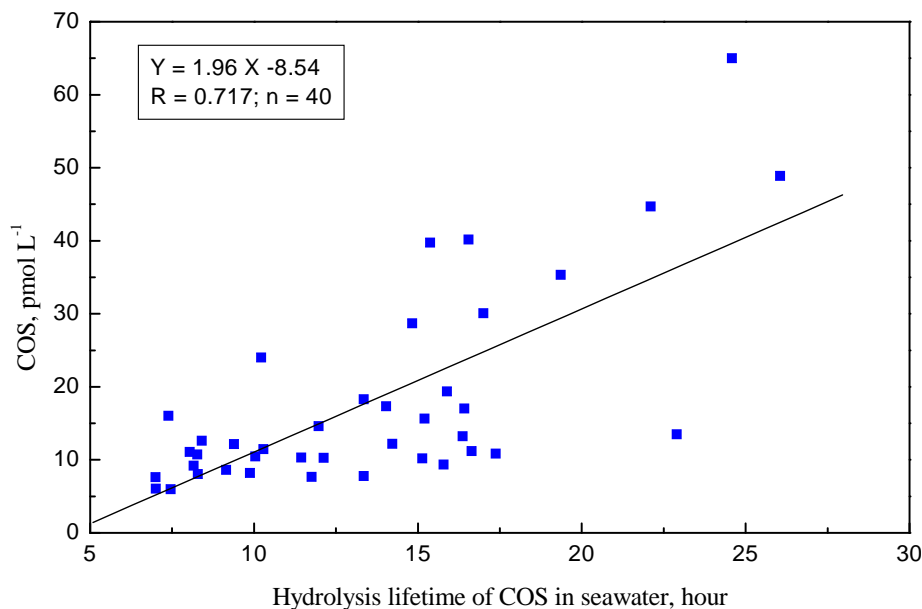
Figure 2.8: Correlation between daily means of the COS concentration and of the hydrolysis lifetime of COS in seawater. The line shows a least square fit to the data. The regression results are shown in the box.

light intensity and concentrations of precursors.

Correlation to Chlorophyll

Chlorophyll is one of the most important pigments in nature. It is found in virtually all photosynthetic organisms, including green plants, blue-green algae, etc. It uses the solar energy to convert carbon dioxide to carbohydrates. Chlorophyll occurs in several distinct forms, among which chlorophylls a and b are the two major types found in higher plants and green algae. Chlorophyll a ($C_{55}H_{72}O_5N_4Mg$) is considered to be a measure of phytoplankton as well as of primary production.

Data in *Johnson and Harrison* (1986) show a certain correlation between the concentrations of seawater COS and of chlorophyll. *Andreae and Ferek* (1992) found a high degree of correlation between the COS concentration and the marine productivity by comparing measurements in different biogeographical regions. From these findings, *Erickson and Eaton* (1993) proposed a linear model for estimating the COS concentration in the surface ocean based on the chlorophyll concentration as derived from the satellite ocean
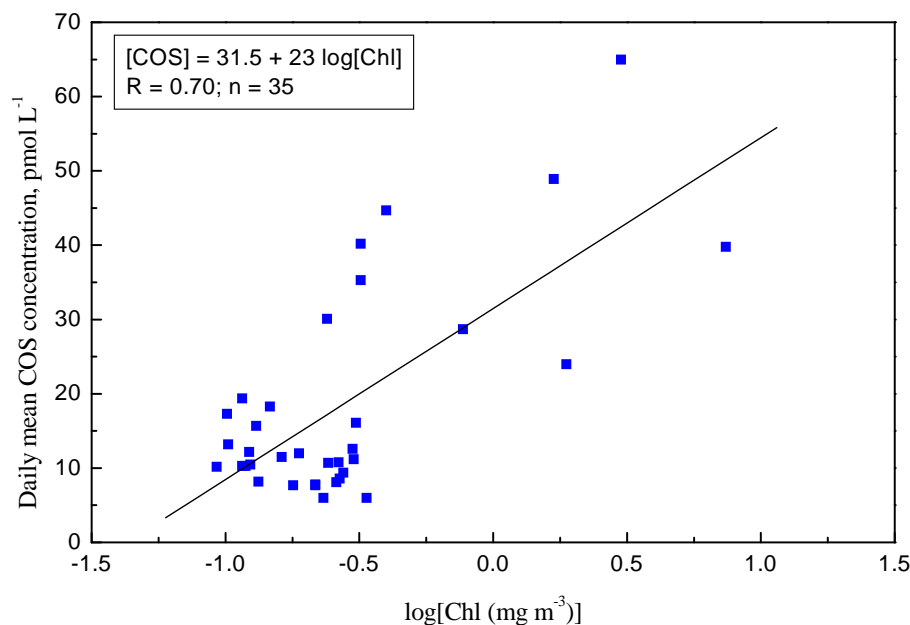
Figure 2.9: Correlation between the daily mean concentration of dissolved COS and the logarithm of the chlorophyll *a* concentration [Chl]. The line shows a least square fit to the data. The regression results are shown in the box.

color data. Combining their linear model with the air-sea flux model of *Liss and Merlivat* (1986), they calculated the global distribution of the surface ocean COS concentration and estimated the global area integrated flux to be 0.47 Tg COS yr^{-1}. However, this method has recently been questioned by *Uher and Andreae* (1997a). Instead, they suggest estimating COS production using CDOM absorbance data, which appear to also be retrievable from satellite databases (*Hoge et al.*, 1995).

In this work, chlorophyll *a* concentrations for different observational days were derived from the ocean color data of SeaWiFs, as described in *Section 2.2.4*. The daily mean COS concentration and the logarithm of the chlorophyll *a* concentration are plotted in *Figure 2.9*. Both quantities are positively correlated at the confidence level of 99%, suggesting an influence of the phytoplankton content on COS production.

As suggested by *Erickson and Eaton* (1993), the chlorophyll content derived from satellite measurements may be considered to be an index of "photochemical lability". This may explain the significant correlation between the concentrations of seawater COS and chlorophyll, reported here and in
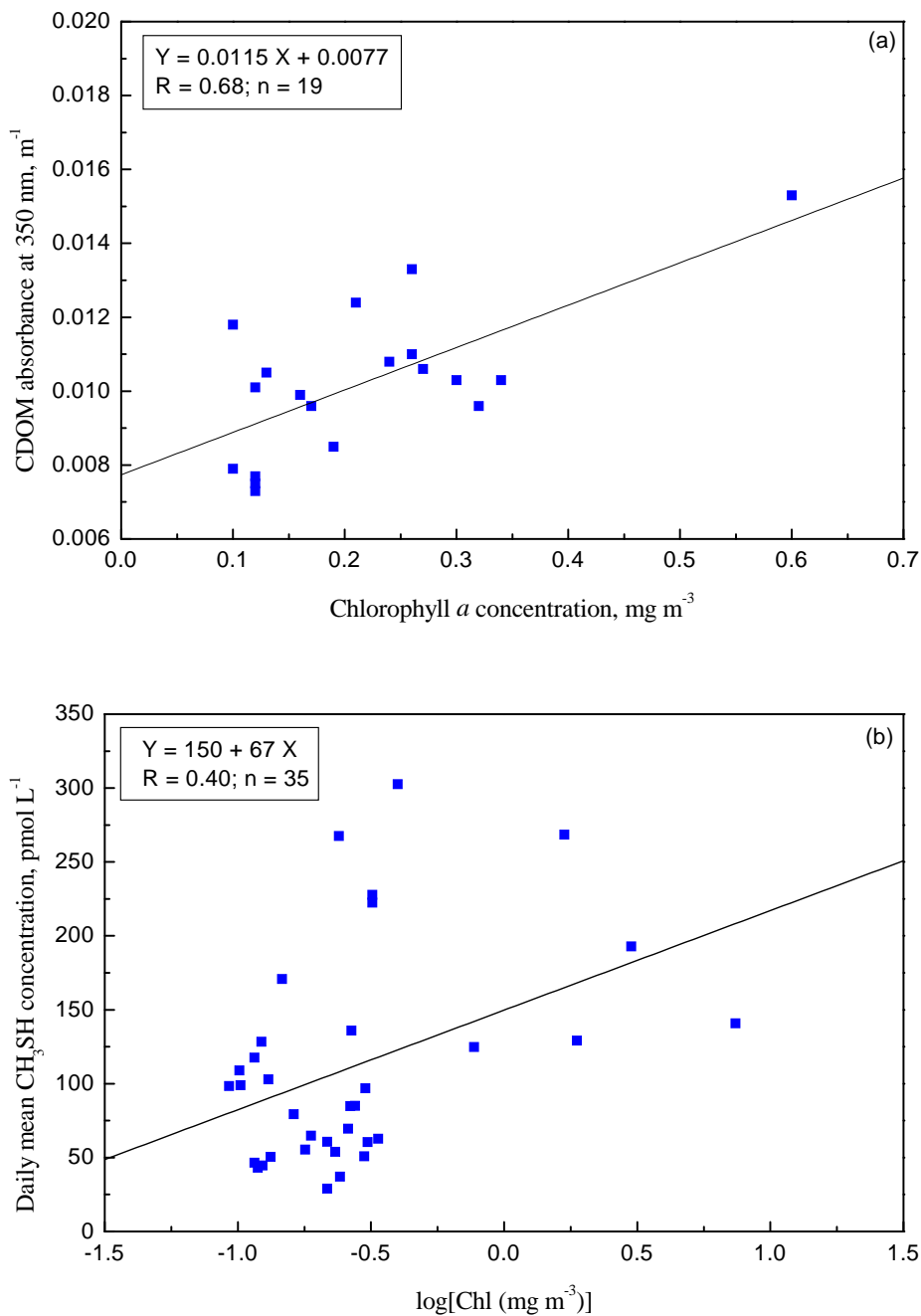
Figure 2.10: Correlation (a) between the CDOM absorbance at 350 nm and the chlorophyll *a* concentration, and (b) between the daily mean concentration of dissolved CH_3SH and the logarithm of the chlorophyll *a* concentration [Chl]. The lines show the least square fits to the data. The regression results are shown in the corresponding boxes.

Andreae and Ferek (1992). For seawater COS, the "photochemical lability" can be promoted by increasing either the concentrations of COS precursors, or the content of CDOM, which may act as photosensitizers, or both. Higher chlorophyll a concentrations or primary productivity may lead to higher concentrations of both COS precursors (CH_3SH, CYS, GSH, etc.), which are released during the decomposition of dead algae, and CDOM, which is the chromophoric fraction of dissolved organic matter (DOM). Actually, there is some evidence supporting this idea. *Figure 2.10* shows that the chlorophyll a content is correlated both to the CDOM absorbance at 350 nm (measured by A. James Kettle, Max Planck Institute for Chemistry, personal communication) and to the daily mean CH_3SH concentration. The confidence levels for the correlations in *Figures 2.10(a)* and *2.10(b)* are 99% and 95%, respectively. Consequently, satellite chlorophyll a data may still be used as a base to estimate the COS concentration in surface seawater, regardless of whether the approach of *Erickson and Eaton* (1993) or *Uher and Andreae* (1997a) is followed.

2.3.4 An Empirical Model for Seawater COS

As shown in *Section 2.3.3*, dissolved COS is correlated with several variables. All the correlations are statistically significant and could be reasonably interpreted based on present knowledge about the production and removal of COS in seawater. However, some data points deviate significantly from the regression line in each of the *Figures 2.5*, *2.6*, *2.8*, and *2.9*. The deviation may be caused by the influence of variables other than those considered. Since all studied factors (radiation intensity, precursor concentrations, and hydrolysis) exert more or less influence on seawater COS and these factors vary relatively independently of each other, changes in the concentration of dissolved COS cannot be perfectly interpreted by only one of these factors. Consequently, a multivariable model should be developed, taking into account the influences of all main factors on seawater COS. This approach was followed by applying a stepwise Multiple Linear Regression Analysis (MLRA) to the data set of daily mean values.

Global radiation (G), the hydrolysis lifetime of COS in seawater (τ), the temperature difference between surface water and air (ΔT), wind speed (W_s), salinity (S), and the chlorophyll a concentration in logarithm ($log[Chl]$) were chosen as independent variables for the analysis. The hydrolysis lifetime is the reciprocal of the hydrolysis rate constant, which has been calculated using *Equations 2.1* and *2.2*. A and E_a values from *Radford-Knoery and Cutter* (1994) and a pH value of 8.3 were used in the calculation. A significance limit of 0.01 was set for the selection of variables to be added into the re-
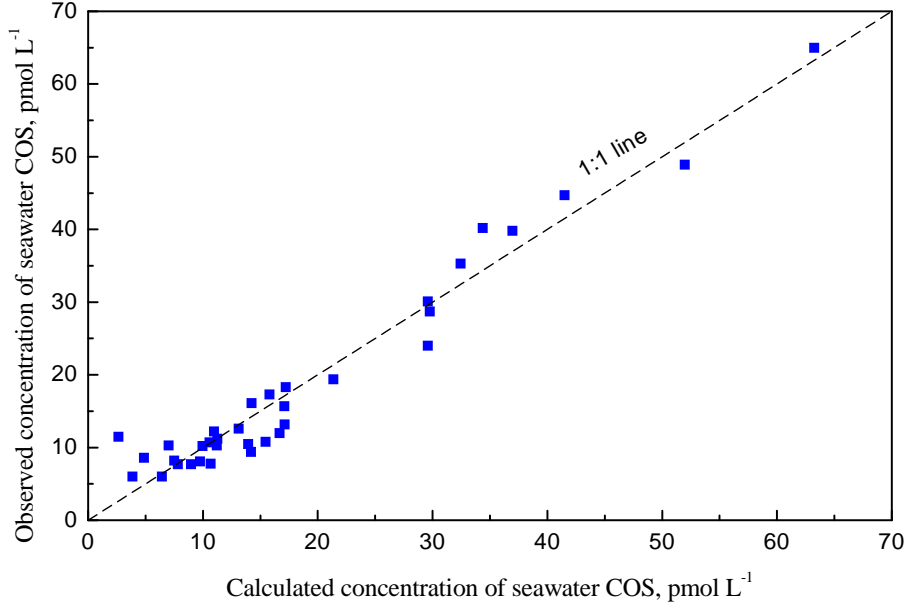
Figure 2.11: A comparison of the observed and calculated daily mean concentrations of seawater COS.

gression equation. Based on the results of the MLRA, the daily mean COS concentration ($[COS]$) can be expressed empirically as:

$$[COS] = 1.8\tau + 13log[Chl] - 1.5W_s + 0.057G - 0.73. \qquad (2.5)$$

The multiple regression coefficient is 0.98 ($n = 35$). The sequence of the parameters on the right-hand side of *Equation 2.5* indicates both the order, in which the parameters have been added, and the order of importance of the variables. The hydrolysis lifetime appears to be the most important factor in controlling the daily mean concentration of seawater COS, followed by the chlorophyll a content and wind speed. Interestingly, global radiation seems to be least important among the four selected parameters. The signs in the equation suggest that longer hydrolysis lifetimes (or lower seawater temperatures), higher chlorophyll concentrations and more intense solar radiation lead to higher daily mean concentrations of seawater COS, while higher wind speeds lead to lower concentrations of seawater COS, which may be a result of enhanced downward mixing of COS in surface seawater and air-sea flux of seawater COS.

 Figure 2.11 shows a scatter plot of the observed daily mean concentrations of seawater COS against those calculated using the empirical model (*Equa-*

tion 2.5). Both agree quite well with each other, suggesting that the daily mean concentration of seawater COS could be reasonably estimated using the hydrolysis lifetime, the chlorophyll *a* content, wind speed and global radiation. Since all these independent parameters can be retrieved from satellite measurements or derived from the retrieved data, such an empirical model appears to be a promising tool for estimating the seawater COS content from satellite data instead of in situ measurements. However, this empirical relationship needs further verification using in situ measurements and satellite data.

2.3.5 COS Air-Sea Flux

As previously shown in *Figure 2.3*, the COS saturation ratio in surface seawater showed large latitudinal, seasonal, and diurnal variations. The calculated COS saturation ratio varied from 0.5 to 6.3 with an average of 1.8 during the cruise *ANT-XV/1*, and from 0.4 to 17.9 with an average of 2.0 during the cruise *ANT-XV/5*.

In order to estimate the net contribution of the Atlantic waters to the atmospheric COS cycle, the COS air-sea flux F was calculated using the model of *Liss and Slater* (1974):

$$F = k_w \left(C_w - \frac{C_a}{H} \right) = k_w \frac{C_a}{H} \left(\mathrm{SR} - 1 \right), \tag{2.6}$$

where C_a and C_w are the mixing ratio of atmospheric COS [pptv] and the concentration of COS in seawater [pmol L^{-1}], respectively, k_w is the air-sea exchange coefficient or piston velocity, H is the Henry's law constant for COS in atm L mol^{-1}, and SR is the saturation ratio of COS in seawater. The dependence of H on the water temperature has been well established by *Johnson and Harrison* (1986) (see *Equation 2.4*). H varies by less than a factor of two over the normal range of seawater temperatures. The air-sea exchange coefficient k_w can be highly variable, and its dependence on atmospheric and oceanic conditions, such as wind speed, boundary layer stability, surfactants, bubbles, etc., has not yet been satisfactorily quantified. Nevertheless, several empirical models are available for calculating k_w. Three models, developed by *Liss and Merlivat* (1986) (LM86), *Wanninkhof* (1992) (W92), and *Erickson* (1993) (E93) have been employed by various authors to estimate the COS air-sea flux (*Mihalopoulos et al.*, 1992; *Ulshöfer et al.*, 1995; *Ulshöfer and Andreae*, 1998; *Weiss et al.*, 1995). The LM86 and W92 models only consider the influence of wind speed on k_w, whereas the E93 model takes into account both wind speed and thermal stability, which is a function of

Table 2.1: Statistics (mean$\pm 1\sigma$) of the COS measurements and flux estimates for the open Atlantic Ocean during the cruises in October-November 1997 and May-June 1998.

Parameter	October-November 1997	May-June 1998
n^a	301	392
$C_w{}^b$, pmol L^{-1}	14.8$\pm$11.4	18.1$\pm$16.1
SR	1.8$\pm$1.2	2.0$\pm$1.6
H, atm L mol^{-1}	61.3$\pm$9.7	59.8$\pm$10.4
Sc^c	543$\pm$95	562$\pm$107
W_s, m s^{-1}	5.4$\pm$2.4	7.5$\pm$2.9
ΔT^d, K	0.9$\pm$0.8	1.3$\pm$1.9
$k_w{}^e$, m d^{-1}	2.1$\pm$0.7	3.7$\pm$2.8
F_{COS}, nmol m^{-2} d^{-1}	13.4$\pm$19.5	28.6$\pm$47.8

[a] Data obtained near the English Channel (north of 48˚N) are excluded to remove the effect of shelf water.

[b] C_w was derived from the COS mixing ratio measured in the headspace air of the equilibrator. The Henry's law constant calculated using the empirical function of *Johnson and Harrison* (1986) was used for the derivation.

[c] Empirical equations, as given by *Siedler and Peters* (1986) were used for calculating the kinematic viscosity of seawater. The molecular diffusivity COS at 25˚C is 1.94×10^{-5} cm^2 s^{-1} (*Sharma*, 1965). The temperature dependence of the gas diffusivity reported by *Himmelblau* (1964) was used to calculate the COS diffusivity at other temperatures.

[d] Here ΔT is derived from the air temperature measured at 27 m a.s.l. and the seawater temperature measured at 5 m depth.

[e] The exchange coefficient was estimated using the stability dependent model (*Erickson*, 1993)

the temperature difference (ΔT) between sea surface and air. Although there is no current consensus as to which model provides the best flux estimate, *Erickson* (1989) suggested that LM86 underestimates the k_w values. This was confirmed by *Putaud and Nguyen* (1996) in a study on DMS air-sea exchange using micrometeorological techniques. Since the marine boundary layer was thermally unstable most of the time during the two cruises, only the E93 stability dependent model was used for calculating k_w in this work.

The E93 model was developed on the basis of the empirical "whitecap" model of *Monahan and Spillane* (1984), who assume a close relationship between the exchange coefficient and the whitecap coverage. The air-sea exchange coefficient k_w is expressed as

$$k_w = k_m (1 - W) + k_t W, \tag{2.7}$$

where k_m and k_t are coefficients representing the conditions for a non-whitecap

area and for a turbulent whitecap area, respectively, and W is the fraction of the sea surface covered by whitecaps. W is proportional to the rate of energy input to a specified ocean area and depends on surface wind speed (V) and the local drag coefficient (C_D), which is itself a function of V and ΔT. Details about the stability dependent model are described by *Erickson* (1993) and references therein. In this work, wind speed and air and seawater temperatures for the calculation of W are taken from the measurements by the ship's sensors during the two cruises. Air temperature was measured at 27 m a.s.l., seawater temperature at 5 m depth. Wind speed measured at 37 m a.s.l. was converted to that at 10 m a.s.l. using a logarithmic wind profile and the neutral drag coefficient of *Trenberth et al.* (1989).

Two sets of k_m and k_t values are available for *Equation 2.7*. One set was derived by *Monahan and Spillane* (1984) based on radon data from projects Geochemical Ocean Sections Study (GEOSECS) and Transient Tracers in the Ocean (TTO). Another set of coefficients ($k_m = 5.0$ cm h^{-1} and $k_t = 1300$ cm h^{-1}) is derived in E93 and attempts to bring the low wind speed results into better agreement with observations while maintaining a global area weighted k_w value of 20.9 cm h^{-1} as obtained for CO_2. In this work the latter set of k_m and k_t values is used to calculate k_w for radon. The k_w values for radon were converted to k_w for COS using the relation:

$$k_{\mathrm{COS}} = k_{\mathrm{Rn}} \left[\frac{Sc_{\mathrm{COS}}}{Sc_{\mathrm{Rn}}} \right]^n \tag{2.8}$$

with the power dependence of the Schmidt number Sc (the ratio of the kinematic viscosity to the molecular diffusivity of a gas) as proposed by *Liss and Merlivat* (1986) and *Jähne et al.* (1987):

$$n = -\frac{1}{2} \text{ for } V \geq 3.6 \text{ m s}^{-1}; \ n = -\frac{2}{3} \text{ for } V < 3.6 \text{ m s}^{-1}.$$

$Sc_{\mathrm{R}n}$ was calculated using the temperature function given by *Erickson* (1993). A set of empirical equations given by *Siedler and Peters* (1986) was used for calculating the kinematic viscosity of seawater. The molecular diffusivity of COS at 25°C is 1.94×10^{-5} cm^2 s^{-1} (*Sharma*, 1965). The temperature dependence of the gas diffusivity as reported by *Himmelblau* (1964) was used for calculating the COS diffusivity at the other temperatures.

The estimated k_w values, as well as COS fluxes and other related parameters for the two cruises, are listed in *Table 2.1*. The large deviations of these flux estimates are mainly due to the strong diurnal and latitudinal variation in the concentration of COS in seawater. *Figure 2.12* shows the regional and seasonal variations in the COS air-sea flux. The largest COS emissions
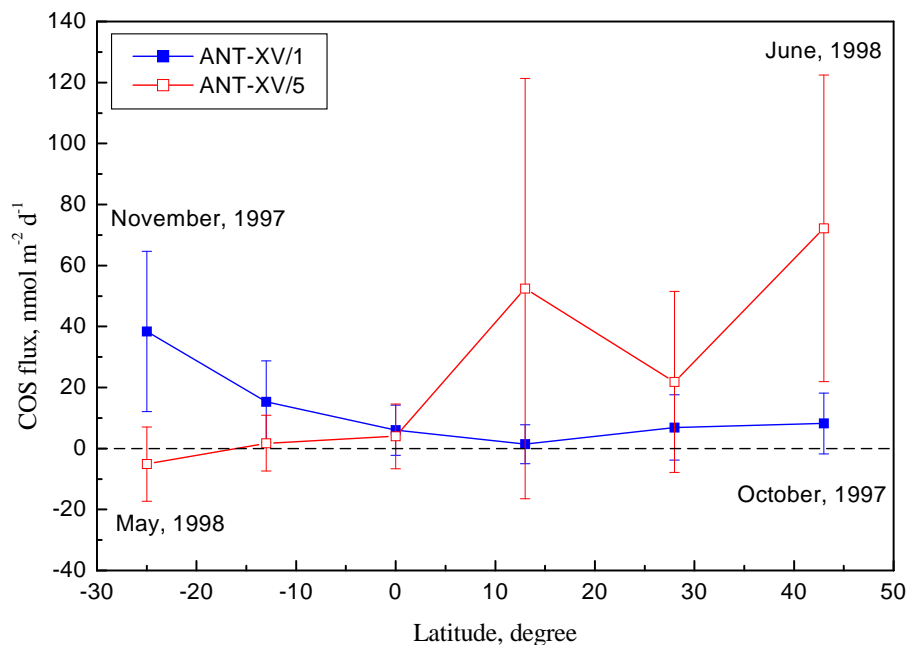
Figure 2.12: Regional and seasonal variation in the estimated COS air-sea flux during the two cruises. The dashed line represents zero flux. The error bars indicate one standard deviation from the mean values.

were observed in the productive regions of the summer hemisphere, i.e., in the Benguela Current in November and in both the Northeast Atlantic and the West African upwelling area in June. A small deposition flux (5.1 nmol COS m^{-2} d^{-1}) existed even in the productive Benguela Current during the southern winter. As shown in *Table 2.1*, the mean flux values for both cruises are positive, indicating a net COS emission from the ocean; however, there is a large variability associated with these values.

By extrapolating the flux estimates for low and middle latitudes from this work and fluxes for the high latitudes (subpolar and polar) given by *Weiss et al.* (1995) to the global open oceans, a global open ocean source of 0.10 Tg COS yr^{-1} was derived from the flux observations. This value should be considered as an upper limit since measurements in this study did not cover the high winter, when COS deposition into the oceans could be stronger, because of the stronger and longer lasting undersaturation of COS in seawater, as shown by *Ulshöfer et al.* (1995). Nevertheless, this flux estimate suggests that the global open ocean is probably a small source of atmospheric COS rather than the minor sink suggested by *Weiss et al.* (1995). On a global scale, the major COS emission of the ocean most likely occurs from coastal

and shelf regions (*Weiss et al.*, 1995; *Ulshöfer and Andreae*, 1998).

2.3.6 Atmospheric COS

The latitudinal distribution of COS in the marine atmosphere is plotted in *Figure 2.13*. The COS mixing ratio averaged 474±33 and 502±38 pptv for the two cruises, respectively. During both cruises, the latitudinal distribution of atmospheric COS was more uniform than that obtained on other cruises with similar instrumentation (*Bingemer et al.*, 1990; *Staubes-Diederich*, 1992). Nevertheless, it displays some characteristic features. The COS level in the subtropical and temperate regions was significantly lower than that observed in the equatorial and tropical regions. A similar distribution, i.e., a steep rise of the COS mixing ratio from the northern subtropical Atlantic towards the equator, was also observed by *Staubes-Diederich* (1992) in the fall of 1988. This author attributed the maximum near the equator to the transport of continental air from Africa. The backward air trajectories in *Figure 2.1* do not indicate any direct transport of air from the African conti-
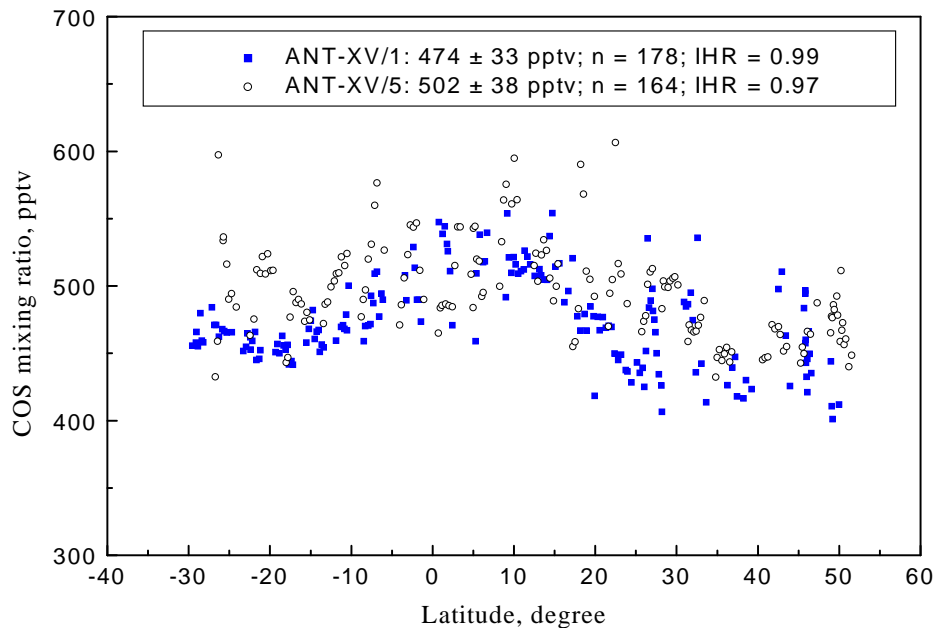

Figure 2.13: Latitudinal distribution of the COS mixing ratio in the marine boundary layer during the cruises *ANT-XV/1* and *ANT-XV/5*. The ITCZ was used to define the boundary of the air masses from the two hemispheres in the calculation of the interhemispheric ratio.

nent to the ship's position during the measurements in this work. However, it is possible that the tropospheric level of COS in the equatorial and the tropical bands was enhanced during the cruises by continental COS sources, such as biomass burning. According to remote observations of the European Space Agency (ESA), the seasonal distribution of the global number of fires peaked around September-October of 1997 and had a secondary maximum in May of 1998, with the latitudinal distribution peaking between 20°S and 20°N (see http://shark1.esrin.esa.it/ionia/FIRE/). As the tropical land surface may act both as a source (biomass burning) and as a sink (assimilatory uptake, see *Chapter 3*) of atmospheric COS, this interpretation remains highly speculative. Enhanced levels of COS in the boundary layer have been observed during aircraft sampling of regional biomass burning plumes over tropical Africa (*Bingemer et al.*, 1992) and over the western Pacific Ocean after long range transport from southeast Asian fires (*Thornton et al.*, 1996). *Thornton et al.* (1996) also reported depletion of COS in air of continental origin due to loss of COS to vegetation.

Interhemispheric Ratios (IHR = M_{NH}/M_{SH}) of atmospheric COS in the range of 0.92-1.25 have been reported by other authors (*Torres et al.*, 1980; *Johnson*, 1985; *Bingemer et al.*, 1990; *Staubes-Diederich*, 1992; *Johnson et al.*, 1993). It has been suggested that higher IHRs are caused by larger anthropogenic emissions in the Northern Hemisphere (*Bingemer et al.*, 1990; *Johnson et al.*, 1993). Taking the ITCZ as the tropospheric boundary between the air masses from both hemispheres, IHRs of 0.99 and 0.97 were observed during the cruises *ANT-XV/1* and *ANT-XV/5*, respectively. Taking into consideration the standard errors of the mean for both hemispheres, these IHR values are not significantly different from unity, at the 95% confidence level.

The IHR values in this work and those of 0.92 reported by *Johnson* (1985) and 0.96 and 0.99 by *Staubes-Diederich* (1992) do not support the idea of a significant contribution of industrial sources in the Northern Hemisphere to atmospheric COS levels. Nevertheless, it does not necessarily mean that such a contribution does not exist. As *Griffith et al.* (1998) point out, in situ measurements of IHR from cruises involve a change of season between hemispheres. On the basis of stationary long-term measurements of total column COS, averaging over several years and all seasons, *Griffith et al.* (1998) derive a mean IHR in the range 1.1-1.2. This robust estimate of IHR allows for significant anthropogenic emission in the Northern Hemisphere.

The variability in the IHR values derived from in situ measurements may be caused mainly by seasonal and geographical variations in the major sources and sinks of atmospheric COS. Ocean emission is highly dependent on the season, as shown by the data from this work and from *Weiss et al.*

([1995](#)). Due to the seasonality in plant physiology, the uptake of atmospheric COS by vegetation may have a seasonal variation, as does the CO_2 assimilation, especially in the middle and high latitudes. In addition, both the ocean source and the vegetation sink of COS may not be equally distributed between the hemispheres because of the asymmetric distribution of the ocean and vegetated areas between the two hemispheres (see *Bates et al.*, 1992). Recent measurements suggest that soil represents a sink for atmospheric COS (*Kuhn et al.*, 1999). *Watts* (2000) recently estimated a soil sink of 0.92 Tg COS yr^{-1} with an uncertainty of 85%. It is not known whether this sink also undergoes a seasonal variability or not. There is very little information about the temporal and geographical distributions of chemical COS sources (i.e., the oxidation of CS_2 and DMS). More studies on COS sources and sinks with emphasis in their temporal and spatial variations are needed. In view of the highly complex variability in time and space of all the major parameters involved, tests of the compatibility between the observed distributions of atmospheric COS and budget estimates are probably only possible in modeling studies.

2.4   Summary

Measurements during two Atlantic cruises showed strong spatial and temporal variations in the concentration of dissolved COS and its saturation ratio. Data indicate that COS undersaturation exists in the low and midlatitudinal Atlantic waters, but that it occurs regularly only during periods with no or low sunlight.

Field evidence for a relationship between the concentrations of COS and CH_3SH in natural ocean water was presented for the first time. The significant correlation between the concentration and the hydrolysis lifetime of COS in seawater indicates the important role of hydrolysis in controlling the geographical distribution of COS in seawater. There is a significant correlation between the concentrations of seawater COS and chlorophyll a, suggesting the importance of biological productivity for COS formation. An empirical model has been developed for estimating the daily mean concentration of seawater COS. The COS concentration calculated using this model agrees well with the observed one, showing a promising way to estimate the COS content of surface seawater using satellite measurements.

COS air-sea fluxes, estimated using the flux model of *Liss and Slater* (1974) and the stability dependent model of *Erickson* (1993) for the exchange coefficient, show strong regional and seasonal variations. The largest COS emissions were observed in productive regions in the warmer seasons. A small

net deposition was found in the Benguela Current during the southern winter. Based on fluxes for low and middle latitudes from this work and the fluxes for high latitudes from *Weiss et al.* (1995), the upper limit for the global open ocean source for COS is estimated to be 0.10 Tg COS yr^{-1}, suggesting that the open ocean makes only a minor contribution to the budget of atmospheric COS.

The COS measurements showed a relatively uniform latitudinal distribution of COS in the marine atmosphere, with mixing ratios of 474±33 and 502±38 pptv for the 1997 and 1998 cruises, respectively. The mixing ratio of atmospheric COS showed several characteristic features in its latitudinal distribution, i.e., an enhanced level in the equatorial and tropical regions and lower levels in the subtropical and temperate regions. However, no significant interhemispheric gradient was observed, which would argue against any significant contribution of industrial sources to the COS abundance in the Northern Hemisphere.

Chapter 3

Investigation of the air-vegetation exchange of COS and CS$_2$

3.1 Introduction

Terrestrial vegetation is recognized as a dominant sink of atmospheric COS, but the magnitude of this sink has not been satisfactorily quantified. This has been one of the reasons for the large uncertainty in the estimate of the COS budget.

Dynamic enclosure techniques were applied in most studies of the exchange of sulfur gases between the atmosphere and vegetation or vegetated soil/marsh surfaces. Most of the earlier chamber studies, which used sulfur-free sweep gases, yielded fluxes that were erroneous in both direction and magnitude, as a consequence of the artificial trace gas gradient imposed on the plant/atmosphere system (*Aneja et al.*, 1979; *Adams et al.*, 1981; *Carroll et al.*, 1986; *Goldan et al.*, 1987; *Lamb et al.*, 1987; *Fall et al.*, 1988; *Staubes et al.*, 1989). The uptake of COS by vegetation was first observed by *Taylor et al.* (1983) and *Kluczewski et al.* (1983, 1985) during laboratory chamber experiments with synthetic air containing 120 ppb and 4 ppb of COS, respectively. *Brown and Bell* (1986) obtained a preliminary estimate of the global vegetation sink of 2-5 Tg COS yr^{-1}, based on data from *Kluczewski et al.* (1983, 1985). However, it is not clear whether it is reasonable to estimate the global uptake of COS by vegetation from results obtained under such extraordinary conditions. Later laboratory experiments with crops by *Goldan et al.* (1988) showed that the uptake of COS and CO$_2$ for atmospheric levels and under daylight conditions has a common pathway, i.e., through the open

stomata, and that the transport resistances for both gases are virtually the same. This similarity led *Goldan et al.* (1988) to estimate the COS vegetation sink on the basis of the atmospheric mixing ratios of COS and CO$_2$ and the primary productivity of terrestrial plants. This estimated vegetation sink ranges from 0.2 to 0.6 Tg COS yr^{-1}, which is one order of magnitude smaller than the estimate of *Brown and Bell* (1986).

Enzymological studies revealed that all enzymes involved in CO$_2$ assimilation can metabolize COS, with carbonic anhydrase (CA) being the key enzyme, which catalyzes the hydrolysis of COS to CO$_2$ and H$_2$S (*Protoschill-Krebs and Kesselmeier*, 1992; *Protoschill-Krebs et al.*, 1995, 1996). According to this finding, all living higher plants should be able to consume COS. This view is consistent with laboratory results (*Kluczewski et al.*, 1983, 1985; *Taylor et al.*, 1983; *Goldan et al.*, 1988; *Fried et al.*, 1993; *Kesselmeier and Merk*, 1993), however, it is not always supported by field studies. While some in-situ experiments clearly showed uptake of COS by plants or soil/plant systems (*Mihalopoulos et al.*, 1989; *Hofmann et al.*, 1992; *Bartell et al.*, 1993; *Dippel and Jaeschke*, 1996; *Kuhn et al.*, 1999; *Simmons et al.*, 1999), other measurements found either no evidence of deposition (*Berresheim and Vulcan*, 1992) or the existence of both deposition and emission (*Kesselmeier et al.*, 1993; *Hofmann*, 1993; *Huber*, 1994). This indicates that the role of vegetation in natural conditions is more complicated than simply taking up or emitting COS. The air-plant exchange of COS appears to be bidirectional and dependent on the ambient mixing ratio of COS, the climatic condition, the plant type, etc. Cuvette studies with agricultural plants demonstrated that a compensation point, at which deposition equals emission, exists for the air-plant exchange of COS (*Kesselmeier and Merk*, 1993). Compensation points were also observed during some field measurements (*Rennenberg et al.*, 1991; *Schröder*, 1993; *Huber*, 1994; *Dippel and Jaeschke*, 1996). The observed compensation points vary from 90 to 515 ppt and are usually much lower than the average tropospheric level of ∼500 ppt COS, suggesting that vegetation tends to take up COS in most cases.

Beside the ambient mixing ratio of COS, the air-plant exchange flux of COS was often found to be correlated to the CO$_2$ assimilation rate, to photosynthetically active radiation (PAR) and to the H$_2$O flux (*Kesselmeier and Merk*, 1993; *Kesselmeier et al.*, 1993; *Bartell et al.*, 1993; *Hofmann*, 1993; *Huber*, 1994), implying the importance of plant physiological processes in controlling COS exchange between the atmosphere and vegetation. The close relationship between COS uptake and CO$_2$ fixation is an encouraging finding, as it allows an estimate of the global vegetation sink of COS on the basis of the observed uptake ratio COS/CO$_2$ and the terrestrial plant productivity. Assuming that the uptake ratio COS/CO$_2$ equals the ratio of the

atmospheric burden of both gases, *Kesselmeier and Merk* (1993) obtained a vegetation sink of 0.86-1.0 Tg COS yr^{-1}, which is in the same range as the estimate of 0.16-0.91 Tg COS yr^{-1} given by *Chin and Davis* (1993). However, the actual value of this COS sink might be larger, since it was observed that the plants investigated prefer to take up COS over CO_2, as indicated by *Kesselmeier and Merk* (1993).

The air-plant exchange of CS_2 has been studied simultaneously in a few studies dealing with air-plant exchanges of other sulfur gases. Emission of CS_2 was usually observed during most earlier chamber studies over vegetated soil or marsh surfaces, due to the problems using sulfur-free sweep gases, or due to strong emissions by marsh soil (*Aneja et al.*, 1979; *Adams et al.*, 1981; *Steudler and Peterson*, 1984, 1985; *Carroll et al.*, 1986; *Goldan et al.*, 1987; *Lamb et al.*, 1987; *Hines and Morrison*, 1992). During the experiments of *Taylor et al.* (1983), vegetation uptake was observed at a high CS_2 level of 120 ppb. *Fall et al.* (1988) found indirect evidence for the uptake of CS_2 by wheat at lower ambient levels. Gradient measurements of sulfur gases in and over a loblolly pine forest did not reveal any evidence of CS_2 uptake by the trees (*Berresheim and Vulcan*, 1992). More recent field and laboratory studies (*Hofmann*, 1993; *Kesselmeier et al.*, 1993; *Huber*, 1994; *Dippel and Jaeschke*, 1996) indicate that CS_2 is both deposited to and emitted by soil/plant systems. It is presently not clear which plant physiological process influences and controls the exchange of CS_2 between the atmosphere and plants. *Giovanelli* (1987) and *Rennenberg* (1991) suggested that CS_2 is one of the volatile intermediates in the metabolism of nonprotein sulfur amino acids. This may explain the emission of CS_2 from plants, but the deposition of this gas to plants remains a mystery.

Considering the high variability of the exchanges of COS and CS_2 between the atmosphere and terrestrial plants, present databases are obviously not adequate to allow reliable estimates of vegetation sinks for both gases. More field measurements over major ecosystems are required to improve our understanding of the role of terrestrial vegetation in the atmospheric cycle of COS and CS_2. This chapter presents measurements of COS and CS_2 fluxes over a forest in central Germany. The R̲elaxed E̲ddy A̲ccumulation (REA) technique was used for the measurements. Details about the REA technique and the development and validation of a REA sampler are discussed in *Section 3.2*. Field measurements are presented in *Section 3.3*.

3.2   Development of a REA Sampler for Flux Measurements

3.2.1   Background

In studies of biogeochemical cycles of substances and the deposition of pollutants to the Earth's surface, it is often necessary to quantify local gas exchange between the atmosphere and soil/plant ecosystems or oceans. Species of interest include major greenhouse gases (CO_2, CH_4, etc.), sulfur compounds (SO_2, DMS, COS, CS_2, H_2S, etc.), nitrogen compounds (NO_2, NO, N_2O, HNO_3, NH_3, etc.), and photochemically reactive hydrocarbons (isoprene, terpenes, etc.). Exchange fluxes of these gases have been measured in numerous studies with varying uncertainty. One of the major sources of uncertainty in quantifying the fluxes has been shortcomings in the techniques used for the measurements.

Both enclosure and micrometeorological techniques are commonly used for measuring gas fluxes. In the former, a chamber or cuvette is used to cover a certain area of soil or plant twigs or leaves. The chamber can be operated either dynamically or statically. In the case of a dynamic enclosure, fluxes are determined from a mass balance of the trace gases between inflow and outflow. In the case of a static enclosure, fluxes are calculated on the basis of the change in the mixing ratios of the trace gases with time within the closed chamber. The enclosure technique is relatively easy to carry out and is very suitable for mechanistic studies under controlled field or laboratory conditions. However, in both cases, the chamber disturbs the natural microclimate, upon which the aerodynamic resistance depends, and the results have only a small spatial representativity. The latter method, i.e., the micrometeorological technique, overcomes these problems and measures the surface fluxes on an ecosystem scale.

A fairly popular micrometeorological technique for measuring fluxes in atmospheric surface layer is the gradient method. This method, relying on the similarity theory of *Monin and Obukhov* (1954), assumes that the vertical flux of an atmospheric constituent is proportional to its vertical concentration gradient, as is the case in molecular diffusion, so that the flux F_c of a species c is expressed as

$$F_C = -K \frac{\partial c}{\partial z},$$ (3.1)

where $\frac{\partial c}{\partial z}$ is the vertical gradient of the species c and K is the turbulent diffusivity. In addition, it is often assumed that the diffusivity K depends only on atmospheric turbulence and is independent of the species being transferred.

Therefore, the flux F_a of species a can be readily derived from the known flux F_b of species b and the ratio of the gradient of a to that of b:

$$F_a = F_b \frac{\Delta a}{\Delta b}. \tag{3.2}$$

The gradient method has proved quite successful for measuring scalar fluxes over short vegetation, such as grass. However, this method is not recommended for measuring surface fluxes over tall vegetation, such as forests (*den Hartog and Neumann*, 1984). One of the problems with this method originates from the scale of turbulence generated by the inherent roughness of tall vegetation. The turbulent diffusivity over rough surfaces, such as a forest canopy, is usually large and the gradients are much smaller over forest than over short grass or smooth surfaces, so that it is difficult to adequately resolve them. Furthermore, the applicability of the similarity theory over forests has been called into question by observations and theoretical considerations (*Thom et al.*, 1975; *Garrat*, 1978, 1980; *Raupach*, 1979; *Denmead and Bradley*, 1985; *Finnigan*, 1985; *Cellier and Brunet*, 1992). The stability functions for sensible heat and water vapor, which are used for calculating the turbulent diffusivity K, deviate significantly above and within the forest canopy from those over smoother surfaces under unstable conditions (*Thom et al.*, 1975; *Garrat*, 1978; *Denmead and Bradley*, 1985). Even counter-gradient fluxes were observed within the canopy (*Denmead and Bradley*, 1985). The main reason for these phenomena is that the quasi-periodic gusts originating from above the canopy contribute largely to flux (*Denmead and Bradley*, 1985; *Finnigan*, 1985). This significant non-local or non-gradient contribution to flux is not represented by the local gradients and influences the entire roughness sublayer, which extends from ground to two or three canopy heights, leading to substantial underestimates of scalar fluxes by the similarity theory (*Thom et al.*, 1975; *Denmead and Bradley*, 1985; *Rannik*, 1998; *Simpson et al.*, 1998; *Pattey et al.*, 1999). Consequently, profiles for flux estimates must either be measured above the roughness sublayer, which is often impracticable over forests because of difficulties in satisfying enhanced fetch requirements (*Thom et al.*, 1975), or must be corrected beforehand, using independent flux measurement techniques, as done by *Rannik* (1998) and *Simpson et al.* (1998).

Eddy correlation (EC), also called eddy covariance, is a widely adopted method and is the most direct method for measuring turbulent fluxes. In this method, the turbulent flux of a trace gas is calculated by averaging the instantaneous transport of the gas over a suitable time interval:

$$F_c = \overline{w'c'}, \tag{3.3}$$

where F_c is the vertical turbulent flux of the gas, and w' and c' represent the fluctuations of the vertical wind speed w and the gas concentration c around their mean values, respectively. As implied by *Equation 3.3*, only measurements of w and c are needed to obtain the flux F_c. However, the method requires fast-response sensors of both wind speed and trace gas concentrations to measure all the fluctuations that contribute to the flux, which can be as fast as 5 to 10 Hz at a few meters above the surface. Although wind measurements at such a high frequency are no longer a problem since the development of the sonic anemometer, fast-response chemical sensors suitable for eddy correlation measurements are still unavailable for most species. Therefore, alternative methods have been developed during the last two to three decades.

Desjardins (1972) proposed an alternative of the conventional eddy correlation method. As w' at a certain time is either positive w^+ (updraft) or negative w^- (downdraft), *Equation 3.3* may be modified as

$$F_c = \overline{w^+ c'} + \overline{w^- c'}. \tag{3.4}$$

Because $\overline{w^+} + \overline{w^-} = \overline{w} = 0$ and $c = \overline{c} + c'$, *Equation 3.4* is identical with

$$F_c = \overline{w^+ c'} + \overline{w^- c'} + (\overline{w^+} + \overline{w^-})\overline{c} = \overline{w^+ c} + \overline{w^- c}. \tag{3.5}$$

Therefore, it is theoretically possible to measure turbulent gas fluxes by firstly collecting the updraft and downdraft air in two reservoirs according to the direction and magnitude of the vertical wind w, and then determining the differences in gas concentrations between the reservoirs. This method for flux measurements, known as eddy accumulation, is attractive since it bypasses the need for fast measurements of trace gases without adding other uncertainties. However this technique has proved difficult to carry out in practice due to technical obstacles, such as its extreme sensitivity to apparently minor bias in wind and volume measurements (*Hicks and McMillen*, 1984; *Speer et al.*, 1985; *Neumann et al.*, 1989). In spite of some improvement attempts, the practical complexities have restricted the field application of this technique (*Buckley et al.*, 1988; *Neumann et al.*, 1989; *Beier*, 1991).

A modification of the eddy accumulation method was proposed by *Businger and Oncley* (1990). They relaxed the requirements of the eddy accumulation and suggested that the condition for sampling may be determined only by the direction of the vertical wind, and that air is sampled at a constant flow rate. The vertical flux of gas c is then expressed as

$$F_c = \beta \sigma_w (\overline{c^+} - \overline{c^-}), \tag{3.6}$$

where $\overline{c^+}$ and $\overline{c^-}$ are the average concentrations associated with updrafts and downdrafts, respectively, β is a dimensionless coefficient, and σ_w is the standard deviation of the vertical windspeed. This method, known as relaxed eddy accumulation (REA) or conditional sampling (CS), has been applied to flux measurements of CO_2, CH_4, pesticides and isoprene, giving reliable results in most cases (*Majewski et al.*, 1993; *Oncley et al.*, 1993; *Pattey et al.*, 1993, 1999; *Beverland et al.*, 1996a,b; *Guenther et al.*, 1996; *Moncrieff et al.*, 1998). However, such success should not be a reason to stop the development of the true eddy accumulation technique and of fast-response chemical sensors for eddy correlation measurements, since the relaxed eddy accumulation is based on a one-and-a-half closure scheme to parameterize the vertical turbulent flux, as recently argued by *Kramm et al.* (1999).

A modeling study by *Wyngaard and Moeng* (1992) revealed that the coefficient β in *Equation 3.6* is determined uniquely by the joint probability density of the vertical windspeed w and the scalar c, and that the theoretical value for β is about 0.6 for bottom-up (flux driven) diffusion in the convective boundary layer, agreeing well with the empirical value obtained by *Businger and Oncley* (1990) based on their simulation. A slightly smaller β value ($\sim$ 0.56) has been obtained during most in situ measurements (*Majewski et al.*, 1993; *Oncley et al.*, 1993; *Pattey et al.*, 1993, 1999; *Beverland et al.*, 1996a,b).

To investigate the role of vegetation in the tropospheric budget of COS, a reliable technique for the measurement of the COS flux over tall vegetation is needed. No suitable analyzer is presently available for eddy correlation measurements of this gas. Therefore, a REA sampler has been developed and validated. Although the intention for the development of the sampler in this work was to measure air/plant exchange fluxes of COS and CS_2, this tool can also be used to measure fluxes of other species, with little or no modification.

3.2.2   Description of the REA Sampler

The setup of the REA sampler is depicted in *Figure 3.1*. A 3-dimensional sonic anemometer-thermometer with a USA-1 sensor (Metek, Germany) was used for monitoring wind components and the virtual temperature. Wind and temperature data at 10 Hz were acquired by a portable PC, connected to the anemometer by an RS-232 cable. Three Teflon solenoid valves (Cole Parmer, USA) were employed to direct air segments into different reservoirs. A control program decided which of the three solenoid valves (V_+, V_0, and V_-) should be opened, according to the direction and scale of the vertical wind w. Digital control signals were sent to a valve controller, which switched the valves electrically. Only one of the valves was opened at any one time
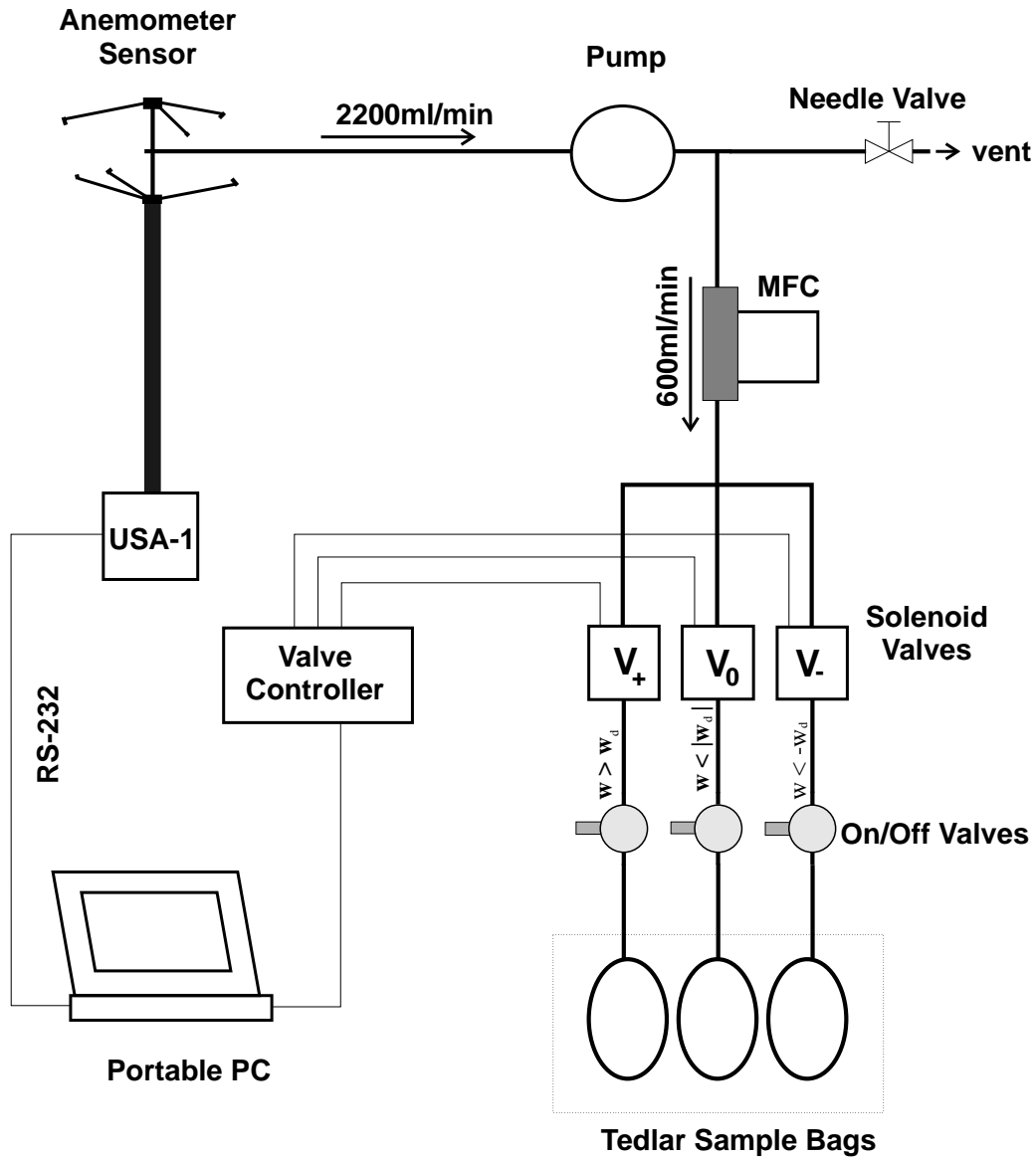
Figure 3.1: Schematic representation of the REA sampler.

during the sampling.

Bags with a volume of 9 L, made of Tedlar PVF film (Du Pont, USA), were used as sample reservoirs. Before sampling, the bags were evacuated and then connected to the solenoid valves. During sampling, air from the height of the anemometer sensor was drawn at a rate of 2200 ml/min through a 3 m Teflon FEP tubing (1/8″ O.D., 1/16″ I.D.) by a Teflon diaphragm pump (N86 KTE, KNF Neuberger, Germany). This flow was split in two sub-streams, one of which was set at 600ml/min by a mass flow controller (MFC, 0-1000ml/min, Bronk Horst, Holland) and directed to the selected reservoir, and the other was vented. Such a layout shortens the lag time of air in the tubing and protects the MFC from the influence of water droplets formed in the outflow of the pump.

3.2.3   Practical Requirements and Problems

Response Time and Switch Frequency

As described in *Section 3.2.1*, no fast measurements of gas concentrations are needed in the REA method. However, measurements of the vertical windspeed and the sampling should be operated at a similarly high frequency to that required for EC measurements. This means that the switching valves directing the updraft and downdraft air into the corresponding reservoirs must be able to react as quickly as the operating frequency of the wind sensor used. In addition, the response time of the valves should be significantly shorter than the interval of wind measurements. These requirements should be fulfilled to avoid erroneous sampling.

The solenoid valves and the valve controller used in the sampler presented here have response times of 15 ms and 40 ms, respectively. Therefore, the switching system is able to work at a frequency of above 10 Hz. As the lifetime of the valves is limited to about 50000 switching operations, the operation at higher frequency may require more frequent replacement of the valves, which is unfavorable both in time and in cost. As a compromise, the valves were switched at 5 Hz with only a few exceptions, although wind signals were acquired at 10 Hz. This compromise prolongs the valve's lifetime without significant reduction in the accuracy of the flux measurements. This is confirmed by a simulation, in which the sensible heat flux (F_H) was supposed to be obtained by the REA method at the sampling frequencies of 5 Hz and 10 Hz, respectively. Field data of wind and temperature (10 Hz) obtained over a spruce stand in the Solling Mountains (see *Section 3.3.1*) were used for the simulation. *Figure 3.2* shows the results of the simulation at both sampling frequencies. With a few exceptions all data points lie on
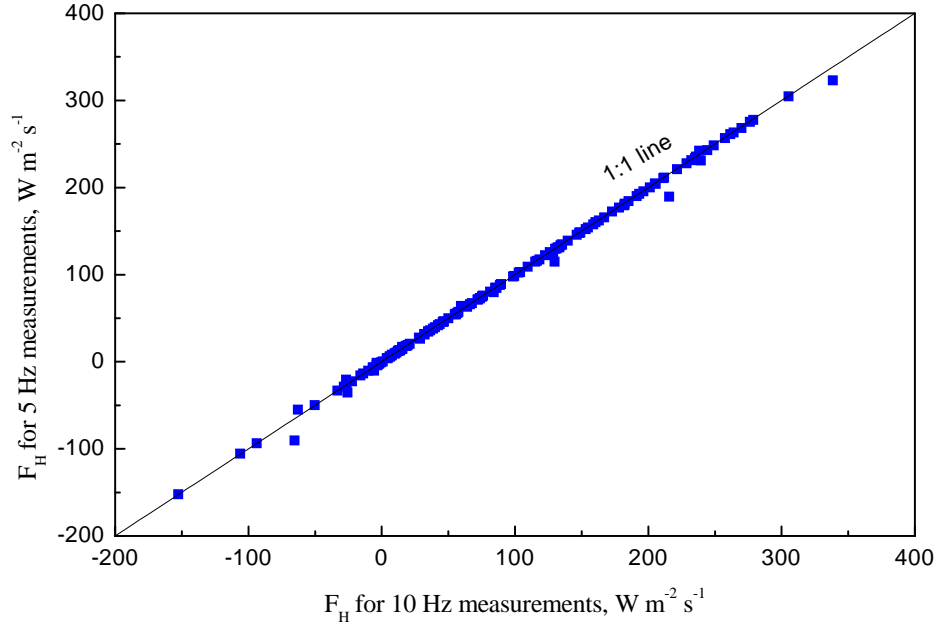
Figure 3.2: Comparison of simulated sensible heat fluxes for measurements at 5 Hz with those made at 10 Hz.

the 1:1 line, suggesting no significant loss of flux by reducing the sampling frequency from 10 Hz to 5 Hz.

Another measure to avoid excessive valve switching is the application of a deadband (w_d). The deadband is an interval of the vertical wind signal, centered at $w = 0$, in which air is not accumulated in any of the reservoirs for up and downdraft. Field practice showed that a deadband of $0.1\sigma_w$ may reduce the number of switching operations by about 10%, on the average.

Lag Time and Damping

During flux measurements, air is transported from the intake point through a tube to the sample reservoirs. The travel time from the intake to the switching valve causes a time lag. In EC measurements, such a delay is usually corrected in post-processing of EC data (*Leuning and Moncrieff*, 1990; *Fan et al.*, 1992). In REA measurements, any erroneous sampling cannot be corrected, once the gas sample is fed to the reservoir. Therefore, the delay must be corrected on-line if it is close to or longer than the interval between two sequential valve operations. Based on the flow rates and the dead volume between the tubing inlet and the solenoid valves (see *Appendix*

B), the lag time of the sampled air mass is estimated to be 1.0 s. This lag time was taken into account in the control program.

Another problem caused by the sampling tube is the damping of concentration fluctuations. Due to the non-uniform distribution of the concentration in the radial axis, the concentration fluctuations in the tube are attenuated. This attenuation effect can lead to underestimates of turbulent fluxes. To ensure the accuracy of the flux measurements, this underestimate should be account for.

The flow in a tube is either laminar or turbulent depending on the Reynolds number Re, as defined by

$$Re = \frac{2rU}{\nu}, \tag{3.7}$$

where r is the tube radius, U is the discharge velocity in the tube, and ν is the kinematic viscosity of air. In the turbulent case, the error due to tube attenuation is negligible, if no absorption or desorption occurs on the tube walls, as shown by *Lenschow and Raupach* (1991) and *Massman* (1991). In the laminar case, the underestimate of the flux depends on the geometry of the tubes, the wind speed during the sampling, the sampling height, etc. (*Philip*, 1963; *Leuning and Moncrieff*, 1990). Re for flow in the sampling tube of the REA sampler presented here is close to 2000, which is less than the critical Reynolds number ($Re_c = 2300$). Therefore, formulae for the laminar case are used here to estimate the possible error caused by the sampling tube.

According to *Leuning and Moncrieff* (1990), the fractional loss of the measured flux (F_{raw}) due to tube attenuation is estimated by

$$\frac{\Delta F_{raw}}{F_{raw}} = 1 - \frac{\int_0^\infty f_t(n) S_{wc} dn}{\int_0^\infty S_{wc} dn}, \tag{3.8}$$

where $f_t(n)$ and S_{wc} are the transfer function and the cospectrum of w and c at frequency n, respectively. The transfer function $f_t(n)$ is given by *Philip* (1963) as

$$f_t^2(n) = e^{-\frac{0.829 n^2 r^2 l}{D_c U}}, \tag{3.9}$$

where l is the tube length, D_c is the diffusivity of c in air, r and U are the same as in *Equation 3.7*. D_c for CS_2 is 0.10 at 19.9°C (*Weast*, 1979). No D_c value for COS is available, but it is estimated to be a little higher than that for CS_2. Here, the D_c for CS_2 is used for estimating the attenuation effect. *Equation 3.9* is an approximation solution. The restrictions for using this approximation are $\frac{2\pi n r^2}{D_c} < 10$ and $\frac{10l}{r} \gg \frac{Ur}{D_c}$. Both are met in the setup of this REA sampler.
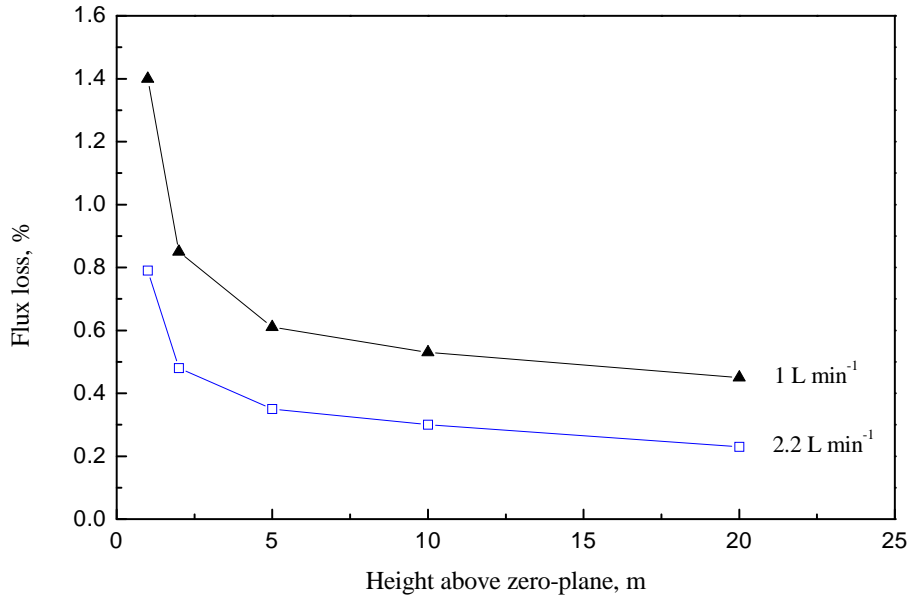
Figure 3.3: Underestimates of gas fluxes due to the damping of concentration fluctuations by the sampling tube, as a function of sampling height and flow rate.

As done by *Leuning and Moncrieff* (1990), the cospectra given by *Kaimal et al.* (1972) for the vertical windspeed and temperature under near-neutral conditions were used for the approximate estimate. The functions are

$$S_{wc} = \begin{cases} - \dfrac{11fu_*T_*}{n(1+13.3f)^{1.75}} \; , & f \leq 1.0 \\ - \dfrac{4.4fu_*T_*}{n(1+3.8f)^{2.4}} \; , & f \geq 1.0, \end{cases} \tag{3.10}$$

where u_* and T_* are the friction velocity and the scaling temperature, respectively, $f = \frac{nz}{u}$ is a dimensionless frequency, with z being the height above the zero-plane and u being the horizontal windspeed.

Leuning and Moncrieff (1990) showed that the underestimates of the gas fluxes increase with increasing windspeed. To estimate the effect under extreme conditions, a windspeed of 10 m s^{-1} was assumed, a case that did not occur during the field measurements in this work. In addition, the REA sampler was supposed to be used at different heights with different sampling flow rates. *Figure 3.3* shows the calculated flux loss as a function of sampling height and flow rate. The data suggest that the impact of damping on this REA sampler is not severe. Even under extreme conditions, i.e., at a low

sampling height (1 m) and with a small flow rate (1 L min^{-1}), the flux loss is still negligibly small for most measurements. For the measurements described in *Section 3.3*, a sampling height of 16.3 m above the zero-plane and a sampling flow rate of 2.2 L min^{-1} were selected, so that a correction for the damping effect seems to be unnecessary.

Flow Stability

The volumetric flow rate in the sampling tube may fluctuate due to changes in the pump's temperature, etc., during a sampling period. Such fluctuations may lead to incorrect sampling, since both the air volume sampled and the lag time vary during the sampling. To resolve this problem, an MFC is used in the sampling system described in *Section 3.2.2*. Unlike volumetric flowmeters, the MFC measures and controls the mass flow with an accuracy of better than 1.0% of full scale.

Effect of a Deadband on the Accuracy

As mentioned previously, a deadband can be used during the REA sampling to prolong the lifetime of the switching valves. Since using a deadband biases the sampling towards larger eddies, this practice can increase the differences (ΔC) in gas concentrations between up and downdraft samples (*Pattey et al.*, 1993) and hence the signal-to-noise ratio in determining the differences (*Oncley et al.*, 1993). The increase in the concentration difference causes an overestimate of the flux, if the dimensionless coefficient β obtained without considering the deadband is used in the flux calculation from *Equation 3.6*. To avoid this overestimate, β should be calculated on the basis of eddies which were actually sampled.

The effect of a certain deadband on the β value varies from run to run, but the relative change in this coefficient seems to be a monotonic function of the deadband normalized to σ_w. Based on simulation studies with data collected over flat terrain in Wyoming (USA), *Businger and Oncley* (1990) obtained the following relationship:

$$\beta(w_d/\sigma_w) \cong \beta(0)e^{-0.75w_d/\sigma_w}, \tag{3.11}$$

where $\beta(w_d/\sigma_w)$ and $\beta(0)$ are β values with and without a deadband, respectively. *Pattey et al.* (1993) made similar simulations with data collected over a soybean field at the Greenbelt farm of Agriculture Canada and obtained a somewhat different empirical model

$$\beta(w_d/\sigma_w) = 1 - b_0[1 - e^{(-b_1 w_d/\sigma_w)}], \tag{3.12}$$

where b_0 and b_1 are the nonlinear regression coefficients. In the case of β for temperature, $b_0 = 0.437$ and $b_1 = 1.958$. For w_d/σ_w values lower than 0.2, there is virtually no difference between these two models. For higher w_d/σ_w, *Equation 3.11* gives a significantly lower value of β.

To investigate the influence of the deadband on β over higher plants, REA experiments were simulated with data collected over a spruce forest (tree height $\sim$ 30 m) in central Germany (see *Section 3.3.1* for details). 160 half-hour runs were used for the simulation. β values based on temperature (β_T), CO$_2$ (β_{CO_2}), H$_2$O (β_{H_2O}), and momentum (β_M) were calculated for deadbands varying from 0.0 σ_w to 0.8 σ_w. The results are plotted in *Figure 3.4*, together with β values predicted by the models of *Businger and Oncley* (1990) and *Pattey et al.* (1993). Some ($\sim$ 5 %) of the simulated values are unrealistically large (> 1) or small (≤ 0), and occurred mostly during neutral atmospheric conditions. They were not included in the statistics. As shown in *Figure 3.4*, for w_d/σ_w values lower than 0.2, the simulation agrees quite
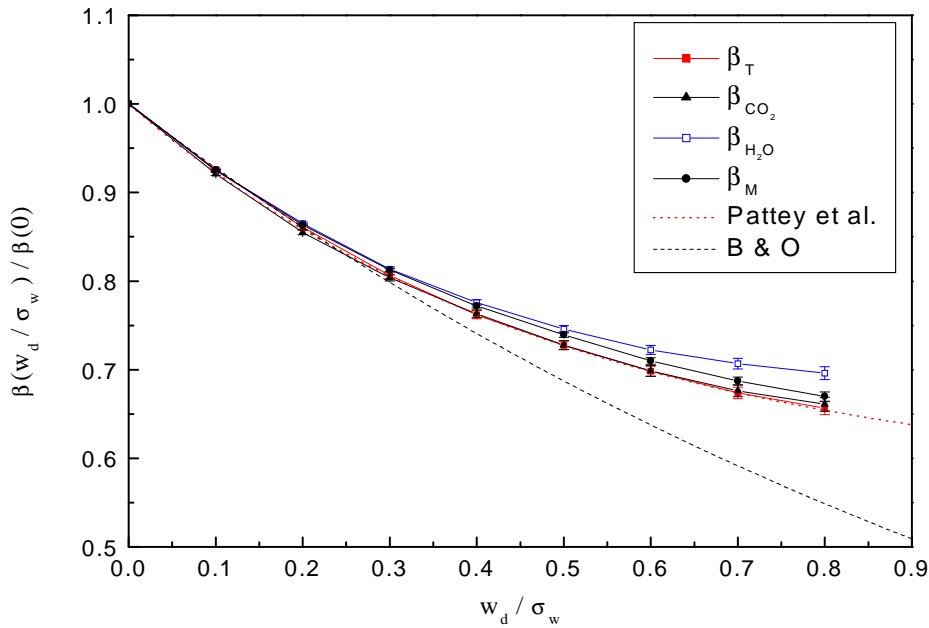

Figure 3.4: Dependence of the coefficient β on the deadband. β_T, β_{CO_2}, β_{H_2O} and β_M are obtained by simulating REA measurements on the data collected over a spruce forest in central Germany. The error bars represent one standard error of the mean. The dashed and dotted lines represent the empirical equations of *Businger and Oncley* (1990) and *Pattey et al.* (1993), respectively.

well with those predicted by the models of *Businger and Oncley* (1990) and *Pattey et al.* (1993). For higher w_d/σ_w, the values predicted by the model of *Pattey et al.* (1993) agree with the results of the simulation to 2 % for β_T, β_{CO_2}, and β_M, and to 6 % for β_{H_2O}. Large discrepancies exist between the simulated values and those predicted by the model of *Businger and Oncley* (1990).

The difference in the $\beta \sim w_d$ relationships might have been caused by different contributions of small eddies to the fluxes at the three sites. The slight deviation of β_{H_2O} from others for higher w_d/σ_w in *Figure 3.4* is not observed by *Businger and Oncley* (1990) and *Pattey et al.* (1993). At present, there is no convincing interpretation for that, nor is it known if such phenomenon also exists over other forest sites.

Effect of a Nonzero $\overline{w}$ on the Accuracy

In the derivation of *Equation 3.6*, the mean value of the vertical windspeed, $\overline{w}$, is assumed to be zero. However, a nonzero mean vertical windspeed, w_b, is often encountered due to uneven terrain, imperfect levelling of the sonic anemometer, or an offset in wind signals, etc. Such a bias in $\overline{w}$ may lead to erroneous sampling and hence to inaccuracies in REA flux measurements. Simulation studies show that β values are not very sensitive to this bias (*Businger and Oncley*, 1990; *Pattey et al.*, 1993). If $\frac{|w_b|}{\sigma_w}$ is smaller than 0.1, changes in β values are usually less than 5%. This conclusion is supported by data obtained in the present work. *Figure 3.5* shows the results from simulations with data collected over the spruce forest. On the average, the β values change less than 5 % for normalized bias $\frac{|w_b|}{\sigma_w}$ smaller than 0.2, which was the case in 70 % of the runs in this work. It is noticeable that the magnitude and direction of the changes in the β values are not necessarily the same for different quantities. For instance, β_T and β_{H_2O} change in opposite directions for a certain $\frac{w_b}{\sigma_w}$. Consequently, slightly different fluxes may be obtained by using β values for different quantities in the calculations. But this difference in the flux value is not usually significant due to the weak sensitivity of β to w_b.

Material Selection

The gas pathway of the REA sampler is composed of Teflon FEP tubes, Nylon unions, a Teflon membrane pump, stainless steel on/off valves, Teflon PTFE solenoid valves. The inertness of these materials ensures no loss or production of trace gases in the plumbing. The sample bags are made of Tedlar PVF film (T-TR-20-SG-4, 50 μm thick, Du Pont), which is as inert as
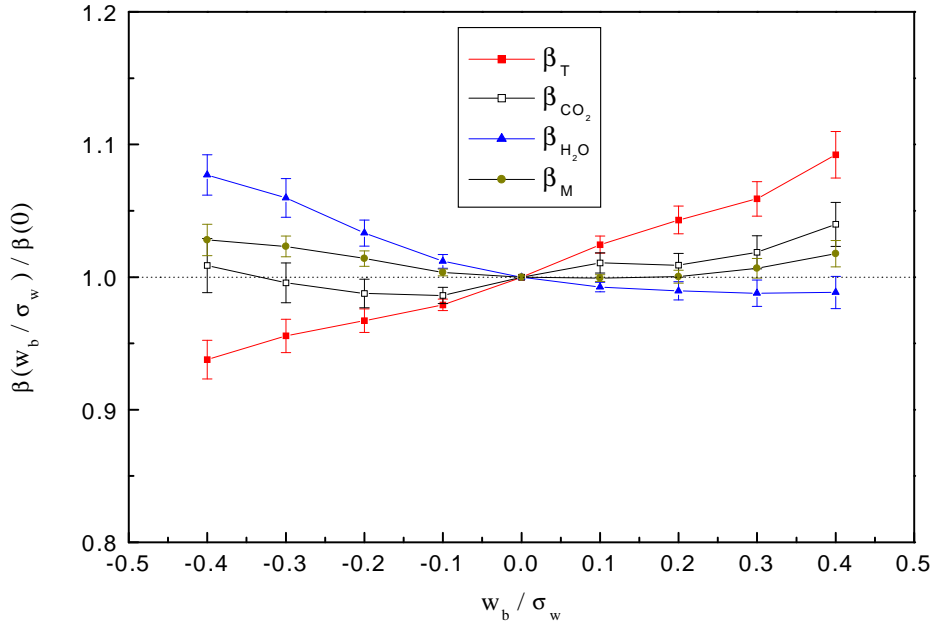
Figure 3.5: Influence of a bias in vertical wind on the coefficient β. The β_T, β_{CO_2}, β_{H_2O}, and β_M values were obtained by simulating REA measurements on the data collected over a spruce forest in central Germany. The error bars represent one standard error of the mean.

Teflon and less permeable and more tensile than Teflon. Tests with ambient air showed that samples can be stored in the Tedlar bags for more than 10 hours without significant changes in the COS and CS$_2$ contents. During field measurements, samples were usually analyzed within 3 hours after sampling.

3.2.4   Validation of the REA Sampler

To verify the reliability of the REA system, CO$_2$ fluxes were measured using the system (see *Section 3.3* for details). These measurements allow an intercomparison with those from EC measurements made by the Institute for Bioclimatology, University Göttingen. 94 pairs of CO$_2$ fluxes measured simultaneously by REA and EC techniques are plotted in *Figure 3.6*. Although there are some outliers, most of the data lie near the 1:1 line. The regression line indicates a slight overestimate of the CO$_2$ deposition flux by REA, but this overestimate is not significant, considering the standard errors of the intercept and the slope, 0.55 and 0.06, respectively. The 95% confidence belt covers the 1:1 line, suggesting reliable performance of this REA
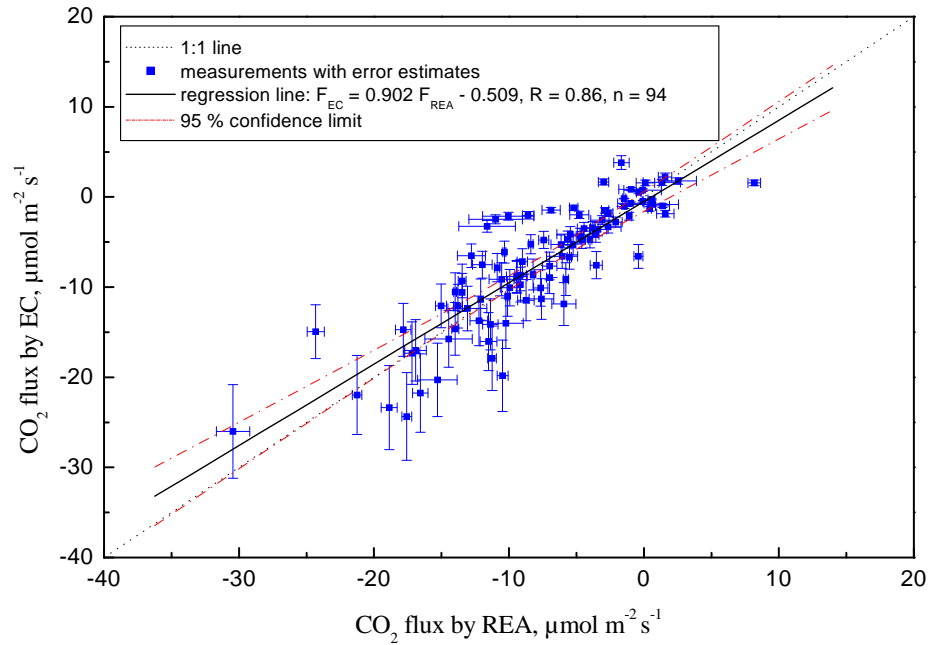
system under most conditions.

Figure 3.6: Intercomparison of the CO_2 fluxes obtained by REA to those from EC measurements.

3.3 Measurement

3.3.1 Site

Measurements were made on a plateau in the Solling Mountains, Germany (51° 46′ N, 9° 35′ E, 505 m a.s.l). The plateau extends about 1300 m and has a slight downward slope of 1° 20′ towards east. *Figure 3.7* shows an aerial picture of the site, taken on July 29, 1992 (from *Laubach et al.* (1994)). All REA flux measurements were taken from a meteorological tower of the Institute for Bioclimatology (IFB), University of Göttingen. The white arrow on the picture indicates the location of the tower.

The site is covered mainly by Norway Spruce (*Picea abies*, dark areas on the picture) planted in 1888, with a tree density of 461 trees ha^{-1} (*Ellenberg et al.*, 1986; *Ibrom et al.*, 1996). The average canopy height of the spruce stand is about 30 m and the leaf area index about 7. A beech stand (*Fagus sylvatica*, bright areas on the picture) with a canopy height of about 29
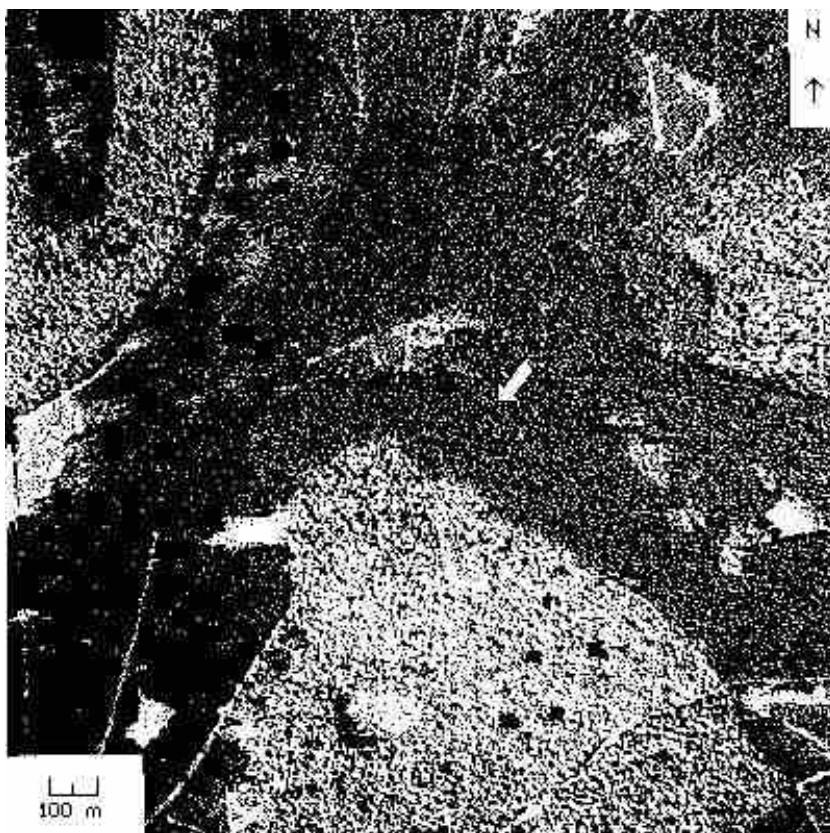
Figure 3.7: An aerial picture of the site at which REA measurements were conducted. Dark and bright areas are covered by spruce and beech trees, respectively. The white arrow indicates the location of the meteorological tower on which the experiments took place. (Courtesy: The Niedersächsische Forstliche Versuchsanstalt)

m is located south and southwest of the tower. The small bright triangle-shaped area located about 200 m northwest of the tower represents younger spruces of about 20 m height. There are some beech patches (small areas with medium brightness) to the southeast of the tower. If these beech patches are neglected, the spruce fetch extends 200-300 m in the south and southwest directions and up to 600-1500 m in other directions from the tower (*Ibrom et al.*, 1996).

Soils at the site are characterized as cambisol with a pH value of 3.5 (*Ellenberg et al.*, 1986). The soils are covered by a humus layer of 5 cm depth. Herbs, such as *Trientaliseuropea*, *Avenellaflexuosa*, *Galiumharcynium*, are the dominant ground plants. They cover 40% of the area. In addition, about 10% of the ground is covered by moss species, such as *Dicranella*

Figure 3.8: The meteorological tower from which air samples for REA measurements were collected. The sonic anemometer-thermometer is mounted at the height of 39 m, which is about 3 m higher than the 3rd platform from the top. (Courtesy: Martin Steinbacher)

heteromalla, *Polytrichum formosum*, etc.

The climate of the site is characterized as montane (sub-oceanic / subcontinental). The annual mean temperature is 6.6°C. The maximum and minimum monthly mean temperatures are approximately 18°C (July) and 4°C (February), respectively. The annual precipitation is about 1045 mm with relatively large interannual variations. There is no clear dry or wet season at the site. The prevailing wind direction is west to southwest.

The meteorological tower (*Figure 3.8*) has a horizontal size of 2.5×2.5 m^2 and a height of 52 m above the ground. Roughly two fifths of the tower is above the top of the canopy. In this work REA flux measurements were taken at 39 m above the ground, where CO_2, H_2O and heat fluxes were continuously measured by the IFB using the eddy correlation method. According to the calculations of *Laubach et al.* (1994), the zero-plane displacement (d) and the roughness length (z_0) for this site are 22.7 (± 0.7) m and 2.5 (± 0.1) m, respectively. As shown by a conservative estimate (*Morgenstern*, 1997), fluxes measured at altitudes above 33 m above the ground should represent the horizontally averaged surface flux.

The largest source area extent (or the footprint) of the Solling site, i.e., the maximum upwind distance from which the observed flux can originate, has been estimated by *Laubach et al.* (1994) and *Ibrom et al.* (1996). Based on the formulation of *Gash* (1986), *Laubach et al.* (1994) calculated the cumulative contribution Q_x of the source area extending from the observation point to the upwind distance x as

$$Q_x = Q \exp\left[-\frac{(z-d)\overline{U}}{u_* \kappa x}\right], \tag{3.13}$$

where Q is the flux density of a certain scalar, z is the observation height, d is the zero-plane displacement, $\overline{U}$ is the height-averaged constant wind speed, u_* is the friction velocity, and $\kappa = 0.4$ is the von Kármán constant. They parameterized $\frac{\overrightarrow{U}}{u_*}$ after *Schuepp et al.* (1990) in terms of the logarithmic wind profile for neutral stratification, i.e.,

$$\frac{\overline{U}}{u_*} = \frac{\ln\left[(z-d)/z_0\right] - 1 + \left[z_0/(z-d)\right]}{\kappa[1 - z_0/(z-d)]}, \tag{3.14}$$

where z_0 is the roughness length. For the measurement height of 39 m, as in the case of this work, they predicted that 80% of the flux originates from a distance of between 0 and 600 m under neutral conditions. *Ibrom et al.* (1996) used a different approach, suggested by *Wilson and Swaters* (1991), in which the influence of stability on the source area is taken into account. The maximal extent x_{max} of the source area is estimated by

$$x_{max} = \frac{\overline{U} z \Phi}{\kappa u_*}, \tag{3.15}$$

where Φ represents the stability function. They obtained a x_{max} ranging from 200 m during the daytime to 600 m during the night, using the empirical stability functions for scalar fluxes above forests as given by *Denmead and Bradley* (1985). Therefore, the fetch requirements are met for flux measurements during the daytime even in the worst case, i.e., southwest wind. Inhomogeneous fetch may be encountered during nocturnal measurements, which only account for 2% of flux measurements in this work.

3.3.2 Sampling

The REA system depicted in *Figure 3.1* was used for collecting updraft and downdraft samples at 39 m from the tower. Details of the REA sampler were described in *Section 3.2*.

The sampling period was 30 min. Because a deadband w_d (see *Section 3.2.3*) was used during the sampling, the effective sampling time was less than 30 min. To establish a suitable deadband, a test run (3-5 min) was made before each REA sampling. The turbulence intensity (σ_w), which was derived from the vertical wind data during the test run, was taken as a reference to select the value of w_d. w_d was usually less than $0.2\sigma_w$. The corresponding effective sampling periods were normally between 25 and 30 min.

Tedlar bags (9 L) were used as sample reservoirs. They were protected with polystyrene boxes, which on one hand prevented photochemical reactions in the samples and on the other hand could easily be transported.

Samples were analyzed for COS, CS_2 and CO_2 either in a small wooden house or a container near the tower or in a castle 20 km away from the site. Most of the samples were analyzed within 3 hour after sampling. The inertness of the Tedlar film ensures no loss or production of these trace gases in the bags before analyzing.

3.3.3   Analysis of COS and CS_2

COS and CS_2 were measured using a gas chromatograph (GC, HP 6890, Hewlett Packard) with a flame photometric detector (FPD, Tracor, USA). *Figure 3.9* shows the analyzing system schematically. It is composed of sample preparation, detection, and data acquisition parts. For determining the mixing ratios of COS and CS_2, sub-samples with a volume of 0.4-0.5 L were cryogenically focused (liquid Argon, -186°C) in a capillary glass trap (20 cm) filled with 2-3 cm silanized glasswool. To prevent the formation of ice in the glass trap, water vapor in the air samples was removed by passing the sample through a Nafion dryer (Perma Pure, KNF Neuberger, Germany). The Nafion membrane in the dryer allows water molecules in the moist air samples to permeate into the outer tube of the dryer, without affecting the contents of sulfur gases in the sample. The outer tube of the dryer was connected to a drying tube (Drierite, Cole Parmer) and a pump, as shown in *Figure 3.9*. Air in the outer tube was dried by circulating it in the direction against the sample flow, so that a large difference in water vapor between the inner (Nafion) and the outer tubes was maintained. This method for drying air samples has proved to be effective and economical.

Two glass traps were connected to a 8-way valve, so that one sample could be focused from the sample bag while the other sample was being analyzed. The sulfur compounds were separated on a $5' \times 1/8''$ Teflon column packed with Chromosil 310 (Supelco, Germany). Nitrogen (99.999%, Messer Griesheim, Germany) was used as a carrier gas. For optimal separation within a short time (4-5 min), a pressure program was used instead of the
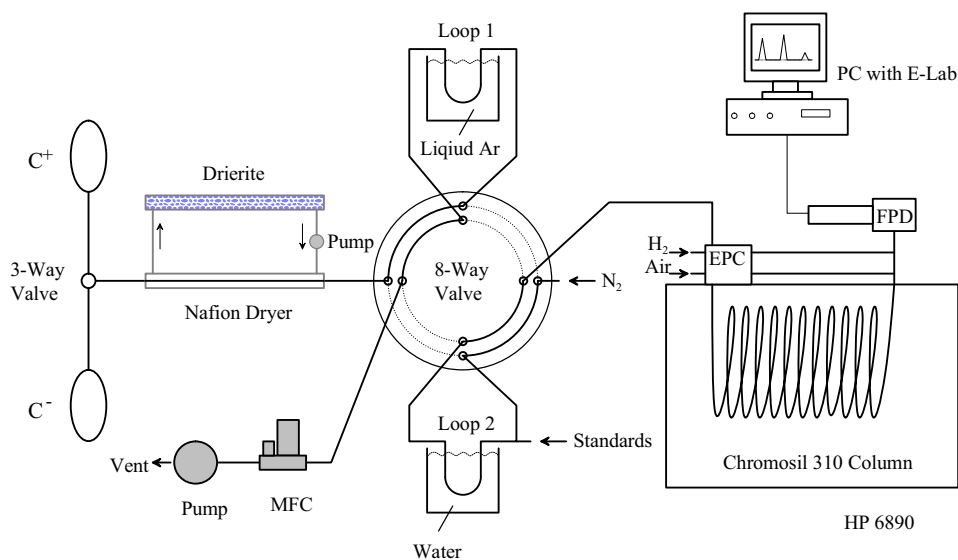
Figure 3.9: A system for the analysis of sulfur gases in air samples collected in Tedlar bags.

conventional temperature program. This was done by routinely changing the carrier gas pressure at the inlet of the column using the electronic pneumatic control (EPC) of the GC. The oven temperature was set to 30±0.1°C. A typical pressure program was: (1) starting at 280 kPa and holding for 0.1 min, (2) decreasing to 120 kPa at a rate of 240 kPa min^{-1} and holding for 2 min, and (3) increasing to 340 kPa at a rate of 1000 kPa min^{-1} and holding for 1.7 min. *Figure 3.10* shows a typical chromatogram for an air sample. COS, CS$_2$, H$_2$S, and the major trace gas CO$_2$ are well separated within 5 min by the Chromosil 310 column. Although the S-mode FPD is rather insensitive to CO$_2$, CO$_2$ can also be detected due to its high atmospheric mixing ratio, which is 6-7 orders of magnitude higher than that of the sulfur gases. Other sulfur compounds, such as SO$_2$, DMS, CH$_3$SH, etc., were not detected by the analysis procedure described here because of their small mixing ratio or the special character of the Chromosil 310 column. Each sample was analyzed at least 3 times to reduce the uncertainty of the measurement in determining amount of sulfur gases.

Analog signals from the FPD were converted by an E-Lab card (OMS-
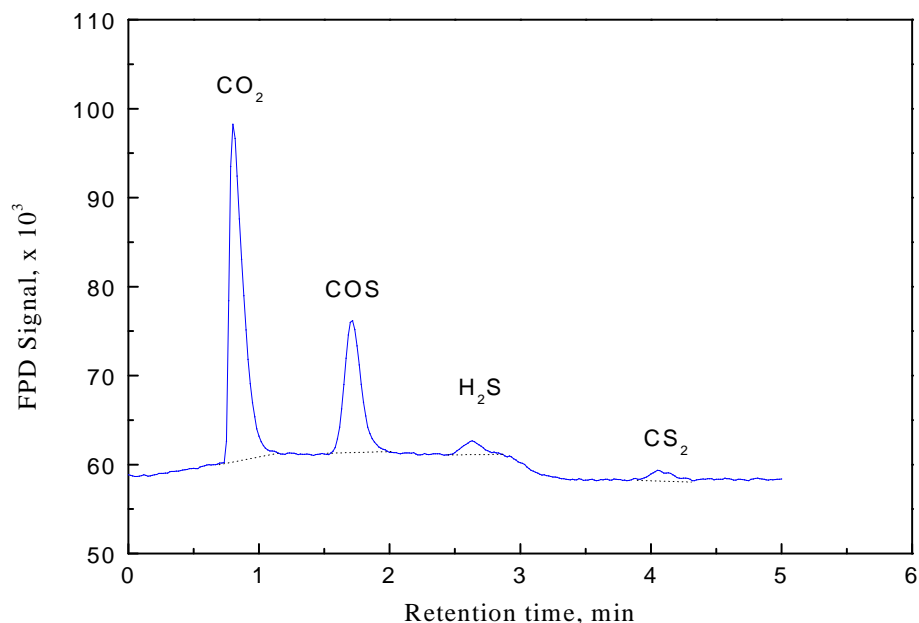
Figure 3.10: A typical air sample chromatogram obtained at the 30°C isothermal
condition using a pressure program for carrier gas. The program steps
were: (1) starting at 280 kPa and holding for 0.1 min, (2) decreasing
to 120 kPa at a rate of 240 kPa min^{-1} and holding for 2 min, and
(3) increasing to 340 kPa at a rate of 1000 kPa min^{-1} and holding
for 1.7 min.

Technology, USA) installed in a PC. Chromatograms were processed using
E-lab's companion software.

The GC/FPD system was calibrated daily by injecting standard samples
with a gas tight Teflon/glass syringe (Precision sampling Corp., USA). The
standard gas mixture (0.6-1 ppm COS and 0.1-0.25 ppm CS_2) was produced
by a permeation dilution device kept at 30±0.1°C (Haunold, Germany). To
determine the permeation rates, permeation tubes (VICI Metronics, USA)
were weighed every one or two months with an electronic balance (0.01 mg,
Sartorius, Switzerland). The permeation rates have a relative standard de-
viation of less than 10%, showing no significant temporal trend. Since no
measures were taken to avoid loss of H_2S during the sampling and analyzing,
as done by *Haunold et al.* (1989), the H_2S peak, which appeared in some of
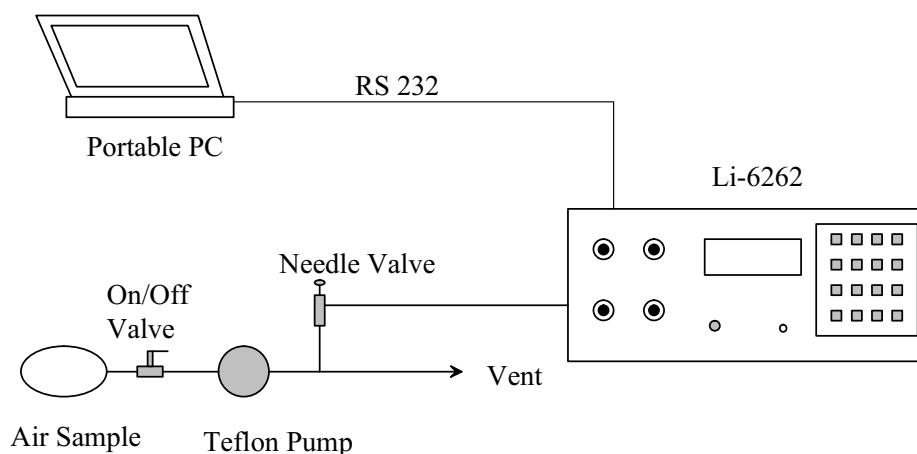the samples, was not quantified.

Figure 3.11: Method for analyzing CO$_2$ in REA samples using the Li-6262 infrared gas analyzer operated in absolute mode.

3.3.4   Analysis of CO$_2$

Most of the samples were also analyzed for CO$_2$, using a Li-6262 infrared CO$_2$ / H$_2$O analyzer (Li-COR, Nebraska, USA). *Figure 3.11* shows the way in which sample bags were connected to the analyzer. Since the Li-6262 was operated in absolute mode, no reference gas was needed. CO$_2$ and H$_2$O in the reference cell were removed by circulating air in the reference cell through an external scrubber filled with Soda Lime / desiccant (Mg(ClO$_4$)$_2$). Soda Lime and desiccant were changed roughly every 40 hours of operation. Pressure changes in the sample cell were measured by a pressure transducer (6262-03, Li-Cor). The Li-6262 was programed to automatically correct for the influence of pressure and H$_2$O fluctuations on CO$_2$ measurements due to dilution and pressure broadening.

During the measurements, air from the Tedlar bags was pumped through a T-connector and a needle valve into the sample cell of the Li-6262. The T-connector was used to vent water droplets formed in the pump's outlet. The air flow into the sample cell of the analyzer was adjusted to 0.3-0.4 L min^{-1} using the needle valve. After the sample cell was flushed with the air samples for roughly 2 min, CO$_2$ was measured statically at a frequency of 5

Hz. Only data from the steady period (0.5-1 min) were used for calculating the average mixing ratios. Each sample was measured at least 3 times.

The Li-6262 analyzer, which was purchased in 1998, was calibrated by the factory against NIST-traceable standards. No further factory calibration was made during this work. Slight zero and span drifts were corrected using working standards, which were calibrated against secondary standards at the Institute for Stratospheric Chemistry, Research Center Jülich, Germany.

3.3.5   Other In Situ Measurements

Continuous eddy correlation measurements of the CO_2, H_2O and heat fluxes as well as measurements of meteorological parameters were conducted by the IFB. Details about the instrumentation were described by *Laubach et al.* (1994) and *Ibrom et al.* (1996).

The EC measurements of the CO_2 and H_2O fluxes were made at 39 m above ground level, at which the REA measurements took place. The same sonic anemometer-thermometer (see *Section 3.2.2*) from Metek was used for the EC and REA measurements. The sensor of the instrument was mounted at the end of a metal bar of 2.5 m length, which was directed towards west, the prevailing wind direction. The CO_2 and H_2O mixing ratios at the height of the sonic sensor were continuously measured at 10 Hz using another infrared CO_2/H_2O analyzer of the same type (Li-6262) as used for measuring CO_2 in the REA samples. For these high frequency measurements, air from the position of the sonic sensor was drawn through a Teflon tube into the sample cell of the Li-6262. Damping of the concentration fluctuations in the tube is negligible (*Ibrom et al.*, 1996). An automatic daily two point calibration of the system was made for both CO_2 and H_2O using CO_2 calibration gases and a stable capacitive humidity sensor, respectively. More details about this EC system are given in *Ibrom et al.* (1996), *Schütz* (1996) and *Tworek* (1996).

3.3.6   Assessment of Errors

As discussed in *Section 3.2.1*, the turbulence flux of the trace gas c is calculated by

$$F_c = \beta \sigma_w (\overline{c^+} - \overline{c^-}) \equiv \beta \sigma_w \Delta C, \tag{3.16}$$

where β is a dimensionless coefficient, σ_w is the standard deviation of the vertical wind speed, $\overline{c^+}$ and $\overline{c^-}$ are the average concentrations associated with updrafts and downdrafts, respectively. The coefficient β is usually obtained by simulating REA flux measurements for sensible heat (or temperature), H_2O, etc.

According to the error propagation theory (see for example *Miller and Miller* (1993)), the relative systematic error in F_c is given by

$$\frac{\Delta F_c}{F_c} = \frac{\Delta \sigma_w}{\sigma_w} + \frac{\Delta \beta}{\beta} + \frac{\Delta(\overline{c^+} - \overline{c^-})}{\overline{c^+} - \overline{c^-}}, \qquad (3.17)$$

where ΔF_c, $\Delta \sigma_w$, $\Delta \beta$, and $\Delta(\overline{c^+} - \overline{c^-})$ are the absolute systematic errors in F_c, σ_w, β, and $(\overline{c^+} - \overline{c^-})$, respectively. Theoretically, the dimensionless coefficient β has no systematic error since any systematic errors in temperature and wind speed are cancelled out during the calculation using *Equation C.8*. In practice, there could be systematic errors associated with β, which are caused by using a deadband during the sampling and by a nonzero mean vertical windspeed. Although corrections for these errors were made in the flux calculations, there may still be a residual systematic error in β. But this error is estimated to be less than 5%. The relative systematic error in σ_w is estimated to be about 2%. According to *Equation C.25*, the relative systematic error in $(\overline{c^+} - \overline{c^-})$ equals to that in the sample volume, which is smaller than 3%. Therefore, the accuracy for the flux measurements is estimated to be better than 10%.

The relative random error in F_c is given by

$$\frac{\delta_{F_c}}{F_c} = \sqrt{\left(\frac{\delta_{\sigma_w}}{\sigma_w}\right)^2 + \left(\frac{\delta_\beta}{\beta}\right)^2 + \left(\frac{\delta_{\Delta C}}{\Delta C}\right)^2}, \qquad (3.18)$$

where δ_{F_c}, δ_{σ_w}, δ_β, and $\delta_{\Delta C}$ are the absolute random errors in F_c, σ_w, β, and ΔC, respectively. Methods for estimating δ_{σ_w}, δ_β, and $\delta_{\Delta C}$ are described in *Appendix C*.

Among the three error sources in the right-hand side of *Equation 3.18*, $\frac{\delta_{\Delta C}}{\Delta C}$ is normally the dominant one. Because of the relatively small $|\Delta C|$ values, and the less perfect precision in the GC measurements of COS and CS$_2$, $\frac{\delta_{\Delta C}}{\Delta C}$ was as large as 10-100% in most REA runs, and even larger than 1000% in a few extreme cases, when the fluxes (or the $|\Delta C|$ values) were close to zero. Consequently, with a few exceptions, random errors in σ_w and β make only negligible contributions to the overall precision for the calculated COS and CS$_2$ fluxes.

CO$_2$ could be measured at higher precision, so that, in spite of the small differences in the CO$_2$ concentrations associated with downdrafts and updrafts, the relative random error in ΔC for CO$_2$ was smaller than 10% in most cases, which was about the same order of the magnitude as the relative random errors in σ_w and β.

3.4 Results and Discussion

3.4.1 COS and CS$_2$ Exchange Fluxes

Six campaigns of 10 to 15 days were conducted in August and September of 1997, in September of 1998, and in May, July and September-October of 1999, respectively. *Table 3.1* summarizes the results of the REA measurements of the COS and CS$_2$ fluxes from all these campaigns.

Table 3.1: Statistics of the COS and CS$_2$ fluxes observed over a spruce forest in the Solling Mountains, Germany.

	F_{COS} (pmol m^{-2} s^{-1})			F_{CS_2} (pmol m^{-2} s^{-1})		
	n	mean$\pm\sigma$	range	n	mean$\pm\sigma$	range
All	154	-93$\pm$11.7	-497$\sim$311	154	-18$\pm$7.6	-305$\sim$236
Deposition	110	-163$\pm$9.7	-497$\sim$-0.03	89	-73$\pm$7.7	-305$\sim$-0.07
Emission	44	81$\pm$11.1	0.03$\sim$311	65	57$\pm$7.6	1.7$\sim$236

The observed COS and CS$_2$ fluxes varied in the range of -497$\sim$311 pmol m^{-2} s^{-1} and -305$\sim$236 pmol m^{-2} s^{-1}, respectively. The exchange of both gases between the atmosphere and the forest is bidirectional, in other words, the spruce forest can both take up and emit COS and CS$_2$. The uptake of both gases occurred mainly during the sunlit period, whereas emission was observed mostly at night (see *Section 3.4.3* for details). *Table 3.1* also shows the statistics of the COS and CS$_2$ fluxes for the cases of deposition and emission, respectively. More than 70% of the measurements indicate the uptake of COS by the forest ecosystem. Nearly 60% of the measurements also show deposition of CS$_2$ to the forest. Overall, the forest is a sink for atmospheric COS and CS$_2$.

To account for the contributions of soils at the site to the exchanges of COS and CS$_2$ between the forest and the atmosphere, air-soil exchanges of both gases were measured in July, August, and September-October of 1999 using dynamic chambers, which were swept with ambient air. Details about these measurements are given in *Steinbacher* (2000). Data from this study show that soils at the site always act as a sink for atmospheric COS, but the soil sink, averaged 0.81$\pm$0.24 pmol m^{-2} s^{-1}, only accounts for less than 1% of the mean deposition of COS into the ecosystem, as observed in the REA measurements. More than 99% of the observed uptake of COS was caused by the trees.

The air-soil exchange of CS$_2$ was found to be bidirectional. As in the case of COS, the observed CS$_2$ flux, ranging from -0.11 pmol m^{-2} s^{-1} to 0.23 pmol

Table 3.2: COS and CS$_2$ deposition velocities over different plant species, calculated on the basis of the leaf area.

Plant	V_d, COS mm s^{-1}	V_d, CS$_2$ mm s^{-1}	PAR μE m^{-2} s^{-1}	Method	Reference
Spruce	1.1±0.68[a]	5.4±5.9	0-930	REA, in situ	This study
Spruce	0-0.6	0-1.5	0-350	Chamber, in situ	Huber (1994)
Grass	16-48[b]		135-1644	Gradient, in situ	Bartell et al. (1993)
Quercus agrifolia	0-0.57		0-200	Chamber, in situ	Kuhn (1997)
Rapeseed	1.34				
Corn	0.69		100-800	Chamber, laboratory	Kesselmeier and Merk (1993)
Corn	1.1				
Soybean	0.7		40-600	Chamber, laboratory	Goldan et al. (1988)
Wheat	1.5				
Alfalfa	1.6				
Various vegetables	0.50				
Lettuce	0.28		350	Chamber, laboratory	Kluczewski et al. (1985)[c]
Ryegrass	0.77				
P. vulgaris	1.4	0.6			
G. max	3.1	1.2	400	Chamber, laboratory	Taylor et al. (1983)[d]
L. esculentum	0.4	0.2			

[a]Emission fluxes were not considered in the calculations.
[b]Based on the ground area. The ambient COS level was between 0.5 to 3.6 ppb.
[c]4ppb COS used
[d]120ppb COS used

m^{-2} s^{-1}, is also negligible compared to the exchange flux of CS$_2$ between the forest and the atmosphere.

For the purpose of comparison, the values of the observed deposition fluxes of COS and CS$_2$ were converted to deposition velocities based on the leaf area, using the relation

$$V_d = \frac{F}{LAI \cdot [C]}, \tag{3.19}$$

where V_d is the deposition velocity, F is the uptake flux, $LAI(=7)$ is the leaf area index of the studied site, and $[C]$ is the mean mixing ratio of COS or CS$_2$ during a certain REA measurement. *Table 3.2* lists the mean deposition velocities and their standard deviations together with those reported by other authors. The mean deposition velocity for COS found during this study is around 1 mm s^{-1}. This agrees well with those obtained in other studies, although quite different plant species were investigated in most of these studies. It is interesting to note the reasonable agreement between the laboratory studies and the in situ experiments.

Only four values of the deposition velocity of CS$_2$ have been reported by other researchers. These values are several factors to one order of magnitude smaller than the one obtained in this work.

3.4.2 Seasonal Variations in the COS and CS$_2$ Fluxes

Field experiments covered the seasons of spring, summer and fall. Because of unsuitable weather conditions (cold, snow coverage, etc.), no field experiment was carried out in the winter months.

Table 3.3 lists statistical data for the REA measurements of the COS and CS$_2$ fluxes in different seasons and years. Data for the CO$_2$ fluxes, photosynthetically active radiation (PAR) and air temperature are also presented in this table.

PAR and air temperature were influenced by the synoptic situation during the campaigns, in addition to seasonal variations of the local climate. The campaigns in 1997 were dominated by sunny days. Weather during the campaigns in September of 1998 and in May and July of 1999 can be characterized as partially sunny and partially cloudy or overcast with little precipitation. During the last campaign, i.e., September-October of 1999, it was rainy, so that measurements during this campaign were mainly done between intermittent showers. It even showered or drizzled during some measurements during this campaign.

Figure 3.12 shows the seasonal variations in the air-plant exchange fluxes of COS, CS$_2$ and CO$_2$. Although COS emission was sometimes observed, the

Table 3.3: REA measurements of COS, CS$_2$ and CO$_2$ fluxes over a spruce forest in Solling, Germany. Mean values and standard errors of the mean are listed for the individual campaigns.

Time	F_{COS} pmol m^{-2} s^{-1}	F_{CS_2} pmol m^{-2} s^{-1}	F_{CO_2} μmol m^{-2} s^{-1}	PAR^a μE m^{-2} s^{-1}	T^a °C
Aug., 1997	-105±47	-44±37	no data	568±101	22
Sept., 1997	-173±51	-17±8	no data	428±87	14
Sept., 1998	-43±27	-32±20	-5.98±0.81	290±40	12
May, 1999	-93±32	1±20	-10.2±1.4	520±75	13
July, 1999	-88±19	5±9	-9.29±1.03	550±44	18
Sept./Oct., 1999	-105±23	-36±19	-5.06±1.26	156±23	10

^{a}Considering only data during the REA measurements
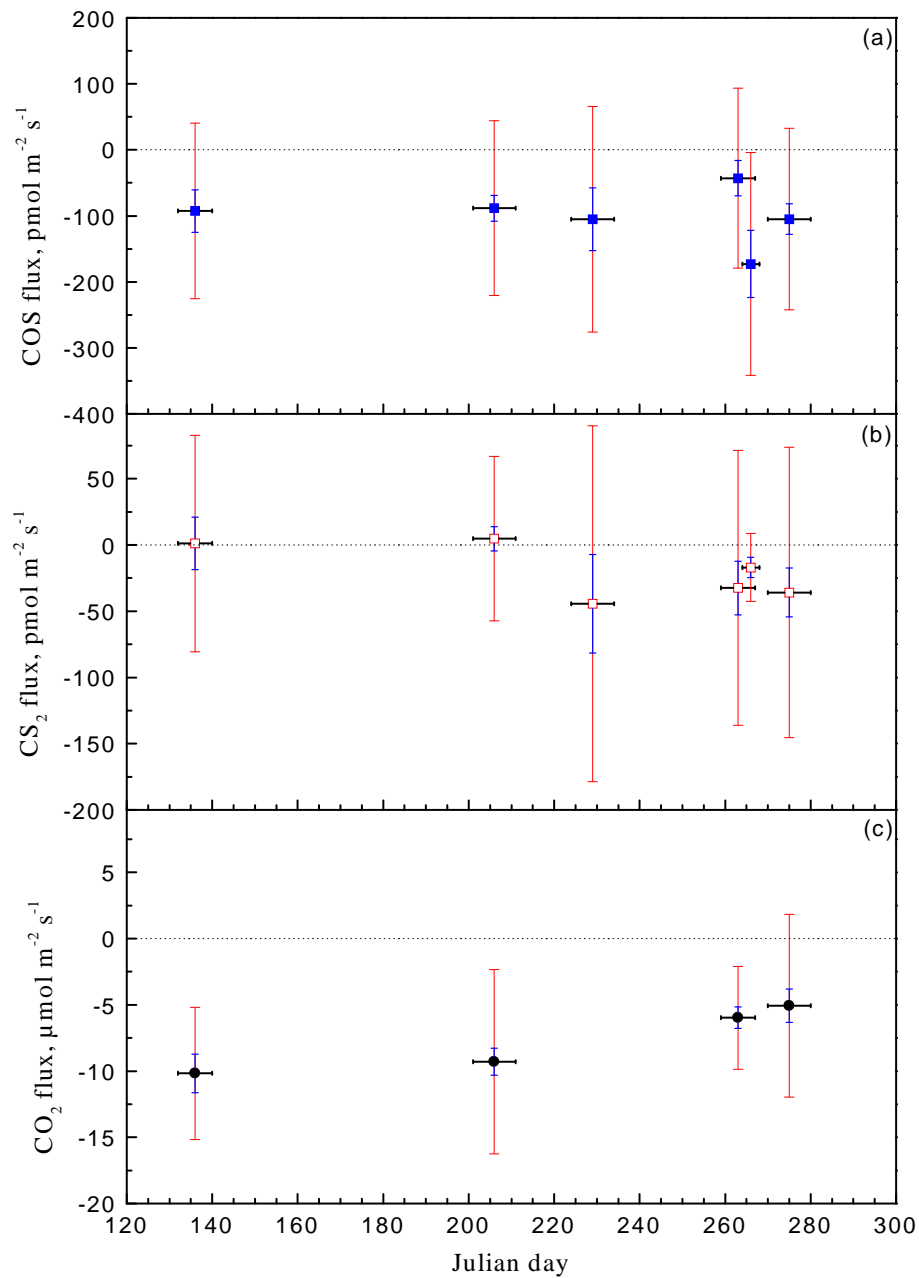
Figure 3.12: Seasonal variations in the air-plant exchange fluxes of COS (a), CS$_2$ (b) and CO$_2$ (c) over a spruce forest in Solling Mountains, Germany. The short and long vertical bars indicate standard errors of mean values and standard deviations, respectively. The horizontal bars indicate the measurement periods of the campaigns.

average flux indicates that COS was taken up by the forest in all the seasons studied. The largest COS deposition was observed in September of 1997, the smallest in September of 1998. There is no clear seasonal trend of the COS flux for its large year-to-year fluctuation in the fall. CS$_2$ data (*Figure 3.12(b)*) show a net deposition in August, September and October and a minor, but insignificant net emission in May and July. As expected, the CO$_2$ flux has a clear seasonal variation. Larger CO$_2$ deposition was observed in later spring and in summer, smaller in fall. This seasonal trend is consistent with that obtained by continuous measurements at the same site (*Ibrom et al.*, 1996).

3.4.3   Diurnal Variations in the COS and CS$_2$ Fluxes

Because of the high variability of the COS and CS$_2$ fluxes and the small number of measurements which could be done on a certain day, it is difficult to find potential diurnal cycles for the COS and CS$_2$ fluxes on the basis of data for individual observational days. Such data do not always show any common features. Some daily profiles are even contradictory. However, the average diurnal variations, presented in *Figure 3.13*, clearly indicate the systematic features of the fluxes of COS and CS$_2$, as well as of CO$_2$. It can be seen in this figure that the uptake of COS and CS$_2$ by the forest occurs during the sunlit hours and that the release of these gases by the forest takes place during the rest of the day, as is clearly the case for the exchange of CO$_2$ between the atmosphere and the forest. The highest deposition of both sulfur gases occurs around local noon, i.e., the period with the most intense solar radiation and the strongest turbulence. The similar diurnal features for COS and CO$_2$ indicate the existence of a common uptake pathway, i.e., the open stomata, as suggested by *Goldan et al.* (1988). The change of stomatal aperture, which is controlled by various environmental factors, such as the light intensity, water stress, etc., may cause the diurnal cycles of the COS and CS$_2$ fluxes, as it does for the CO$_2$ flux. This is supported by the correlations shown in the following sections.

3.4.4   Correlations of the COS and CS$_2$ Fluxes to PAR and to the H$_2$O Flux

Figures 3.14 and *3.15* show the relationships of the COS and CS$_2$ fluxes to PAR and to the H$_2$O flux, respectively. The correlation coefficients in *Figures 3.14(a)* and *3.15(a)* indicate that the COS flux is significantly ($\alpha < 0.01$) correlated both to PAR and to the H$_2$O flux. The CS$_2$ flux also appears to be correlated to PAR and the H$_2$O flux, however, the correlations to
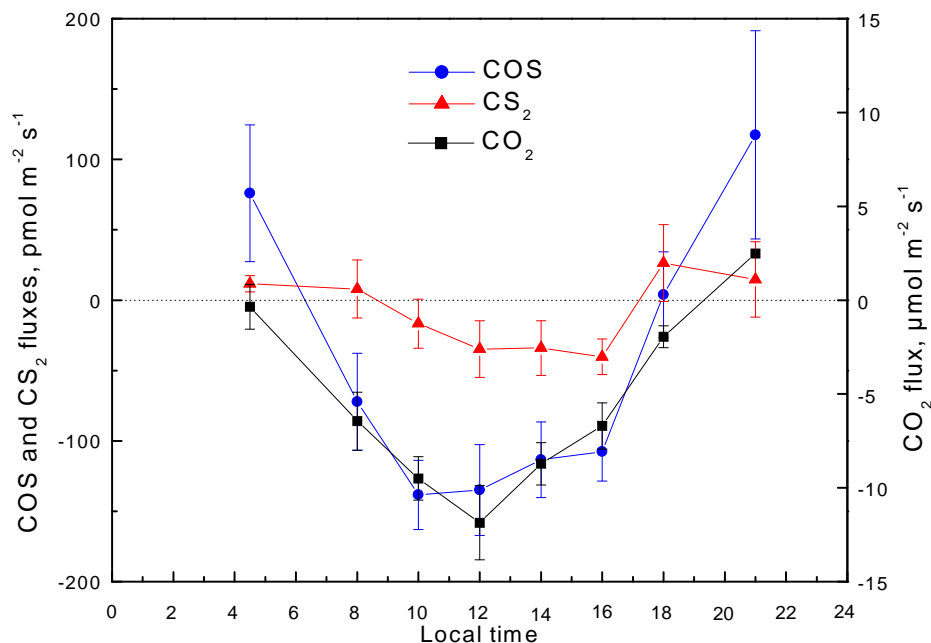
Figure 3.13: Average diurnal variation in the COS, CS_2 and CO_2 fluxes. The error
bars indicate standard errors of the mean.

both quantities are only significant at confidence levels of 75% and 87%,
respectively.

As implied by the slopes of the regression lines in *Figures 3.14* and *3.15*,
the uptake of COS and CS_2 increases with increasing PAR and H_2O flux.
This may be a result of physiological regulation through stomatal aperture,
which is related to both PAR and the H_2O flux. If PAR is higher, the trees
tend to take up more COS and CS_2 and release more water vapor because of
decreased stomatal resistance.

The data presented here suggest that CS_2 seems to be taken up through
the same pathway as COS and CO_2, i.e., through the open stomata of higher
plants. However, this suggestion should be treated with caution, not only
because of the lower significance of the correlations between the CS_2 flux
and PAR and the H_2O flux, but also because of the possibility that other
processes may cause the slight correlation. There is no known enzymological
interpretation to the uptake of CS_2 by plants. *Hofmann* (1993) postulated
that vegetation might be an indirect rather than a direct sink of atmospheric
CS_2. This author suggested that CS_2 is transported into the canopy, and has
a chemical sink close to the surface, which oxidizes CS_2 to COS. This COS
is then removed by vegetation. The major oxidant for CS_2, the OH radical,
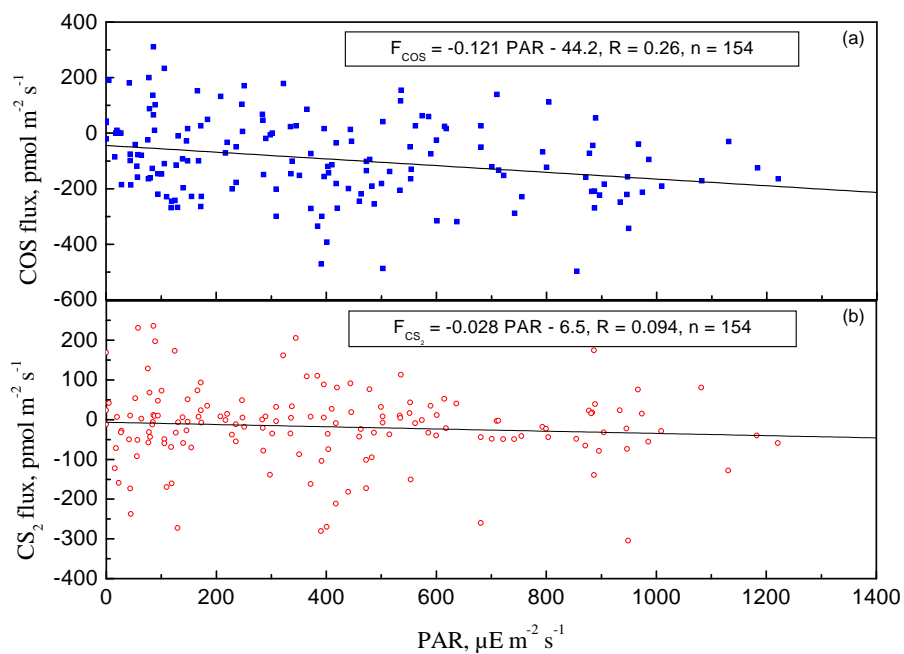
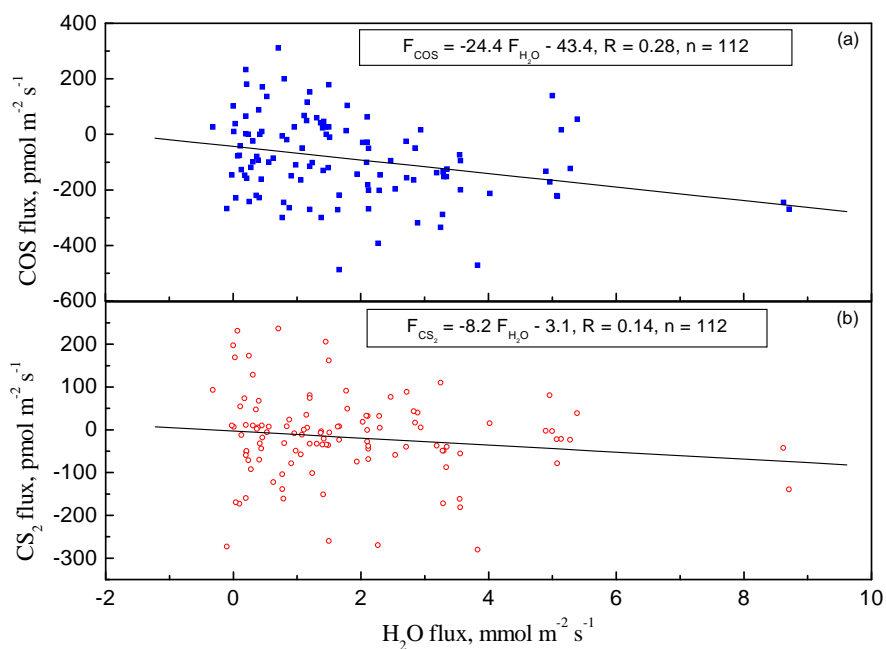*Figure 3.14:* Correlations between the COS and CS$_2$ fluxes and PAR.

Figure 3.15: Correlations between the COS and CS$_2$ fluxes and the H$_2$O flux.

might be produced in the vicinity of plants by reactions of ozone with reactive alkenes emitted by the plants. This postulation can qualitatively explain the observed CS_2 deposition to plants and the correlations between the CS_2 flux and PAR and the H_2O flux, but it needs to be tested by appropriate experiments and simulations. If such an indirect vegetation sink of CS_2 were confirmed, the consequence would be that vegetation is able to take up more COS than the COS fluxes observed.

Although the correlations in *Figures 3.14* and *3.15* show plausible relationships between gas fluxes and physiological parameters, they are not suitable for parameterization purposes since the correlations capture only a very small fraction ($< 10\%$) of the variance.

3.4.5 Correlation of the COS Flux to the CO_2 Flux

Laboratory studies show that COS is consumed by plants in nearly the same way as CO_2, after being split by the key enzyme, CA (*Protoschill-Krebs and Kesselmeier*, 1992; *Protoschill-Krebs et al.*, 1995, 1996). This finding not only reveals the physiological background of the uptake of COS by higher plants, but also implies the possibility of extrapolating measurements to obtain the global COS deposition to vegetation, using the ratio of the COS uptake to CO_2 assimilation and the global CO_2 fixation, which is better quantified. Measurements in this work support this idea. *Figure 3.16* shows that the COS and CO_2 fluxes are positively correlated at the 99% confidence level. Although the data points are relatively scattered, the correlation line is well defined, as indicated by the dotted lines which represent the 95% confidence belt of the regression line.

There is a certain correlation between the CS_2 and CO_2 fluxes, too. However, the correlation (with a confidence level of 90%) is not as significant as that between the COS and CO_2 fluxes.

The regression line in *Figure 3.16* contains a small intercept (-19.6 pmol m^{-2} s^{-1}). Both the intercept and the origin lie in the 95% confidence belt, suggesting that the deviation of this intercept from the origin is not significant. This is consistent with the idea that both COS and CO_2 are taken up by vegetation through a common pathway, i.e., the open stomata. On the other hand, since the soils at the site are a permanent source of CO_2 and a minor sink of COS, it is to be expected that a small negative intercept should exist.

The slope (10.0 with a standard deviation of 1.7) of the regression line in *Figure 3.16* can be considered as a representative value for the uptake ratio COS/CO_2. Such uptake ratio were also investigated in several laboratory, as well as in situ, studies (*Hofmann*, 1993; *Kesselmeier and Merk*, 1993;
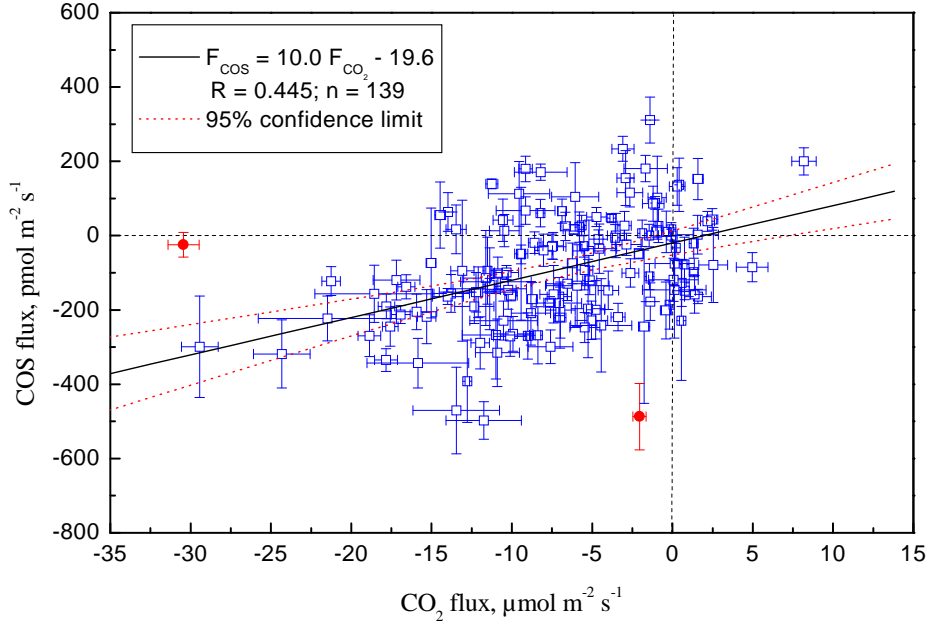
Figure 3.16: Correlation between the COS and CO$_2$ fluxes. The vertical and horizontal bars present the estimated errors of the observed COS and CO$_2$ fluxes. The two outliers marked with filled circles were not included in the regression since the results are too sensitive to them.

Kesselmeier et al., 1993; *Velmeke*, 1993; *Huber*, 1994; *Kuhn*, 1997). *Table 3.4* lists various values of the uptake ratio which were reported in these articles, along with the one obtained in this work. The values in *Table 3.4* show large differences between the plants studied. In addition to this work, there are two studies dealing with spruce trees. *Hofmann* (1993) and *Huber* (1994) measured exchanges of COS and CO$_2$ between the atmosphere and a spruce forest (80 years) in Schachtenau (Nationalpark Bayerischer Wald), Germany, using the gradient and chamber methods, respectively. The uptake ratio obtained in this work agrees well with the one derived from the measurements of *Huber* (1994) within bounds of the uncertainty, but is about one order of magnitude higher than the one derived from the measurements of *Hofmann* (1993). When compared with the other uptake ratios listed in *Table 3.4*, the uptake ratio from this work falls roughly in the middle of the values reported.

Table 3.4: Measurements of the uptake of COS by different plants in relation to CO_2 assimilation.

Plant	COS/CO_2, pmol μmol^{-1}	Method	Reference
Spruce	10.0±1.7	REA, in situ	This work
Spruce	11.7±4.8	Chamber, in situ	Huber (1994)
Quercus agrifolia	2.2	Chamber, in situ	Kuhn (1997)
Spruce	0.8±0.1	Gradient, in situ	
Wheat	5.7±1.0		Hofmann (1993)
Corn	11.2±3.8	Chamber, in situ	
Pea	6.2±2.1		
Pea	0.3-4.2		Kesselmeier and Merk (1993)
Rapeseed	0.9-1.4	Chamber, laboratory	
Corn	1.9-16.7		
Sacoglottis gabonensis	14.4(0.8-38.4)	Chamber, in situ	Kesselmeier et al. (1993)
Porterandia cladantha	1.7(0.14-6.0)		
Querscus petrea	2.2	Chamber, laboratory	Velmeke (1993)
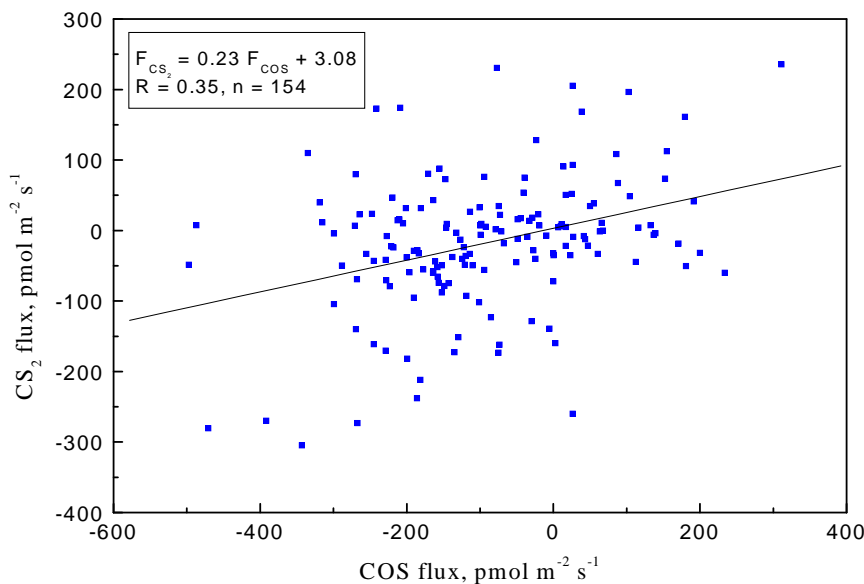
Figure 3.17: Correlation between the COS flux and the CS$_2$ flux.

3.4.6   Correlation of the COS Flux to the CS$_2$ Flux

Figure 3.17 plots the CS$_2$ flux against the simultaneously measured COS flux. A linear regression indicates that the fluxes of both gases are highly significantly ($\alpha < 0.0001$) correlated. As discussed in *Section 3.4.4*, CS$_2$ may be directly or indirectly taken up by trees. No matter which of the two cases is true, a correlation between the COS and CS$_2$ fluxes can be expected since both the uptake pathway for the gases (stomata) and the photochemical removal of CS$_2$ are closely related to a common factor, i.e., the intensity of solar radiation.

If the small intercept of the regression line in *Figure 3.17* is neglected and the slope taken as an uptake ratio, COS/CS$_2$, one can say that COS and CS$_2$ are taken up by trees at roughly a ratio of 5:1.

3.4.7   Relationship between Ambient Concentrations and Fluxes

The COS and CS$_2$ fluxes appear to also be correlated to the ambient mixing ratios of COS and CS$_2$, respectively (*Figure 3.18*), in addition to their correlation to PAR, the H$_2$O and CO$_2$ fluxes. Such a flux-concentration correlation for COS was also observed during the cuvette experiments by

Kesselmeier and Merk (1993) and *Huber* (1994). Since the fluxes measured under natural conditions are subject to the influence from many factors, the relationship between exchange flux and ambient concentration is not as clear as that observed under laboratory conditions. The correlations in *Figures 3.18* capture only a very small fraction of the variance. Influences of other factors on the COS and CS_2 fluxes are much larger. Nevertheless, the correlations in *Figures 3.18(a)* and *3.18(b)* are statistically significant at the confidence levels of 99% and 85%, respectively. A compensation point, i.e., the point of zero net exchange, can be derived from each regression line. The compensation points for COS and CS_2 are 300±51 ppt and 24±15 ppt, respectively. It should be pointed out that the correlation in *Figure 3.18(b)* strongly depends on the data points with mixing ratios of higher than 100 ppt. If these points are not included in the statistics, the correlation disappears. Therefore, the compensation point for CS_2 should be viewed with caution.

For the purpose of comparison, various compensation points for different plant species are listed in *Table 3.5*. The data reported by *Huber* (1994) for spruce and wheat show that the compensation points of COS depend on both the vegetation type and the growth stage of a certain plant. The compensation point of COS for elder spruce is lower than that for younger spruce. In the case of wheat, the situation is reversed. There seems no substantial difference in the compensation point of CS_2 between the growth stages of the plants. In most cases, the compensation point of COS is lower than its atmospheric mixing ratio ($\sim$500 ppt). This suggests that vegetation should be a permanent sink of COS. However, COS emission has often been observed under natural atmospheric conditions. Therefore, other factors (such as the radiation intensity, plant physiological processes, etc.) also appear important in reversing the direction of the COS exchange between vegetation and the atmosphere.

The CA catalyzed hydrolysis of COS in plant leaves can explain the deposition of COS to plants, but not the emission of COS from plants. Cuvette experiments on various deciduous trees showed that COS was emitted from leafless twigs and taken up leafy twigs (*Velmeke*, 1993). This may at least partially explain the observed COS emission from the plants. The actual processes leading to the production of COS by the twigs are not clear. Nor is it clear, whether or not there are any mechanisms that produce COS in the leaves.

During early chamber measurements using sulfur-free air as a sweep gas, only the emission of CS_2 from plants was observed (*Goldan et al.*, 1987; *Fall et al.*, 1988; *Hines and Morrison*, 1992). However, both emission and deposition of CS_2 were observed in more recent cuvette measurements with
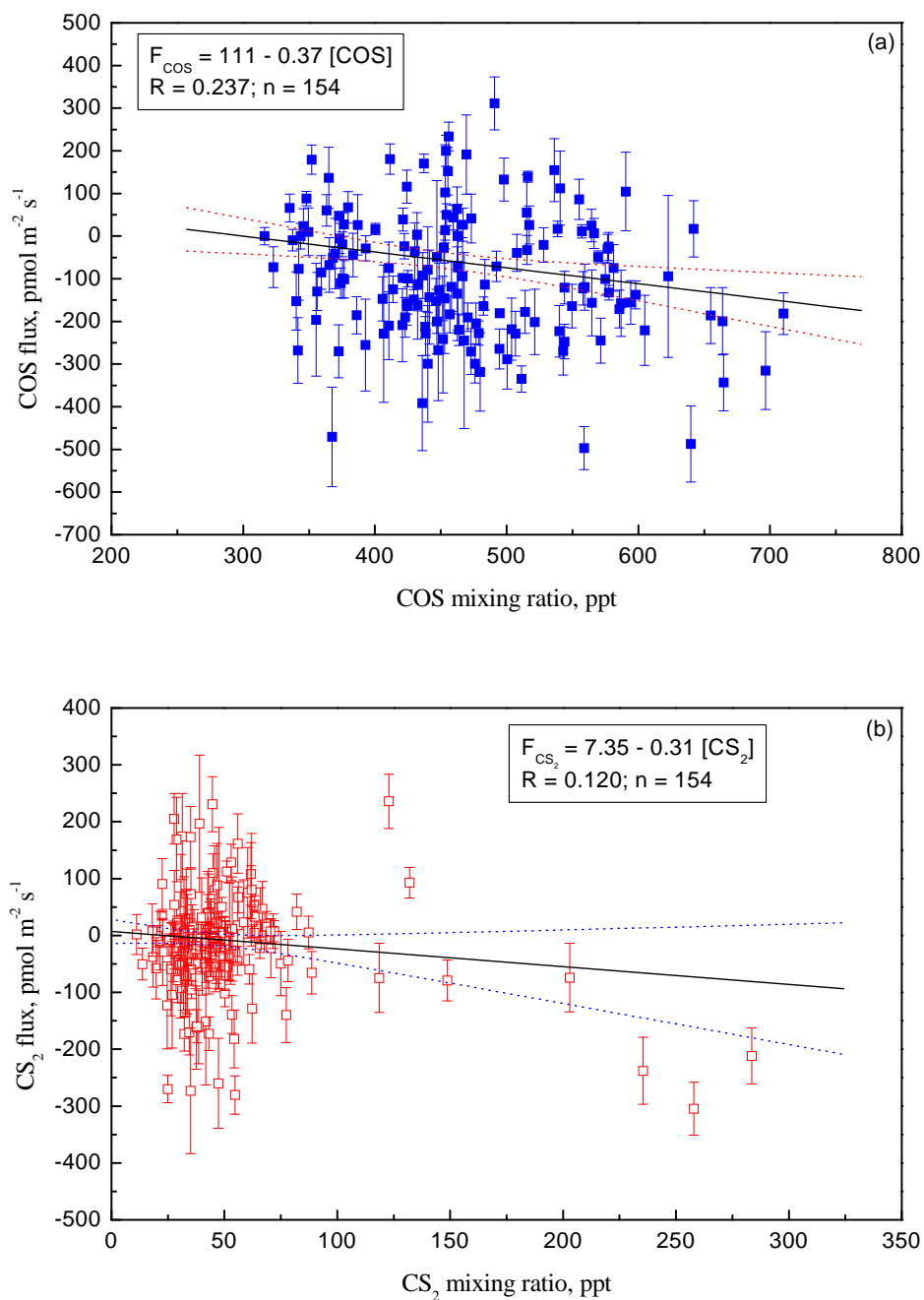
Figure 3.18: Relationship between the ambient concentrations and the fluxes of COS (a) and CS$_2$ (b). The vertical bars present the estimated errors. The regression is obtained using the errors as weighting factors.

Table 3.5: Compensation points for the exchange of COS and CS_2 between the atmosphere and different plants.

Plant	COS, ppt	CS_2, ppt	Method	Reference
Spruce (110 years)	300±51	24±15	REA, in situ	This work
Spruce (80 years)	124	6		
Spruce (10 years)	399-515	2.4-3.4	Chamber, in situ	*Huber* (1994)
Wheat (G.S. 31)[a]	115	23		
Wheat (G.S. 75-85)[a]	518	28		
Corn (3-4 weeks)	144 (0-328)		Chamber, laboratory	*Kesselmeier and Merk* (1993)
Rapeseed (4-6 weeks)	90 (57-135)			

[a]Growth stage according to *Lancashire et al.* (1991)

different plants (*Hofmann*, 1993; *Kesselmeier et al.*, 1993; *Huber*, 1994), as they were in this work. At present, we have hardly any knowledge about the processes controlling the air-plant exchange of CS$_2$.

3.4.8   Global Vegetation Sinks of COS and CS$_2$

One of the intentions of the simultaneous measurement of the COS and CO$_2$ fluxes over vegetation was to obtain a global estimate of the vegetation sink of atmospheric COS by extrapolating the quantitative relationship between COS uptake and CO$_2$ fixation which was derived from the flux measurements. Obviously, this extrapolation will have a rather small uncertainty if there is a good correlation between the fluxes of both gases. As shown in *Section 3.4.5*, such a correlation was obtained for the spruce forest studied in this work. Measurements over a 80 year spruce stand in Bavaria using the gradient method (*Hofmann*, 1993) and the cuvette method (*Huber*, 1994) also showed a significant correlation between the COS and CO$_2$ fluxes. However, such a correlation was not found during cuvette experiments on young (10 years) spruce trees (*Huber*, 1994). A poor correlation between the COS exchange und the CO$_2$ assimilation was found by *Kesselmeier et al.* (1993) during field experiments on tropical plants (*Poterandia cladantha* and *Saccoglottis gabonensis*), while a good correlation was observed by *Kuhn* (1997) during experiments on a temperate plant (*Quercus agrifolia*). Laboratory studies on agricultural plants (wheat, corn, rapeseed and pea) showed a certain correlation of the COS uptake to the CO$_2$ assimilation (*Hofmann*, 1993; *Kesselmeier and Merk*, 1993), while no relationship between COS and CO$_2$ exchanges was observed over a wheat field (*Hofmann*, 1993). These inconsistent results indicate the uncertainty in estimates of the COS vegetation sink based on the extrapolation mentioned above. Nevertheless, it is worthwhile to use this extrapolation method until better methods become available. Based on the uptake ratio COS/CO$_2$ of 10.0±1.7 pmol μmol^{-1} obtained in this work and the recent estimate of the terrestrial net primary production (NPP) of about 45±5 Pg C yr^{-1} (or 90 Pg dry matter yr^{-1}) from *Matthews* (1997)[1], the global vegetation sink is estimated to be 2.3±0.5 Tg COS yr^{-1}. This value lies within the ranges 2-5 Tg COS yr^{-1} and 1-3.4 Tg COS yr^{-1} estimated by *Brown and Bell* (1986) and *Hofmann* (1993), respectively, but is much larger than the estimates of 0.24-0.59 Tg COS yr^{-1}, 0.16-1.0 Tg COS yr^{-1}, and 0.86-1.0 Tg COS yr^{-1} by *Goldan et al.* (1988), *Chin and Davis* (1993), and *Kesselmeier and Merk* (1993), respectively. The COS vegetation

---

[1]This estimate was obtained using a variety of data-based and modeled-based techniques. It is at the low end of the range of historical estimates of 45-60 Pg C yr^{-1}.

sink derived from the REA measurements should not be considered to be the current best estimate of the uptake of COS by global vegetation. The range for the sink can be estimated from the range of uptake ratios for COS/CO_2 reported in the literature (see *Table 3.4*). A plausible range for the uptake ratio seems to be 2-12 pmol μmol^{-1}, corresponding to a sink of 0.5-2.8 Tg COS yr^{-1}. The uptake ratio obtained in this work falls within this range, however, as it is derived from a larger number of in-situ data covering several years and seasons, it should be given special consideration.

The method for estimating the vegetation sink of COS can be applied to tentatively estimate the vegetation sink of CS_2. A linear fit shows $F_{CS_2} = (1.9 \pm 1.2)F_{CO_2} - 3.8$. Assuming that the uptake ratio CS_2/CO_2 is also equal to 1.9±1.2 pmol μmol^{-1}, the global vegetation sink is estimated to be 0.54±0.35 Tg CS_2 yr^{-1}. However, this preliminary estimate of the vegetation sink of atmospheric CS_2 should be viewed with caution since the correlation between the CS_2 and CO_2 fluxes is only significant at the 90% confidence level. Considering the large uncertainty in this estimate, further studies are necessary to quantify the air-vegetation exchange of CS_2.

3.5 Summary

Among the various techniques for the measurements of the trace gas fluxes over tall plants, the REA method appears to be suitable for flux measurements of those gases which can not be analyzed at frequencies high enough for EC measurements. A REA sampler for the measurement of turbulent fluxes over forests has been developed and verified for COS, CS_2 and CO_2. This sampler employs a 3-D sonic anemometer-thermometer for measuring wind at high frequency and fast response solenoid valves controlled by a program for directing up and downdraft air into corresponding reservoirs. A series of technical requirements and error sources have been taken into account. The REA system has an adequately short response time, and the damping of the concentration fluctuations in the tubing is negligible. Simulations using data collected over a high spruce forest show that β values decrease substantially with increasing deadband, but are not very sensitive to a bias in $\overline{w}$. Effects of both the deadband and the bias in $\overline{w}$ on the accuracy should be corrected for in the flux calculations. Intercomparison showed that the CO_2 fluxes measured by REA agreed well in most cases with those from EC, suggesting reliable performance of the REA sampler.

Exchange fluxes of COS and CS_2 between a tall spruce forest and the atmosphere were measured using the REA system developed and validated in this work. Both deposition and emission of COS and CS_2 were observed.

On average, however, the forest acted as a net sink of both gases. The overall average fluxes for COS and CS$_2$ were -93$\pm$11.7 pmol m^{-2} s^{-1} and -18$\pm$7.6 pmol m^{-2} s^{-1}, respectively. The uptake of COS by the forest showed no clear seasonal trend. CS$_2$ data showed a net deposition in August, September and October and a minor net emission in May and July. The average diurnal profile of the fluxes shows maximum deposition around noon, indicating the importance of stomata in controlling the air-plant exchange of COS and CS$_2$. This is supported by the correlations of the fluxes of both gases to PAR and to the H$_2$O and CO$_2$ fluxes. The ambient mixing ratios of both sulfur gases also appear to affect the air-plant exchange. Compensation points were derived from the flux-concentration correlations for the studied plants and site. They are 300$\pm$51 ppt for COS and 24$\pm$15 ppt for CS$_2$. Based on the uptake ratio COS/CO$_2$ (10.0$\pm$1.7 pmol μmol^{-1}) and a recent estimate of the NPP, the global COS vegetation sink is estimated to be 2.3$\pm$0.5 Tg COS yr^{-1}. This estimate is much larger than that of *Chin and Davis* (1993), which has usually been adopted in budget reviews of atmospheric COS. This large vegetation sink of COS may limit the residence time of atmospheric COS to about 2 years and cause significant seasonal variation in the mixing ratio of tropospheric COS at the middle and high latitudes of the Northern Hemisphere. The vegetation sink of atmospheric CS$_2$ is tentatively estimated to be 0.54$\pm$0.35 Tg yr^{-1}, based on the measurements from this work.

Chapter 4

Indirect evidence for a large vegetation sink of atmospheric COS

4.1   Introduction

As indicated in *Chapter 3*, the large vegetation sink of atmospheric COS should cause a significant seasonal variation in the mixing ratio of tropospheric COS. However, such a seasonal variation has not been observed in earlier in situ measurements. Most earlier measurements of atmospheric COS were conducted during campaigns with a duration of a few days to a maximum of two months (e.g. *Torres et al.*, 1980; *Johnson and Harrison*, 1986; *Bingemer et al.*, 1990; *Bandy et al.*, 1992; *Staubes-Diederich*, 1992; *Johnson et al.*, 1993; *Weiss et al.*, 1995; *Thornton et al.*, 1996). While these campaigns were suitable for revealing the spatial variability of atmospheric COS, they were not designed to measure the temporal variability of atmospheric background COS, especially the seasonal variation. Because the major sink of atmospheric COS, i.e., terrestrial vegetation, has an seasonal component, a seasonal variation of atmospheric COS, similar to that of atmospheric CO_2, is to be expected. To understand the variability of background COS on seasonal and interannual scales, it is desirable to make long-term observations of this component at remote locations, far from anthropogenic sources.

So far, only a few such long-term measurements have been reported. *Mihalopoulos et al.* (1991) made a 2-year observation of COS in the marine boundary layer at the Amsterdam Island (37° 50′ S, 77° 31′ E). They did not observe any measurable seasonal variation, nor significant interannual trend. However, apparent seasonal cycles of total column COS with a sum-

mer maximum and a winter minimum were observed by *Rinsland et al.* (1992) and *Griffith et al.* (1998), using ground-based solar infrared absorption spectroscopy. They reported peak-to-peak amplitudes of 6-18%, about 2-6% of which are attributed to the seasonal change in the tropopause height and the reminder to seasonal fluctuations of the COS mixing ratio in the troposphere. The most profound peak-to-peak amplitude (12% after subtracting influences due to the tropopause height changes) was found by *Griffith et al.* (1998) at Wollongong (34.45° S, 150.88° E), Australia. The authors suggested that the seasonal cycle was caused at least partially by a summer coastal ocean source and a winter land-based sink. *Rinsland et al.* (1992) observed peak-to-peak amplitudes of 6%-14% at two continental stations in the Northern Hemisphere, i.e., Kitt Peak (31.9° N, 111.6° W), United States, and Jungfraujoch (46.5° N, 8.0° E), Switzerland. Apparently there are factors other than tropopause height changes causing the observed seasonal cycles. Theoretically, a strong terrestrial assimilatory sink of COS would cause a summer minimum and a winter maximum of the COS level in the tropospheric mixing layer over the continents. However, the phase of such a potential seasonal signal does not agree with that of the observed seasonal cycles of total column COS. But the phase of the terrestrial sink and of total column COS must not necessarily be the same, as several other processes (such as the marine source, biomass burning, the reaction with OH, and transport) with a seasonal component also contribute to the atmospheric COS burden and mixing ratio.

Since 1993, atmospheric COS has been measured at the Taunus Observatory of the University of Frankfurt (*Bingemer, personal communication*). The database from these measurements allows a close look at the temporal variability of the COS mixing ratio in the continental background atmosphere. With Dr. Bingemer's agreement, the COS data from the period 1993-1999 were evaluated as the current work. This chapter presents the main results of these long-term observations, especially regarding the seasonal and inter-annual variations of atmospheric COS at this continental site. Details about the location, sampling, and analysis are described in *Appendix D*.

4.2   Results and Discussion

4.2.1   Data Screening

A total of 2136 groups of samples were effectively measured between February, 1993 to December, 1999. The mixing ratio of atmospheric COS for each sampling period was calculated by averaging the individual measurements
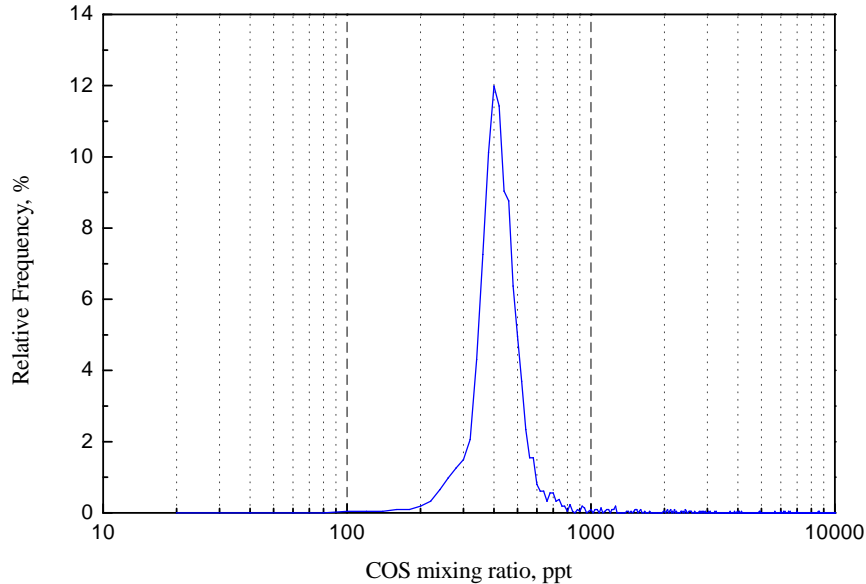
Figure 4.1: Frequency distribution of the COS mixing ratio measured at the Taunus Observatory.

in the period and excluding outliers which lie outside the range of mean $\pm$ 2σ. The group-averaged mixing ratios lie in the range of 96-11077 ppt. The values appear to be log-normally distributed, as shown in *Figure 4.1*. The frequency distribution curve peaks at about 400 ppt. More than 96% of the measurements lie in the range of 100-1000 ppt.

Figure 4.2 shows the influences of wind direction and thermal stability on COS levels at the site. COS mixing ratios above 1000 ppt were mainly observed in the northeast to southeast wind sector during inversions. Such a dependence on wind direction suggests possible anthropogenic emissions in the NE-SE sector. These high values cannot be considered to be background levels of atmospheric COS, and, therefore, should be screened.

Taking into account the above analysis, the data were screened by (1) excluding all values higher than 1000 ppt and (2) excluding all values corresponding to wind directions between 40° and 120° and obtained during inversions. The number of data points was reduced from 2136 to 1990 after this screening. Based on the screened data, the mixing ratio of atmospheric COS at the site averaged 422.5 ppt, with a standard deviation of 91.8 ppt and a standard error of the mean of 2.1 ppt during the 1993-1999 period. If the data between May 6 and October 29, 1998 are excluded, as systematic errors happened in the COS calibrations (see *Appendix D*), the average is
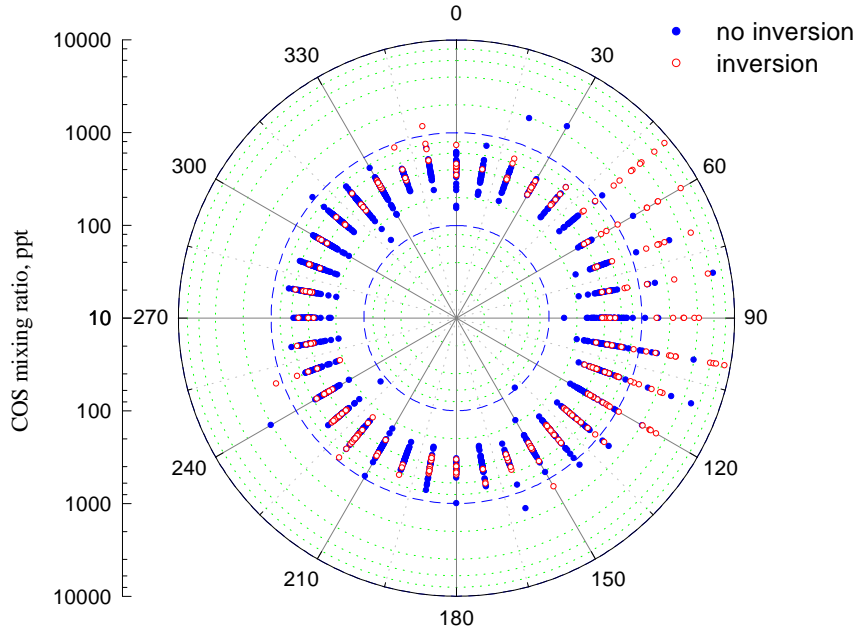
Figure 4.2: Influence of wind direction and thermal stability on the mixing ratio of atmospheric COS at the Taunus Observatory.

then 420.0 ppt.

4.2.2   Seasonal variation of Atmospheric COS

The relatively long data series of atmospheric COS at the Taunus Observatory makes it possible to check if there are periodic features in the COS mixing ratio, especially seasonal variations. Therefore, a forward Fast Fourier Transform (FFT) analysis was conducted on the COS data series.

The Fourier transform decomposes a waveform or function into sinusoids of different frequencies which sum to the original waveform. It creates a representation of the signal in phase space or frequency domain (*Stull*, 1988). The forward Fourier transform of a discrete function $A(k)$ is defined as

$$F(n) = \frac{1}{N} \sum_{k=1}^{N-1} W(k)A(k)e^{-\frac{i2\pi nk}{N}}, \tag{4.1}$$

where $F(n)$ is the discrete Fourier transform, $W(k)$ is a window function which is used to reduce leakage caused by sharp edges of a data window, N
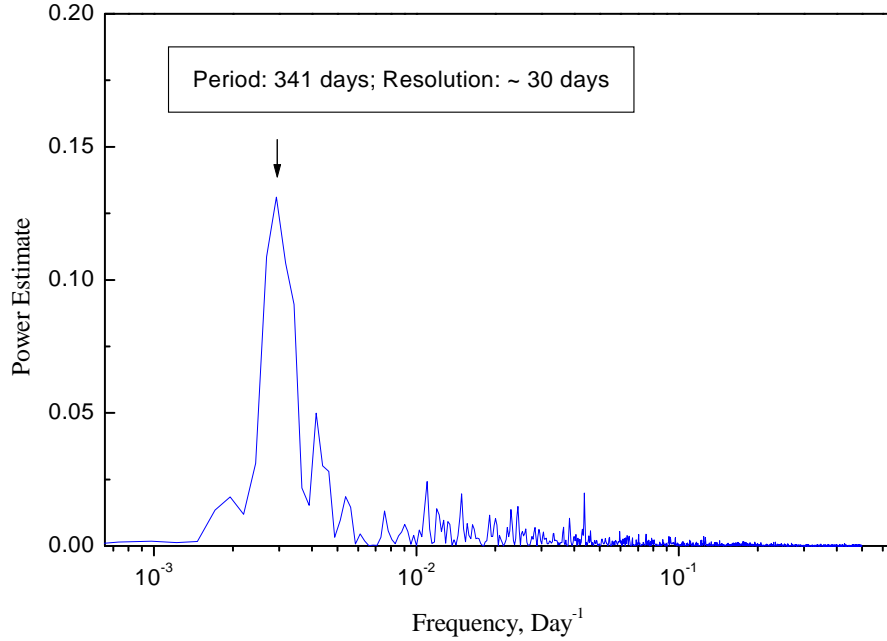
Figure 4.3: FFT power spectrum of the data series of the daily mean COS mixing
ratio at the Taunus Observatory.

is the total number of the points in a discrete data series, n and k are in the
range of 0 to $N-1$.

Contributions of individual frequencies to the variance of $A(k)$ are esti-
mated from the FFT power $G(n)$ with

$$G(n) = |F(n)|^2. \tag{4.2}$$

To fulfill the homogeneity requirement of the FFT to the input data,
COS daily means were calculated from the group measurements. Gaps in the
daily mean series were interpolated since the FFT requires a homogeneous
distribution of values. The data series was then detrended by subtracting
annual means obtained by a running mean. A Welch window function was
selected for modifying the edges of the data window. It is defined as

$$W(k) = 1 - \left[\frac{2k - (N-1)}{N+1}\right]^2. \tag{4.3}$$

Figure 4.3 shows the FFT power spectrum. It has a clear maximum at
the frequency of 0.00293 day^{-1}, corresponding to a period of 341 days. This
is virtually a one-year period, considering the resolution of about 30 days.
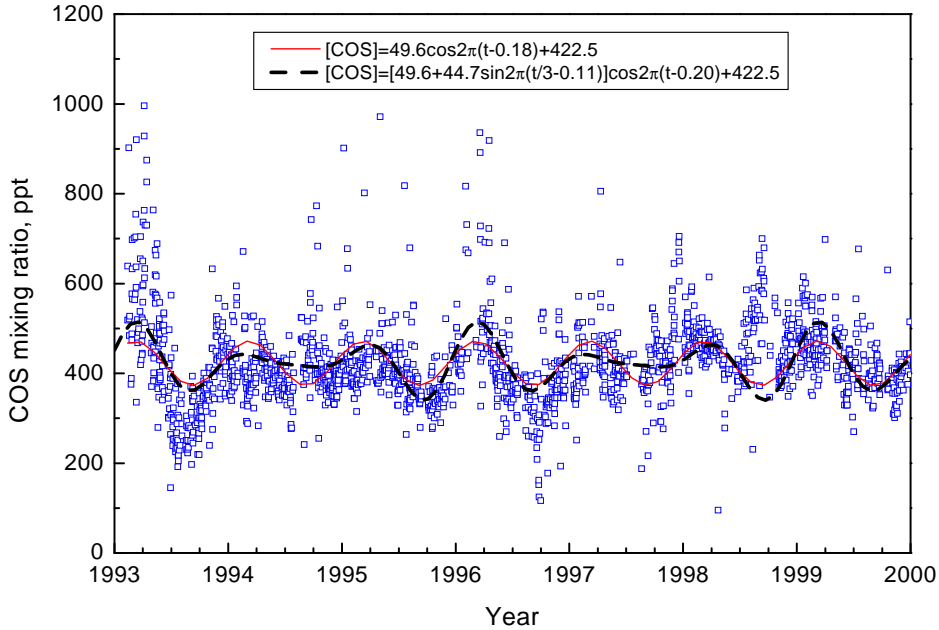
Figure 4.4: A time series of the COS mixing ratio observed at the Taunus Observatory between 1993 and 1999. The solid line shows a nonlinear fit with a fixed amplitude. The dashed line represents a nonlinear fit with a variable amplitude.

This result suggests that there is an annual cycle or seasonal variation in the time series of atmospheric COS at the site, and that this cycle is the most important contributor to the variance of the COS mixing ratio. The phase of this seasonal signal, with a minimum in summer (*Figure 4.4*), agrees with the known seasonality of the continental assimilatory sink of carbon dioxide (see *Section 4.2.3*).

Assuming that the COS mixing ratio fluctuated as a cosine form around its overall mean (422.5 ppt), the following nonlinear fitted function was obtained

$$[COS] = 49.6 cos2\pi(t - 0.18) + 422.5, \tag{4.4}$$

where $[COS]$ represents the mixing ratio of atmospheric COS, t is the time in years. This empirical function indicates that the COS mixing ratio oscillates around 442.5 ppt with an average peak-to-peak amplitude of about 100 ppt. However, the amplitude of the seasonal variation seems to be very variable from year to year, as can be seen in *Figure 4.4*. A quite profound amplitude was observed in the years 1993, 1995 and 1996, while only a small to medium

amplitude occurred in the other years. To take this characteristic of the amplitude into consideration, another model was chosen for the nonlinear fit. In this model the amplitude is composed of a constant term and a variable term which is a sine function of time. The best fit is

$$[COS] = [49.6 + 44.7sin2\pi(\frac{t}{3} - 0.11)]cos2\pi(t - 0.20) + 422.5. \qquad (4.5)$$

This fitted function suggests that the amplitude of the mixing ratio of atmospheric COS at the Taunus Observatory varies with a period of 3 years. The composite results of the sine and cosine parts in *Equation 4.5* shows that the amplitude varies from 156 ppt in the first year, to 29 ppt in the second year, and to 122 ppt in the third year. Correlation coefficients between the measured COS mixing ratios and those modeled using *Equations 4.4* and *4.5* are 0.36 and 0.43 (n=1990), respectively, indicating a better fit of *Equation 4.5* to the observed data.

Both models have shortcomings in describing the measurements. For instance, the amplitude in 1993 and 1996 appears to be underestimated by both models. The observed COS mixing ratios between May and October, 1998 do not agree with the fitted curves at all. This last disagreement can not be fully attributed to the nonlinear fits, since data from this period are quite uncertain, even after the correction for systematic errors in COS calibrations (see *Appendix D*).

Equations 4.4 and *4.5* suggest that there is a phase shift of about 0.18-0.2 year or 2.2-2.4 months (relative to the winter solstice) in the cosine function. On the average, the mixing ratio of atmospheric COS at the site arrives its maximum in March and minimum in September.

4.2.3 Relationship between COS and CO$_2$ and Implications

Three factors may cause a seasonal variation in atmospheric COS. They are: (1) the dilution effect due to tropopause height changes, (2) the seasonal variation in the source strength of COS and/or (3) the seasonal variation in the sink strength of COS. Theoretically, an enhanced tropopause height in the summer may bring more stratospheric air with lower COS mixing ratios into the troposphere, leading to a dilution of tropospheric COS. But the peak-to-peak amplitude of tropospheric COS caused by this dilution effect may not be larger than 2% ($\sim$10 ppt), if the tropopause height changes from 10 km in winter to 12 km in summer and if the average stratospheric COS mixing ratio is 380 ppt as estimated by *Chin and Davis* (1995). Oceans, the major natural source of atmospheric COS, may emit more COS in summer than in

winter. The COS production from the oxidation of CS_2 is higher in summer than in winter. These are contradictory to the features of the seasonal COS variation observed at the Taunus Observatory. COS photolysis or reaction with OH may reduce more COS in summer than in winter, but these sinks are so weak that they are unable to cause such strong seasonal variations as shown in *Figure 4.4*. Therefore, the seasonal variation of atmospheric COS at the site was most likely caused by terrestrial vegetation.

Although the flux measurements discussed in *Chapter 3* did not show any clear seasonality in the COS uptake by vegetation at the site studied, it is reasonable to suppose the existence of the seasonality in COS uptake by vegetation, taking into consideration the stomatal control of the COS uptake, and the significant correlation between the COS and CO_2 fluxes, and the pronounced seasonality of CO_2 assimilation (*Tans et al.*, 1989). As in the case of CO_2, terrestrial vegetation (especially deciduous trees) is expected to take up more COS in the summer half year than in the winter half year, due to apparent seasonal variations in plant physiology, causing an annual cycle such as shown in *Figure 4.4*. However, the intensity of this seasonality may depend on the latitude, as does the CO_2 seasonality. For CO_2 the seasonality is approximately one order of magnitude stronger at the middle and high latitudes in the North Hemisphere than at the low to middle latitudes in the South Hemisphere, as shown by CO_2 measurements (*Tanaka and Aoki*, 1987; *Tans et al.*, 1989). This may be the reason that *Mihalopoulos et al.* (1991) did not observed any significant seasonal variation of atmospheric COS at Amsterdam Island (37° 50′ S, 77° 31′ E), where the seasonality of atmospheric CO_2 is close to its minimum.

There was no parallel measurement of atmospheric CO_2 at the Taunus Observatory. Instead, CO_2 data obtained at the station Schauinsland (47°55′ N, 7°55′ E, 1205 m a.s.l.) were used for the purpose of comparison. The station Schauinsland is a member of GAW (Global Atmospheric Watch) for background measurements. The surrounding area of this station is well covered with vegetation, forest and grass, similar to that of the Taunus Observatory.

The daily mean mixing ratios of atmospheric CO_2 observed at Schauinsland between 1993 and 1998 are plotted in *Figure 4.5*. As expected for a continental site at midlatitudes, the CO_2 mixing ratio has a clear seasonal variation in each year and a increasing trend of the CO_2 mixing ratio. A nonlinear fit was done on the CO_2 data series by assuming a seasonal cycle in form of cosine and a linear increase with the time. This fit gives

$$[CO_2] = 7.2cos2\pi(t - 0.10) + 1.93t - 3496. \tag{4.6}$$

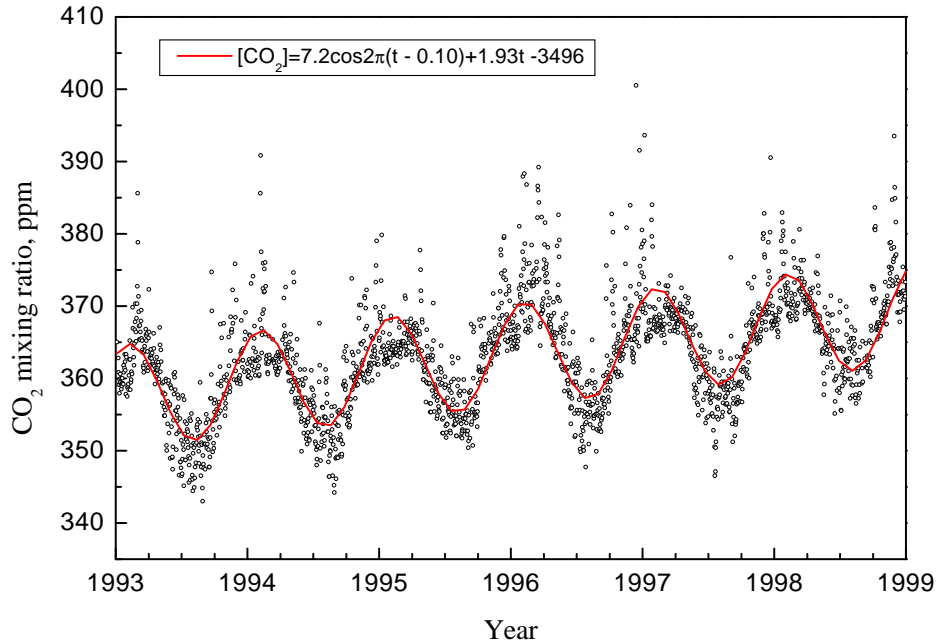This result suggests that the CO_2 mixing ratio at Schauinsland increased at

Figure 4.5: Time series of the daily mean CO_2 mixing ratio observed at the station Schauinsland between 1993 and 1998 (source: Umweltbundesamt, Germany). The solid line is a nonlinear fit to the CO_2 data.

a rate of 1.93 ppm yr^{-1} and had a seasonal variation with an average peak-to-peak amplitude of 14.4 ppm, a maximum in February and a minimum in August.

The amplitude of the CO_2 mixing ratio also appears to vary from year to year, although this variation is not as large as that in the amplitude of the COS mixing ratio. Furthermore, there is a positive correlation between the amplitudes of both gases. Even though the significance of the correlation is only 80%, there seem to be some common factors affecting both amplitudes.

A recent study by scientists at NOAA/CMDL indicates that the global growth rate of atmospheric CO_2 varied significantly from year to year during the period from 1981 to 1999 (URL:"http://www.cmdl.noaa.gov/ccgg/figures /co2trend_global.gif"). Comparing the results of this study with the amplitudes obtained above shows that the estimated global growth rate of atmospheric CO_2 is negatively correlated to the amplitude of the COS mixing ratio at the Taunus Observatory (*Figure 4.6(a)*) and to the amplitude of the CO_2 mixing ratio at Schauinsland (*Figure 4.6(b)*). The confidence levels for both correlations are close to 95%. It has been suggested, that the variation
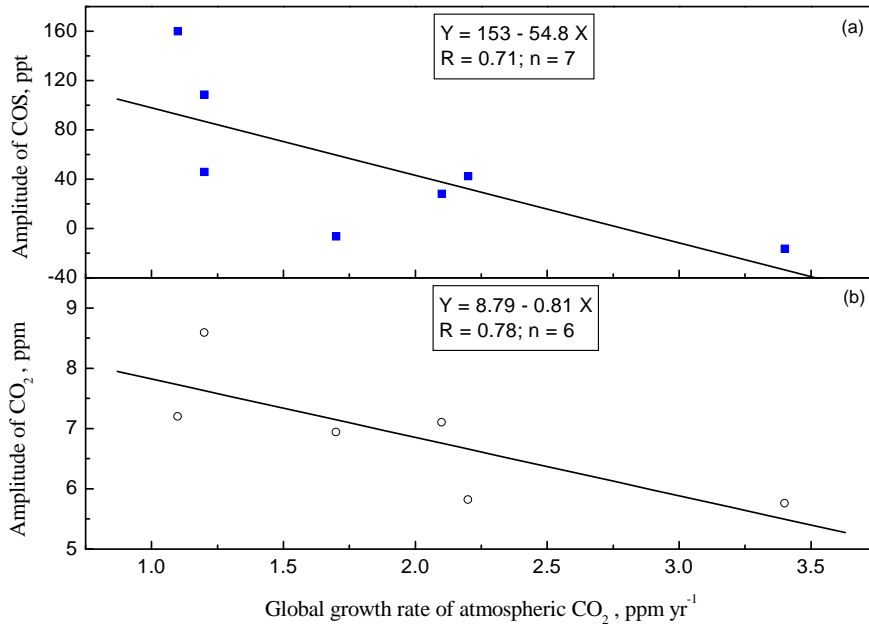
Figure 4.6: Negative correlation of the global growth rate of atmospheric CO_2 to the seasonal amplitudes of atmospheric COS at the Taunus Observatory (a) and CO_2 at Schauinsland (b). Data of the global growth rate of atmospheric CO_2 are from NOAA/CMDL.

in the growth rate of atmospheric CO_2 is mainly caused by the fluctuation in CO_2 exchange between the atmosphere and the terrestrial biosphere, which is believed to be the major sink of atmospheric CO_2 (*Kindermann et al.*, 1996; *Hofmann*, 2000). The negative correlation shown in *Figure 4.6* agrees with the idea that terrestrial vegetation is a major sink of atmospheric CO_2 and COS, affecting their tropospheric burden and surface mixing ratios.

Kindermann et al. (1996) studied the interannual variation of carbon exchange fluxes in terrestrial ecosystems during the period 1980-1994, using the Frankfurt Biosphere Model (FBM). Results from their study suggest that the interannual variation in the growth rate of atmospheric CO_2 is caused mainly by the complex temperature and precipitation responses of the net primary production (NPP) and heterotropic respiration (R_h), with the temperature response being the most important factor. In cold regions, the NPP increases with increasing temperature, whereas in tropical and subtropical regions, the NPP always decreases with increasing temperature. Consequently, the terrestrial biosphere changes from a net sink to a net source of atmospheric

Table 4.1: Parameters for estimating the global vegetation sink of COS.

Parameter	Value	Source
S_{CO_2}	45±5 (Gt C yr^{-1})	*Matthews* (1997)
B_{CO_2}	655±11 (Gt C)	derived from CO_2 data[a]
Ω_{CO_2}	14.4±0.3 (ppm)	nonlinear fit, Equation 4.6
$[CO_2]$	363.2±0.2 (ppm)	Schauinsland, average 1993-1998
B_{COS}	4.63±0.23 (Tg)	*Chin and Davis* (1995)[b]
Ω_{COS}	99.2±5.8 (ppt)	nonlinear fit, Equation 4.4
$[COS]$	422.5±2.1 (ppt)	Taunus, average 1993-1999

[a]derived from the global average mixing ratio of atmospheric CO_2 from CMDL
[b]supposing an uncertainty of 5%

CO_2, if the global mean temperature increases significantly, as in the years with strong El Niño. It is possible that this phenological response to the climate parameters caused the year-to-year variation in the COS amplitude observed at the Taunus Observatory.

Supposing that vegetation uptake is the only factor leading to decreases in the mixing ratio of atmospheric CO_2 and COS from their maxima to minima, one can estimate the global vegetation sink of COS using the NPP and the observed peak-to-peak amplitudes of atmospheric COS and CO_2. The following formula can be used for such an estimate:

$$\frac{S_{COS}/B_{COS}}{S_{CO_2}/B_{CO_2}} = \frac{\Omega_{COS}/[COS]}{\Omega_{CO_2}/[CO_2]}, \tag{4.7}$$

where B_{COS} and B_{CO_2} are the tropospheric burdens of COS and CO_2, respectively, Ω_{COS} and Ω_{CO_2} are the amplitudes of COS and CO_2, respectively, $[COS]$ and $[CO_2]$ are the mixing ratios of tropospheric COS and CO_2, respectively, S_{COS} represents the global vegetation sink of COS, and S_{CO_2} equals the terrestrial NPP. The values used for these parameters are listed in *Table 4.1*. Calculations give a global vegetation sink of 1.9±0.3 Tg COS yr^{-1}. This estimate agrees well with that obtained on the basis of the flux measurements presented in *Chapter 3* (2.3±0.5 Tg COS yr^{-1}). Since both methods extrapolate measurements at one site to the global scale, it is possible that the uncertainties in the estimates are even larger than those given here. Nevertheless, the good agreement between these two independent methods suggests that the vegetation uptake of atmospheric COS may be significantly larger than the estimate of 0.43 Tg COS yr^{-1} by *Chin and Davis* (1993).
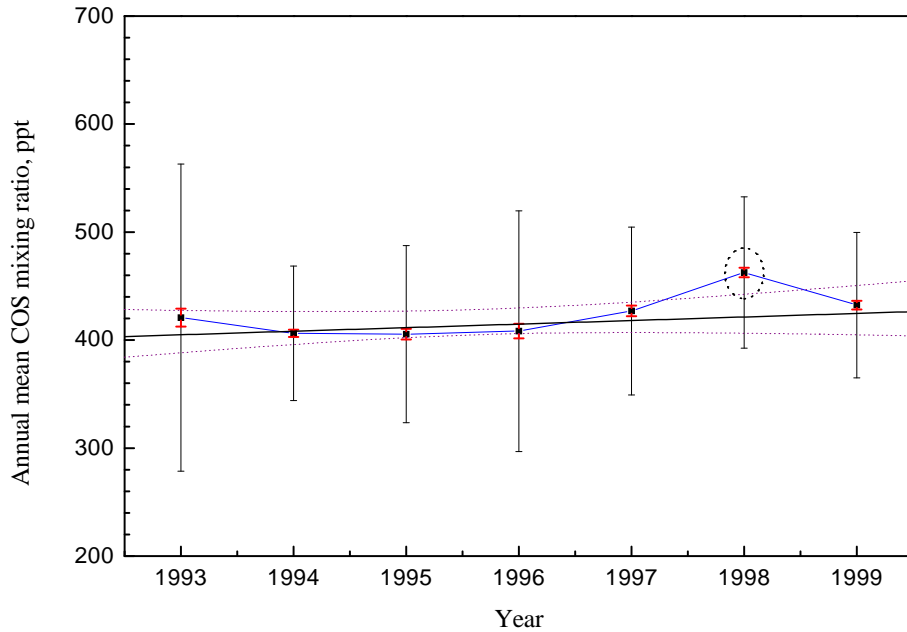
Figure 4.7: Long-term trend of atmospheric COS observed at the Taunus Observatory. Annual mean mixing ratios with standard deviations (long error bars) and standard errors of the mean (short error bars) are plotted. The solid line shows the linear fit with a slope of 3.3 ± 2.1 ppt yr^{-1}. The dotted lines show the 95% confidence belt. The annual mean from 1998 is not included in the linear fitting due to its high uncertainty.

4.2.4   Long-term variation of Atmospheric COS

One of the aims in conducting long-term measurements of atmospheric COS is to study whether or not there is a secular trend in the COS mixing ratio. *Figure 4.7* shows statistics for the COS measurements at the Taunus Observatory for individual years. Initially appears that the annual mean mixing ratio of atmospheric COS peaked in 1998. However, the annual mean from 1998 is highly uncertain because of the erroneous calibration of some measurements (see *Appendix D*). Therefore, it should not be included in the trend analysis. A linear fit to the other annual means indicates an increase of 3.3 ± 2.1 ppt yr^{-1} or $0.8(\pm0.5)\%$ yr^{-1}. The trend is not significant at the 95% confidence level, considering the standard deviation of 0.5% yr^{-1}. This result is in accordance with the trends estimated on the basis of measurements of the COS mixing ratio in the troposphere (*Mihalopoulos et al.*, 1991; *Bandy et al.*, 1992) and the total column COS observations (*Rinsland et al.*, 1992;

Griffith et al., 1998). If the linear fit is weighted by the standard error of the mean, it yields a trend of 4.9 ± 0.9 ppt yr^{-1} or $1.2(\pm 0.2)\%$ yr^{-1}, which is significant at the 99% confidence level. This result suggests that the mixing ratio of atmospheric COS could be slightly increasing, but is sufficiently small that further studies are needed to confirm this observation.

4.3   Summary

Long-term measurements since 1993 of atmospheric COS at the Taunus Observatory show that the mixing ratio of atmospheric COS has a seasonal variation with a maximum in the late winter and a minimum in the late summer. This is confirmed by an FFT analysis on the COS time series. The seasonality is most likely a result of the COS uptake by terrestrial vegetation. A nonlinear fit to the COS measurements gives an average peak-to-peak amplitude of 99.2 ppt. The magnitude of the amplitude varied strongly from year to year, probably caused by the interannual variation in large-scale CO_2 assimilation by the terrestrial biosphere and concomitant COS uptake.

A global COS vegetation sink is estimated to be 1.9 ± 0.3 Tg yr^{-1} on the basis of the average amplitudes of atmospheric COS and CO_2, the COS and CO_2 burdens in the troposphere, and the NPP. This estimate agrees well with that obtained on the basis of the REA measurements of COS fluxes over the Solling Forest. Results from the two independent methods suggest that the vegetation sink of atmospheric COS may have been significantly underestimated in some budget estimates, such as the one by *Chin and Davis* (1993).

The mixing ratio of atmospheric background COS at the Taunus Observatory averaged 422.5 ppt with a standard deviation of 91.8 ppt. A slight increase of 4.9 ± 0.9 ppt yr^{-1} was derived from the annual mean COS mixing ratios. This secular trend is statistically significant, however, further studies are necessary to confirm it.

Chapter 5

Summary and Recommendations

5.1 Summary

This work is an investigation into the tropospheric cycle of COS, with emphasis on the exchange of COS between the ocean and the atmosphere, and between terrestrial vegetation and the atmosphere. The main results of the study are:

Strong spatial and temporal variations in the concentration of dissolved COS and its saturation ratio were observed in the open Atlantic Ocean between 30°S and 50°N during the cruises in the fall of 1997 and in the summer of 1998. The concentration of dissolved COS averaged 14.7 pmol L^{-1} and 18.1 pmol L^{-1} for the fall and summer cruises, respectively.

The concentration of dissolved COS showed pronounced diurnal cycles. Seawater was supersaturated with COS with respect to the atmosphere during the sunlit period of the day, whereas it was undersaturated almost regularly during periods with no or little sunlight, even in the warm seasons and in productive regions. The open ocean thus acts as a sink of atmospheric COS during the late night and early morning, and as a source during the rest of the day.

Field evidence shows that dissolved CH$_3$SH is one of the key precursors of COS in seawater and its concentration can be used as an indicator for the COS production potential. The CH$_3$SH concentration is correlated with the content of chlorophyll a in seawater, implying a close relationship between the CH$_3$SH level and the marine primary productivity.

Significant correlations have been found between the daily mean global radiation and the peak-to-peak amplitude of marine COS, between the daily

mean concentrations of COS and CH_3SH in seawater, and between the daily mean concentration and the hydrolysis lifetime of COS in seawater. This supports the idea that COS in seawater is mainly produced by the photochemical reactions of its precursors and removed from seawater by hydrolysis.

An empirical model has been developed for estimating the daily mean concentration of seawater COS from satellite measurements. According to this model, the daily mean COS concentration can be calculated from the hydrolysis lifetime of COS in seawater, the chlorophyll a content, wind speed, and global radiation. The calculated concentrations compare well with the observations.

COS air-sea fluxes were estimated using the flux model of *Liss and Slater* (1974) together with the stability dependent model of *Erickson* (1993) for the exchange coefficient. The estimated fluxes show strong regional and seasonal variations, with the largest emissions from productive regions during the warmer seasons, and a small net deposition in the Benguela Current during the southern winter. An extrapolation suggests that the global open ocean is a source of up to 0.10 Tg COS yr^{-1}.

The measurements showed a relatively uniform latitudinal distribution of COS in the marine atmosphere, with average mixing ratios of 474±33 pptv and 502±38 pptv for the 1997 and 1998 cruises, respectively. Enhanced mixing ratios of atmospheric COS were observed in the equatorial and tropical latitude belts, whereas lower levels were found in the subtropical and temperate regions. The interhemispheric ratios of atmospheric COS were not significantly different from unity during the two cruises.

A REA sampler for the measurements of the air-vegetation exchange of COS and CS_2 was developed, tested, and validated. Exchange fluxes of COS and CS_2 between the atmosphere and a tall spruce forest were measured for the first time on a tower in the Solling Mountains using the REA technique. Both deposition and emission of COS and CS_2 were observed, with deposition occurring mostly during the daytime and emission during the dark period. On the average, however, the forest acts as a net sink for both gases. The average fluxes for COS and CS_2 were -93±11.7 pmol m^{-2} s^{-1} and -18±7.6 pmol m^{-2} s^{-1}, respectively. The COS flux did not show any clear seasonality between May and October, whereas the CS_2 flux showed a net deposition between August and October and a minor net emission in May and July.

The mean diurnal cycles of the COS and CS_2 fluxes parallel that of the CO_2 flux, i.e., the maximum deposition is found around noon and a small emission during the dark period. The fluxes of both gases were correlated to the fluxes of PAR, H_2O and CO_2. The results support the idea that the air-plant exchange of COS and CS_2 is controlled by the stomata.

Compensation points have been derived from the flux-concentration cor-

relations. They are 300±51 ppt for COS and 22±15 ppt for CS_2.

Based on the uptake ratio COS/CO_2 (10.0±1.7 pmol μmol^{-1}) and the terrestrial NPP, the global COS vegetation sink is estimated to be 2.3±0.5 Tg COS yr^{-1}. This sink may limit the residence time of atmospheric COS to about 2 years, and cause a significant seasonal variation in the mixing ratio of tropospheric COS at the middle and high latitudes of the North Hemisphere.

A vegetation sink of atmospheric CS_2 of 0.54±0.35 Tg yr^{-1} has been derived using the data presented this work. If this preliminary estimate is confirmed by future studies, a modification of the CS_2 budget will be necessary.

Analysis of long-term measurements of atmospheric COS at the Taunus Observatory between 1993 and 1999 shows that the mixing ratio of atmospheric COS has a seasonal variation with a maximum in late winter and a minimum in late summer. This seasonality provides indirect evidence for a large vegetation sink for atmospheric COS. A nonlinear fit to the COS data series shows an average peak-to-peak amplitude of 99.2 ppt. The magnitude of the amplitude varied strongly from year to year. This is probably caused by the interannual variation in the large-scale CO_2 assimilation by the terrestrial biosphere and the concomitant COS uptake.

A global vegetation sink of 1.9±0.3 Tg COS yr^{-1} has been derived from the mean amplitudes of atmospheric COS and CO_2, the tropospheric burdens of COS and CO_2, and the NPP. This estimate agrees well with that obtained on the basis of the REA measurements. Results from the two independent methods suggest that the vegetation sink of atmospheric COS might have been significantly underestimated in some budget estimates, such as the one by *Chin and Davis* (1993).

The background signal of atmospheric COS at the Taunus Observatory shows an average mixing ratio of 422.5 ppt with a standard deviation of 91.8 ppt and a secular trend of 4.9±0.9 ppt yr^{-1}.

5.2 Recommendations for Future Research

In view of the small contribution of open oceans to atmospheric COS, future studies of seawater COS should be mainly focused on the role of coastal and shelf regions. The production and removal mechanisms of seawater COS should be emphasized in these studies to reduce the uncertainty in the estimate of the ocean source of atmospheric COS.

It is highly desirable to develop global models for seawater COS. Local kinetic and empirical models should be improved to make more accurate estimates of the concentration of seawater COS using data from satellites. They

should be integrated into 3-D global models to study the air-sea exchange of COS and its geographic and seasonal variations.

More in situ measurements of the air-vegetation exchange of COS over major ecosystems are needed to extend the database for estimating the global vegetation sink of atmospheric COS. Reliable methods, such as the one used in the work (i.e., the REA technique), should be applied to such measurements. There is a need to develop and improve COS sensors to allow more precise, and faster measurements of the COS flux.

Long-term observations should be continued since they are an inevitable tool for detecting seasonal and interannual variations in atmospheric COS. Monitoring atmospheric COS at different latitudes may help to answer the question of whether or not the seasonal cycle of the vegetation sink of COS has a latitudinal dependence similar to that of the CO_2 assimilation.

The vegetation sink of $\sim$2 Tg COS yr^{-1}, as estimated in this work, appears large enough to cause detectable vertical gradients of the COS mixing ratio in the troposphere. This should be confirmed by measuring profiles of tropospheric COS, preferably in winter and in summer over well vegetated regions in middle and high latitudes. Results from such measurements may also be used to clarify the different phase shifts observed in the COS total column (maximum in the late summer) and in the mixing ratio of COS in the boundary layer (maximum in the late winter).

The role of soils in the budget of atmospheric COS is highly uncertain. Since most earlier measurements of the COS air-soil exchange are unreliable because of artifacts in the measurements, few data are presently available for estimating the soil contribution to atmospheric COS. Apparently, more field measurements of the air-soil exchange of COS are required.

Further studies of anthropogenic emissions of COS are of importance for the following reasons: First, information on the major (indirect) anthropogenic source of COS (i.e., industrial emission of CS_2) is currently only inferred from statistic of commercial production of more than two decades ago, based on the assumed release factors. The estimated contribution from this source is close to 20% of the total COS source, but no experimental evidence for this exists. Second, COS episodes were occasionally observed, but the actual sources of the high levels of atmospheric COS have seldom been identified. Third, anthropogenic emissions are closely related to the future trend of COS abundance in the atmosphere, since they may undergo potential long-term changes. Fourth, if the magnitude of the COS vegetation sink estimated in this work is confirmed by future studies, the estimated total sink will become larger than the known total source. This gap may most possibly be filled by anthropogenic emissions.

Relatively broad databases of the mixing ratio and total column of atmo-

spheric COS have been established by measurements in the last two to three decades. The compatibility between the observed distribution, the estimated sources and sinks, and the transport of atmospheric COS should be tested using 3-D global models.

Zusammenfassung

In der hier vorliegenden Arbeit wurde der troposphärische Kreislauf von Carbonylsulfid (COS) untersucht. COS ist ein Quellgas des stratosphärischen Sulfat-Aerosols, das die Strahlungsbilanz beeinflussen und den chemischen Abbau des stratosphärischen Ozons beschleunigen kann. Trotz zahlreicher Studien sind die Quellen und Senken des atmosphärischen COS bisher nur unzulänglich quantifiziert. Insbesondere bestehen große Unsicherheiten in den Abschätzungen der Beiträge des Ozeans und der anthropogenen Quellen, sowie der Senkenstärke der Landvegetation. Schiffs- und flugzeuggetragene Messungen des atmosphärischen COS ergaben kein einheitliches interhemisphärisches Verhältnis (IHR=M_{NH}/M_{SH}). Während die Messungen von *Bingemer et al.* (1990), *Staubes-Diederich* (1992) und *Johnson et al.* (1993) ein IHR zwischen 1.10 und 1.25 zeigten, fanden die Messungen von *Torres et al.* (1980), *Staubes-Diederich* (1992), *Weiss et al.* (1995) und *Thornton et al.* (1996) keinen oder nur einen geringfügigen N/S-Gradienten. Die Untersuchung von *Chin und Davis* (1993) zeigt ein N/S-Verhältnis der COS-Quellstärke von 2.3, das hauptsächlich auf die stärkeren anthropogenen Quellen auf der Nordhalbkugel zurückzuführen ist. Es ist unklar, ob der zeitweilige Konzentrationsüberschuß der Nordhemisphäre Zeichen anthropogener Quellen dort oder Teil eines durch die Senkenfunktion der Landpflanzen verursachten saisonalen Signals ist. Die Konsistenz der Breitenverteilung des COS-Mischungsverhältnisses mit den geographischen bzw. saisonalen Variationen der COS-Quellen und -Senken muß überprüft werden. Dazu werden genaue Kenntnissen der Quell- und Senkenstärken des atmosphärischen COS und ihrer raumzeitlichen Variabilität benötigt. Vor dem obigen Hintergrund ergeben sich als Schwerpunkte dieser Arbeit: (1) der Austausch von COS zwischen Atmosphäre und Ozean sowie (2) zwischen Atmosphäre und terrestrischer Vegetation und (3) die raumzeitliche Variabilität des atmosphärischen COS.

Zur Untersuchung des Austausches von COS zwischen Atmosphäre und Ozean wurde das Konzentrations-Ungleichgewicht von COS zwischen Ozean und Atmosphäre durch Messungen des COS im Seewasser und in der Meeres-

luft ermittelt und die resultierenden Austauschflüsse mit einem Modell berechnet. Die Messungen fanden an Bord des Forschungsschiffs *Polarstern* während der Fahrten ANT/XV-1 (15.10.-6.11.1997, Bremerhaven-Kapstadt) und ANT /XV-5 (26.5.-6.20.1998, Kapstadt-Bremerhaven) statt. Die Konzentration des gelösten COS und das Sättigungsverhältnis von COS zwischen Ozean und Atmosphäre zeigen ausgeprägte Tagesgänge und saisonale und geographische Variationen. Die mittlere Konzentration von COS im Seewasser beträgt 14.7 pmol L^{-1} für die Herbst-Fahrt bzw. 18.1 pmol L^{-1} für die Sommer-Fahrt. Höchste COS-Konzentrationen werden in der jeweiligen Sommer-Hemisphäre und in Gebieten mit hoher biologischer Produktivität beobachtet, d.h. im Benguela-Strom im November, im Nordost-Atlantik im Juni und in den Auftriebgebieten vor Westafrika im Oktober bzw. Juni. In den übrigen Gebieten sind die Konzentrationen um eine Größenordnung niedriger.

Die Konzentration von COS im Seewasser steigt frühmorgens von ihrem tiefsten Stand an. Um ca. 15 Uhr Ortszeit erreicht sie ihr Maximum, danach nimmt sie ab. Der Tagesgang unterstützt die Theorie, daß COS im Seewasser photochemisch produziert wird. Während der Tagesstunden wird eine Übersättigung des offenen Ozean für COS gefunden. Dagegen ist eine Untersättigung des Ozeans in den späten Nachtstunden zu beobachten. Der Ozean wirkt in den Tagesstunden als COS-Quelle, in der späten Nacht als COS-Senke. Die Untersättigung tritt sogar im Sommer in produktiven Meeresgebieten regelmäßig auf. Eine Konsequenz dieser Beobachtung ist die weitere Reduzierung der ozeanischen Quelle von COS gegenüber bisher publizierten Abschätzungen.

Methylmercaptan (CH$_3$SH) ist in allen Seewasserproben zu beobachten. Der Tagesmittelwert der CH$_3$SH-Konzentration variiert zwischen 29 und 303 pm L^{-1} und ist 3-16 fach größer als der der COS-Konzentration. Der Tagesgang der CH$_3$SH-Konzentration zeigt ein Minimum um die Mittagszeit. Die Tagesmittel der CH$_3$SH- und COS-Konzentrationen sind signifikant miteinander korreliert. Diese Daten liefern den Beweis dafür, daß CH$_3$SH eine der wichtigen Vorgängersubstanzen von COS ist. Die Regressionslinie der Korrelation zwischen den mittleren COS- und CH$_3$SH-Konzentrationen weist nur einen geringfügigen Achsenabschnitt auf. Somit kann die CH$_3$SH-Konzentration als ein Indikator der Konzentration von COS-Vorgängern benutzt werden. Es besteht außerdem eine Korrelation zwischen der CH$_3$SH-Konzentration und dem Logarithmus der Konzentration des gelösten Chlorophyll *a*. Diese Korrelation deutet darauf hin, daß der Gehalt von CH$_3$SH im Seewasser eine enge Beziehung zur marinen Primärproduktion hat.

COS wird im Seewasser durch Hydrolyse abgebaut. Die Abbaurate hängt von der Temperatur des Seewassers ab. Je wärmer das Seewasser ist, desto schneller wird COS abgebaut, und um so kürzer ist die Lebenszeit von COS

im Seewasser. Die Lebenszeit kann einerseits durch das Reaktionsgeschwindig-keits-Gesetz von Arrhenius berechnet werden, andererseits läßt sie sich durch exponentielle Anpassung an den nächtlichen Konzentrationsverlauf (d.h. bei Abwesenheit von Photoproduktion) abschätzen. Eine solche Anpassung des exponentiellen Abklingens wurde anhand von dicht gestaffelten Messungen während einiger Nächte vorgenommen. Die gefitteten Lebenszeiten stimmen mit den theoretischen Werten gut überein, obwohl die gefittete Lebenszeit neben Hydrolyse noch von anderen Prozessen (z.B. Transport nach unten, Air-Sea-Austausch, usw.) beeinflußt wird. Diese gute Übereinstimmung unterstützt die Aussage, daß die Hydrolyse eine bedeutende Rolle beim Abbau von COS im Seewasser spielt. Die berechnete Hydrolyse-Lebenszeit ist mit dem Tagesmittel der COS-Konzentration korreliert. Da die Tagesmittelwerte sowohl zeitliche wie auch räumliche Mittelwerte der COS-Konzentrationen darstellen, zeigt diese Korrelation, daß Hydrolyse eine bedeutende Rolle in der raumzeitlichen Variabilität der COS-Konzentration einnimmt.

Da die Konzentration des gelösten COS von mehreren Faktoren abhängig ist, scheint eine multivariable Betrachtung sinnvoll. Hierfür wurde eine "Multiple Linear Regression Analysis" (MLRA) ausgeführt. Diese Analyse ergibt ein empirisches Modell der folgenden Form für die Berechnung des Tagesmittels der COS-Konzentration:

$$[COS] = 1.8\tau + 13 log[Chl] - 1.5W_s + 0.057G - 0.73,$$

mit $\quad [COS]$ = mittlere Konzentration von COS in pmol L^{-1}
$\quad\quad\quad \tau$ = Hydrolyse-Lebenszeit in Stunde
$\quad\quad\quad [Chl]$ = mittlere Konzentration von Chlorophyll a in mg m^{-3}
$\quad\quad\quad W_s$ = Windgeschwindigkeit in m s^{-1}
$\quad\quad\quad G$ = Intensität der Globalstrahlung in W m^{-2}.

Die Parameter auf der rechten Seite der Gleichung können direkt oder indirekt von Satelliten aus gemessen werden, deshalb kann dieses Modell für die Abschätzung der Konzentration von COS im Seewasser anhand von Satelliten-Daten verwendet werden. Das empirische Modell soll noch durch weitere Messungen bestätigt bzw. verbessert werden.

Der Austauschfluß von COS zwischen der Atmosphäre und dem offenen Ozean wurde mit dem Air-Sea-Fluß-Modell von *Liss and Slater* (1974) zusammen mit dem Modell von *Erickson* (1993) für den Austauschkoeffizienten berechnet. Die berechneten Flüsse weisen starke regionale bzw. saisonale Unterschiede auf, mit Mittelwerten von 13.4±19.5 nmol COS m^{-2} d^{-1} für die Fahrt im nordhemisphärischen Herbst und 28.6±47.8 nmol COS m^{-2} d^{-1} für die Fahrt im nordhemisphärischen Sommer. Die größten Emissionen treten in

den produktiven Gebieten während der wärmeren Jahreszeiten auf. Im Mittel stellt der offene Ozean zu den Meßzeiten eine Quelle für atmosphärisches COS dar, außer im Benguelastrom, wo im südhemisphärischen Winter eine kleine Deposition auftritt. Durch Extrapolation der Austauschflüsse aus dieser Arbeit für die niedrigen und mittleren Breiten und jener von *Weiss et al.* (1995) für die höheren Breiten (subpolare und polare Regionen) wurde eine Quellstärke von 0.10 Tg COS yr^{-1} für den globalen offenen Ozean abgeschätzt. Der offene Ozean spielt somit nur eine kleine Rolle beim troposphärischen Kreislauf von COS. Weitere Untersuchungen sollten sich auf die Küsten-Gebiete konzentrieren.

Das atmosphärische COS-Mischungsverhältnis über dem Atlantik weist während beider Meßfahrten eine relativ homogene Breitenverteilung auf. Die durchschnittlichen COS-Mischungsverhältnisse für ANT/XV-1 und -5 sind 474±33 pptv bzw. 502±38 pptv. Beide Breitenverteilungen zeigen eine glockenförmige Struktur, mit höchsten Mischungsverhältnissen in den Tropen und niedrigsten in den subtropischen bzw. gemäßigten Breiten. Die erhöhten COS-Mischungsverhältnisse in den Tropen lassen sich nicht mit einem direkten Transport von COS aus den Kontinenten erklären. Die Beobachtung von Vegetationsbränden durch die "European Space Agency" (ESA) zeigt eine erhöhte Anzahlen von Feuern zwischen 20°S und 20°N vor bzw. zu den Zeiten, als die Messungen stattfanden. Dies deutet an, daß die höheren COS-Mischungsverhältnisse in den Tropen möglicherweise von der dortigen Biomassenverbrennung verursacht wurden. Die interhemisphärischen Verhältnisse des atmosphärischen COS-Mischungsverhältnisses sind nahe bei eins und liefern keinen Hinweis für einen starken Beitrag von anthropogenen Quellen in der Nordhemisphäre zum atmosphärischen COS.

Unter den Methoden zur Bestimmung des Austausches von Spurenstoffen zwischen Atmosphäre und Pflanzen eignet sich die "Relaxed Eddy Accumulation"-Technik (REA) zur Messungen des Austauschflusses von Gasen wie z.B. COS und CS_2, für die keine schnellen Sensoren verfügbar sind. Zur Messung der turbulenten Austauschflüsse von COS und CS_2 oberhalb eines Pflanzenbestandes wurde ein REA-Sammler entwickelt. Die Zuverlässigkeit des Sammlers wurde durch Parallelmessungen von CO_2-Flüssen mit REA und mit EC ("Eddy Correlation") bestätigt.

Austauschflüsse von COS und CS_2 zwischen Atmosphäre und einem terrestrischen Ökosystem wurden zum ersten Mal mit der REA-Methode gemessen. Die Messungen fanden über einem Fichtenwald im Solling während mehrerer Meßkampagnen zwischen 1997 und 1999 statt. Die Austauschflüsse beider Gase zeigen sowohl Deposition wie auch Emission, wobei Deposition überwiegend während der Tageslicht-Stunden und Emission überwiegend während der Nacht stattfindet. Im Mittel wirkt der Wald jedoch als Senke

für beide Gase. Die mittleren Flüsse betragen -93±11.7 pmol m^{-2} s^{-1} für COS und -18±7.6 pmol m^{-2} s^{-1} für CS$_2$. Der Austausch von COS und CS$_2$ zwischen Atmosphäre und dem Waldboden wurde von *Steinbacher* (2000) parallel untersucht. Die Ergebnisse zeigen, daß der Waldboden nur 1% der beobachteten Depositionsflüsse aufnimmt. Der Waldboden spielt im Austausch von COS und CS$_2$ zwischen Atmosphäre und dem Waldökosystem nur eine geringfügige Rolle.

Die COS-Flüsse zeigen keine eindeutige saisonale Abhängigkeit im Zeitraum zwischen Ende Mai und Anfang Oktober. Die CS$_2$-Flüsse zeigen eine Netto-Senke zwischen August und Oktober, und eine geringe Netto-Emission im Mai und Juli.

Die mittleren Tagesgänge der COS- und CS$_2$-Flüsse verlaufen parallel zu den CO$_2$-Flüssen, d.h. sie weisen die stärkste Deposition um die Mittagszeit und eine gerinfügige Emission während der Nacht auf. Die Flüsse von COS und CS$_2$ sind korreliert mit denen der PAR-Strahlung (photosynthetically active radiation), des H$_2$O und des CO$_2$, wobei die COS- und CS$_2$-Flüsse den H$_2$O-Flüssen entgegengerichtet sind. Bei hohen Strahlungsflüssen (hoher CO$_2$-Aufnahme und H$_2$O-Abgabe) werden COS und CS$_2$ aufgenommen, bei geringen Strahlungsflüssen werden sie abgegeben. Diese Ergebnisse unterstützen die Idee, daß der Austausch von COS und CS$_2$ zwischen Atmosphäre und Landvegetation von den Stomata gesteuert wird und mit der CO$_2$-Assimilation zusammenhängt.

Die Austauschflüsse von COS und CS$_2$ sind mit den atmosphärischen Mischungsverhältnissen der Gase negativ korreliert. Mit zunehmendem Mischungsverhältnis wird eine stärkere Aufnahme beider Gase beobachtet. Anhand der Regressionslinien der jeweiligen Korrelationen wurden Kompensationspunkte (d.h. das Mischungsverhältnis, bei dem der Netto-Fluß sein Vorzeichen wechselt) berechnet. Sie betragen 300±51 ppt für COS and 22±15 ppt für CS$_2$.

Das Verhältnis der Aufnahme von COS relativ zu CO$_2$ wurde aus der Steigung der Regressionsgeraden zwischen den COS- und den CO$_2$-Flüssen mit 10.0±1.7 pmol μmol^{-1} bestimmt. Auf der Basis dieses Aufahme-Verhältnisses und der neueren Abschätzung der terrestrischen Nettoprimärproduktion (NPP) von 45±5 Gt C yr^{-1} wird die globale Landvegetation als eine Senke von 2.3±0.5 Tg COS yr^{-1} abgeschätzt. Bei einer gesamten COS-Masse der Troposphäre von ca. 4.6 Tg, entspricht diese COS-Senke einer troposphärischen Verweilzeit des COS von ca. 2 Jahren. Eine so kurze Verweilzeit, zusammen mit der Saisonalität der Assimilation, wird eine signifikante Jahresvariation im troposphärischen Mischungsverhältnis von COS verursachen, insbesondere in den nördlichen mittleren und hohen Breiten, wo auch die stärkste Saisonalität des atmosphärischen CO$_2$ zu beobachten ist.

Die gleiche Methode wie im Fall von COS wurde zur Abschätzung des Beitrages der Landvegetation zum atmosphärischen CS_2 benutzt. Daraus läßt sich eine globale Aufnahme von 0.54 ± 0.35 Tg CS_2 yr^{-1} durch die Landvegetation ableiten. Wenn diese vorläufige Abschätzung durch weitere Untersuchungen bestätigt wird, muß das CS_2-Budget revidiert werden.

Um die von den REA-Messungen abgeleitete große COS-Senke in terrestrischer Vegetation durch weitere Beweise zu unterstützen, wurde eine langfristige Zeitreihe des atmosphärischen COS ausgewertet. Diese Messung wird am Taunus Observatorium seit 1993 von Herrn Dr. H.G. Bingemer betrieben, der die Meßdaten zwischen 1993 und 1999 zur Verfügung stellte. Um das von anthropogen Kontaminationen weitgehend unbeeinflußte Hintergrund-Niveau des atmosphärischen COS zu ermitteln, wurden COS-Daten von Episoden mit Inversionsbedingungen sowie von Winden aus dem Sektor 40°-120° aussortiert. Die bereinigten Daten weisen ausgeprägte Jahreszyklen mit Maxima im späten Winter und Minima im späten Sommer auf. Eine "Fast Fourier Transform"-Analyse zeigt ein Maximum um ca. 1 Jahr (341 ± 30 Tage) im "Power Spectrum". Die Ergebnisse zeigen eine klare Saisonalität des Mischungsverhältnisses von COS am Taunus Observatorium, die als bedeutendster Faktor zur Varianz des COS-Mischungsverhältnisses beiträgt.

Zwei nichtlineare Anpassungen an die COS-Zeitreihe wurden ausgeführt, unter der Annahme, daß das COS-Mischungsverhältnis in Form eines Kosinus mit der Zeit schwingt. Aus der ersten Anpassung, bei der die Amplitude festgesetzt wird, ergibt sich eine Kosinus-Funktion mit einer "peak-to-peak"-Amplitude von 99.2 ppt. Da die Amplitude von Jahr zu Jahr variiert, wird in der zweiten Anpassung die Amplitude als eine Sinus-Funktion angenommen. Die Ergebnisse dieser Anpassung simulieren die COS-Zeitreihe besser und zeigen, daß die COS-Amplitude in einer Periode von 3 Jahren variiert, mit den "peak-to-peak"-Amplituden von 156ppt, 29ppt bzw. 122 ppt. Beide Anpassungen ergeben eine Phasenverschiebung von 2.2-2.4 Monaten gegen die astronomische Wintersonnenwende. Eine ähnliche Analyse wurde mit der CO_2-Zeitreihe der Meßstation Schauinsland ausgeführt, die ca. 240 km vom Taunus Observatorium entfernt ist, und ählich wie das Taunus Observatorium in einer stark bewaldeten Region liegt. Diese Analyse ergibt eine mittlere "peak-to-peak"-Amplitude von 14.4 ppm CO_2 und eine Phasenverschiebung von 1.2 Monaten. Wie im Fall von COS, zeigt auch die CO_2-Amplitude Unterschiede zwischen verschiedenen Jahren. Die COS- und CO_2-Amplituden der einzelnen Jahre wurden mit den globalen Wachstumraten des atmosphärischen CO_2 (Quelle: NOAA/CMDL) dieser Jahre verglichen. Eine Korrelation zwischen der globalen Wachstumrate des atmosphärischen CO_2 und der COS- bzw. CO_2-Amplitude läßt sich erkennen (Wahrscheinlichkeit: 95%). Dies deutet darauf hin, daß die starken Unterschiede der

COS-Amplitude zwischen den Jahren wahrscheinlich durch die Variationen der großräumigen CO_2-Assimilation und der begleitenden COS-Aufnahme verursacht worden sind.

Die globale Aufnahme von COS durch die Landvegetation wurde anhand der gewonnenen Jahresamplituden der COS- und CO_2-Mischungsverhältnisse abgeschätzt, mit der Annahme, daß die Abfälle der Mischungsverhältnisse von COS und CO_2 zwischen Winter und Sommer ausschließlich von terrestrischer Vegetation verursacht sind. Die Abschätzung ergibt eine globale COS-Aufnahme der Landvegetation von 1.9 ± 0.3 Tg COS yr^{-1}. Diese Abschätzung stimmt mit jener aus den REA-Messungen gut überein. Damit wird die große COS-Senke der Landvegetation indirekt bestätigt. Die Ergebnisse aus den beiden unabhängigen Methoden deuten darauf hin, daß die pflanzliche Senke von COS in den bisherigen Budget-Abschätzungen wahrscheinlich signifikant unterschätzt wurde.

Das Mischungsverhältnis des atmosphärischen COS am Taunus Observatorium zwischen 1993 und 1999 beträgt im Mittel 422.5 ppt, mit einer Standardabweichung von 91.8 ppt. Aus den Jahresmitteln läßt sich ein Trend von 4.9 ± 0.9 ppt yr^{-1} ableiten. Dieser Trend ist zwar statistisch signifikant, aber ausreichend klein, so daß weitere Untersuchungen benötigt werden, um ihn zu bestätigen.

Appendix A

Calibration of CH$_3$SH Peaks Using COS Calibration Curves

No CH$_3$SH permeation tube was available for the direct calibration of CH$_3$SH peaks during the cruise ANT-XV/1. The CH$_3$SH peaks from this cruise were therefore calibrated indirectly, using the COS calibration curve from the same day. Because the FPD is more sensitive to COS than to CH$_3$SH, this nonspecific calibration needs to be corrected for the sensitivity difference between COS and CH$_3$SH. A correction factor has been derived from the COS and CH$_3$SH calibration curves obtained during the *ANT-XV/5* cruise, when direct calibrations were conducted simultaneously for both compounds. The derivation of the correction factor is described below.

Suppose that the COS and CH$_3$SH masses in a sample are M_{COS} and M_{CH_3SH}, respectively, and the peak areas for both compounds are A_{COS} and A_{CH_3SH}. The calibration yields a logarithmic relationship between mass and peak area.

$$\log(M_{COS}) = a_{cos} + b_{cos} \log(A_{COS}), \tag{A.1}$$
$$\log(M_{CH_3SH}) = a_{CH_3SH} + b_{CH_3SH} \log(A_{CH_3SH}), \tag{A.2}$$

where a_{cos} and b_{cos} are the intercept and slope of the COS calibration curve, respectively, and a_{CH_3SH} and b_{CH_3SH} are the intercept and slope of the CH$_3$SH calibration curve, respectively. If a CH$_3$SH peak is quantified using the COS calibration curve, the CH$_3$SH mass, M'_{CH_3SH}, is calculated as:

$$\log(M'_{CH_3SH}) = a_{cos} + b_{cos} \log(A_{CH_3SH}). \tag{A.3}$$

M'_{CH_3SH} needs to be corrected for the sensitivity difference between COS and CH$_3$SH.

The combination of *Equations A.2* and *A.3* yields

$$\log\left(\frac{M'_{CH_3SH}}{M_{CH_3SH}}\right) = (a_{COS} - a_{CH_3SH}) + (b_{COS} - b_{CH_3SH})\log(A_{CH_3SH}), \quad \text{(A.4)}$$

where $\frac{M'_{CH_3SH}}{M_{CH_3SH}}$ is defined as the correction factor r. From *Equations A.3* and *A.4*, a theoretical relationship between r and M'_{CH_3SH} can be derived:

$$\log(r) = \frac{a_{COS}b_{CH_3SH} - b_{COS}a_{CH_3SH}}{b_{COS}} + \left(1 - \frac{b_{CH_3SH}}{b_{COS}}\right)\log(M'_{CH_3SH}). \quad \text{(A.5)}$$

However, this theoretical relation could not be directly applied for the ANT-XV/1 cruise, since the a_{CH_3SH} and b_{CH_3SH} values are not available. Fortunately, the intercept and the slope in Equation A.5 can be determined empirically. A least squares fit to the data from the cruise ANT-XV/5 resulted in the empirical equation

$$\log(r) = 0.22(\pm 0.005)\log(M'_{CH_3SH}) - 0.167(\pm 0.021). \quad \text{(A.6)}$$

The number of data points for this fit is 100, and the correlation coefficient is 0.975, indicating a very high level of significance. This empirical equation was used for correcting the sensitivity difference between COS and CH_3SH.

Appendix B

Determination of the dead volume in the tubing of the REA sampler

The dead volume in the tubing of the REA sampler was determined using a pressure manifold shown in *Figure B.1.* The apparatus consists mainly of a vacuum pump (Turbotronik NT50, Leybold, Germany), a glass vacuum tube, a pressure sensor (Datametrics, Schaefer, Germany) and a pressure display (Datametrics 1500, Schaefer, Germany).

The method presented here for volume determining is based on the ideal gas law

$$PV = nRT, \tag{B.1}$$

where V is the volume of a closed container of any form, P is the inner gas pressure in the container, T is the absolute temperature of a gas or gas mixture in the container, n is the mole number of the gas or gas mixture, and R is the gas constant. The state of a gas in the vacuum tube with a volume V_0 and that of a gas in a container whose volume V_x is to be determined (here the tubing of the REA sampler) can be described by

$$P_0 V_0 = n_0 R T_0 \tag{B.2}$$

and

$$P_x V_x = n_x R T_x. \tag{B.3}$$

If we connect both containers, allow gases to mix, and keep the temperature constant (such as room temperature T), the result will be

$$P_b(V_0 + V_x) = (n_0 + n_x)RT = P_0 V_0 + P_x V_x, \tag{B.4}$$
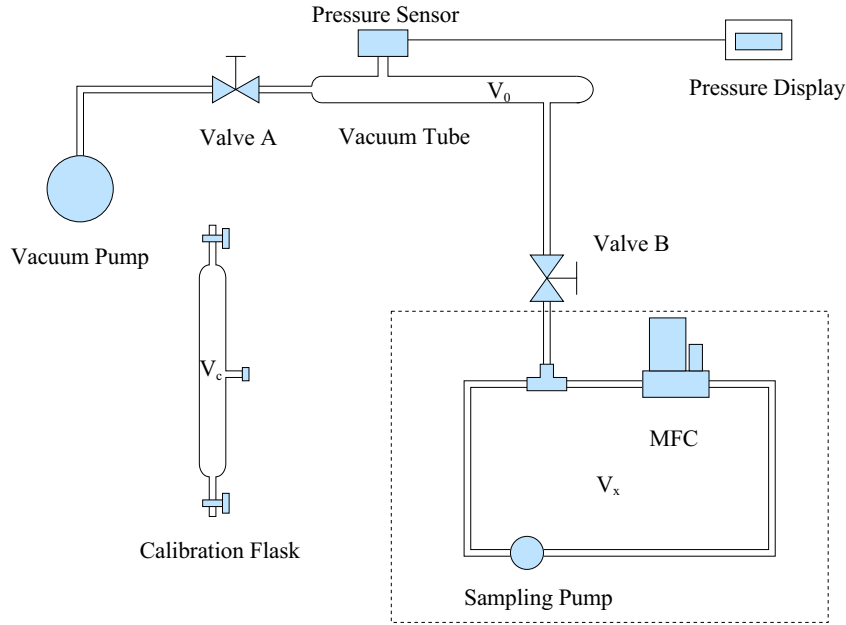
Figure B.1: The apparatus used for determining the dead volume in the tubing of the REA sampler.

where P_b is the balanced pressure. Rearranging this equation gives

$$V_x = V_0 \frac{P_b - P_0}{P_x - P_b}. \tag{B.5}$$

Therefore, V_x can be easily calculated using *Equation B.5*, if P_o, P_x, P_b and V_0 are known. In this work, P_o, P_x and P_b were precisely measured using the pressure sensor. V_0 was calibrated using the calibration flask depicted in *Figure B.1*. The volume (V_c) of the calibration flask was determined to be 327.19 ml by weighing the distilled water that the flask could contain, using an electronic balance (Mettler P1200, Germany). V_0 was found to be 257.44±0.14 ml. The dead volume in the tubing of the REA sampler (*Figure 3.1*) before the split was determined to be 12.14±0.05 ml, and after the split 7.01±0.03 ml.

Appendix C

Estimates of Errors in σ_w, β and $\left(\overline{c^+} - \overline{c^-}\right)$ in REA measurements

C.1 Error in σ_w

Suppose that w values measured by the sonic anemometer have both systematic and random errors. The systematic error (if any) can usually be considered to be a linear function of the true value. The random error is a small value about zero. Therefore, the w value at ith measurement point is given by

$$w_i = aw_{0i} + b + \delta_{w_i}, \tag{C.1}$$

where w_{0i} is the true value of w at ith point, a and b are constants, and δ_{w_i} is the random error for ith measurement. Since the true mean value of w is calculated as

$$\overline{w_0} = \frac{1}{n} \sum_{i=1}^{n} w_{0i} \tag{C.2}$$

with n being the total number of measurements of w during the sampling period ($n = 18000$ for 30 min), the mean value of w, calculated from w_i is then

$$\overline{w} = a\overline{w_0} + b. \tag{C.3}$$

The standard deviation of w, σ_w, is

$$\sigma_w^2 = \frac{1}{n} \sum_{i=1}^{n} (w_i - \overline{w})^2, \tag{C.4}$$

while the ideal standard deviation of w, σ_{w_0}, is

$$\sigma_{w_0}^2 = \frac{1}{n} \sum_{i=1}^{n} (w_{0i} - \overline{w_0})^2, \tag{C.5}$$

Combining *Equations C.1*, *C.2*, *C.3*, *C.4*, and *C.5* and considering $\sum\limits_{i=1}^{n}(w_{0i} - \overline{w_0})\delta_{w_i} \to 0$ give

$$\sigma_w^2 = a^2\sigma_{w_0}^2 + \frac{1}{n}\sum_{i=1}^{n}\delta_{w_i}^2. \tag{C.6}$$

Differentiating *Equation C.6* and dividing both sides by σ_w^2 results in an expression for the maximum relative error of σ_w

$$\frac{\delta_{\sigma_w}}{\sigma_w} = \frac{\sum\limits_{i=1}^{n}\delta_{w_i}^2}{n\sigma_w^2} \leq \frac{\delta_w^2}{\sigma_w^2}, \tag{C.7}$$

where δ_w is the maximum random error in measuring the vertical wind speed. According to the specifications of the sonic anemometer-thermometer (USA-1, Metek) used in this work, δ_w should be about 0.05 m s^{-1} for the range of w_i encountered during this work. Estimates using *Equation C.7* and σ_w data from the REA measurements show that for most of the measurements $\frac{\delta_{\sigma_w}}{\sigma_w}$ was less than 0.01 with a maximum of 0.11 when σ_w was very low.

C.2   Error in β

Since no substantial differences exist between the β values for the fluxes of various properties and temperature is commonly observed simultaneously during the REA measurements, β_T (i.e., β value for temperature) was chosen for calculating the REA fluxes for the gases. Provided that the sensible heat flux calculated using the EC method equals the flux calculated using the REA method, β_T can be expressed as

$$\beta_T = \frac{\overline{T'w'}}{\sigma_w(\overline{T^+} - \overline{T^-})} \equiv \frac{\overline{T'w'}}{\sigma_w \Delta T}, \tag{C.8}$$

where T' and w' represent the fluctuations of the air temperature and the vertical wind speed, respectively, T^+ and T^- represent the air temperatures associated with updrafts and downdrafts, respectively, and the overbars indicate averaging over the sampling period (30 min).

According to the error propagation theory, the relative error in β_T may be calculated from

$$\left(\frac{\delta_{\beta_T}}{\beta_T}\right)^2 = \left(\frac{\delta_{\overline{T'w'}}}{\overline{T'w'}}\right)^2 + \left(\frac{\delta_{\Delta T}}{\Delta T}\right)^2 + \left(\frac{\delta_{\sigma_w}}{\sigma_w}\right)^2, \tag{C.9}$$

where δ_{β_T}, $\delta_{\overline{T'w'}}$, $\delta_{\Delta T}$, and δ_{σ_w} are absolute errors in β_T, $\overline{T'w'}$, ΔT, and σ_w, respectively. Based on the statistics, $\overline{T'w'}$ is the covariance between T and w and may be expressed as

$$\overline{T'w'} = r_{Tw}\sigma_T\sigma_w, \tag{C.10}$$

where r_{Tw} is the correlation coefficient between T and w, σ_T and σ_w are the standard deviations in T and w, respectively. Differentiating *Equation C.10* leads to the following expression for $\delta_{\overline{T'w'}}$

$$\delta_{\overline{T'w'}} = r_{Tw}(\sigma_T\delta_{\sigma_w} + \sigma_w\delta_{\sigma_T}). \tag{C.11}$$

Combining *Equations C.10* and *C.11* gives

$$\frac{\delta_{\overline{T'w'}}}{\overline{T'w'}} = \frac{\delta_{\sigma_T}}{\sigma_T} + \frac{\delta_{\sigma_w}}{\sigma_w}. \tag{C.12}$$

Using the same approach to that used to derive *Equation C.7*, one can obtain

$$\frac{\delta_{\sigma_T}}{\sigma_T} = \frac{\sum_{i=1}^{n} \delta_{T_i}^2}{n\sigma_T^2} \le \frac{\delta_T^2}{\sigma_T^2}, \tag{C.13}$$

where T_i is the ith instant temperature, δ_{T_i} is the absolute error in T_i, and δ_T is the maximum random error in measuring the air temperature and is estimated to be about 0.01 Kelvin. The $\frac{\delta_{\sigma_T}}{\sigma_T}$ estimated for most REA runs was negligibly small (less than 0.005). In an extreme case, it reached a value of 0.02.

To estimate $\frac{\delta_{\Delta T}}{\Delta T}$ in *Equation C.9*, it is supposed that $\overline{T^+}$ and $\overline{T^-}$ had the same absolute error, i.e., $\delta_{\overline{T^+}} = \delta_{\overline{T^-}}$.

$$\overline{T^+} = \frac{1}{m}\sum_{i=1}^{m} T_i^+, \tag{C.14}$$

where $m \simeq \frac{n}{2}$. Error propagation results in

$$\delta_{\overline{T^+}} = \frac{1}{m}\sqrt{\sum_{i=1}^{m} \delta_{T_i^+}^2}. \tag{C.15}$$

Since $\delta_{T_i^+}$ is smaller than δ_T (the maximum random error of T),

$$\delta_{\overline{T^+}} \le \frac{\delta_T}{\sqrt{m}}. \tag{C.16}$$

Therefore,

$$\delta_{\Delta T} = \sqrt{\delta_{T^+}^2 + \delta_{T^-}^2} = \sqrt{2\delta_{T^+}^2} \leq \delta_T \sqrt{\frac{2}{m}} \qquad (C.17)$$

and

$$\frac{\delta_{\Delta T}}{\Delta T} \leq \frac{\delta_T}{\Delta T} \sqrt{\frac{2}{m}}. \qquad (C.18)$$

Combining *Equations C.7*, *C.9*, *C.12*, *C.13*, and *C.18* gives an estimate for the relative error in β_T,

$$\left(\frac{\delta_{\beta_T}}{\beta_T}\right) \leq \sqrt{\left(\frac{\delta_T^2}{\sigma_T^2} + \frac{\delta_w^2}{\sigma_w^2}\right)^2 + \frac{2}{m}\left(\frac{\delta_T}{\Delta T}\right)^2 + \left(\frac{\delta_w}{\sigma_w}\right)^4}. \qquad (C.19)$$

C.3 Error in $\left(\overline{c^+} - \overline{c^-}\right)$

Let V_s being the analyzed sample volume from the reservoirs for both updrafts and downdrafts, and $\overline{M^+}$ and $\overline{M^-}$ being the corresponding average masses of COS in the samples, the average COS concentrations for updrafts $\left(\overline{c^+}\right)$ and downdrafts $\left(\overline{c^-}\right)$ are calculated by

$$\overline{c^+} = \frac{\overline{M^+}}{V_s} \qquad (C.20)$$

and

$$\overline{c^-} = \frac{\overline{M^-}}{V_s}, \qquad (C.21)$$

respectively. Suppose that the systematic errors in the COS mass and the sample volume are ΔM and ΔV, respectively, then the relative systematic errors in $\overline{c^+}$ and $\overline{c^-}$ may be estimated by

$$\frac{\Delta\left(\overline{c^+}\right)}{\overline{c^+}} = \frac{\Delta M}{\overline{M^+}} + \frac{\Delta V_s}{V_s} \qquad (C.22)$$

and

$$\frac{\Delta\left(\overline{c^-}\right)}{\overline{c^-}} = \frac{\Delta M}{\overline{M^-}} + \frac{\Delta V_s}{V_s}, \qquad (C.23)$$

respectively. Since $\overline{M^+}$ and $\overline{M^-}$ are nearly simultaneously determined on the same analyzing system, $\Delta\left(\overline{c^+}\right)$ and $\Delta\left(\overline{c^-}\right)$ are not independent of each other, i.e., they have the same sign. Therefore, the systematic error in $\left(\overline{c^+} - \overline{c^-}\right)$ may be estimated by

$$\Delta\left(\overline{c^+} - \overline{c^-}\right) = \Delta\left(\overline{c^+}\right) - \Delta\left(\overline{c^-}\right). \qquad (C.24)$$

Combining *Equations C.20, C.21, C.22, C.23, and C.24* gives

$$\frac{\Delta\left(\overline{c^+} - \overline{c^-}\right)}{\overline{c^+} - \overline{c^-}} = \frac{\Delta V_s}{V_s}. \tag{C.25}$$

This is the formula for estimating the relative systematic error in $(\overline{c^+} - \overline{c^-})$. The random error in $(\overline{c^+} - \overline{c^-} \equiv \Delta C)$, i.e., $\delta_{\Delta C}$, may be estimated by

$$\delta_{\Delta C} = \sqrt{\delta^2_{\overline{c^+}} + \delta^2_{\overline{c^-}}}, \tag{C.26}$$

where $\delta_{\overline{c^+}}$ and $\delta_{\overline{c^-}}$ are the random errors in $\overline{c^+}$ and $\overline{c^-}$, respectively. To realistically estimate $\delta_{\Delta C}$, the standard errors of the mean for $\overline{c^+}$ and $\overline{c^-}$ are considered to be the representives of $\delta_{\overline{c^+}}$ and $\delta_{\overline{c^-}}$, respectively.

Appendix D

Measurements of atmospheric COS at the Taunus Observatory

D.1 Site

Atmospheric COS was measured at the Taunus Observatory (*Figure D.1*) on the summit of Kleiner Feldberg, Germany (50° 13′ N, 8° 27′ E, 815 m a.s.l). Kleiner Feldberg and the neighboring Grosser Feldberg (878 m a.s.l) form the highest crest of the Taunus mountains in the nature park Hochtaunus. Grosser Feldberg is located about 2 km northeast of Kleiner Feldberg. This orographic structure leads to a minimum of the wind frequency in the northeast direction at the sampling site. The prevailing wind directions are west to northwest.

Kleiner Feldberg is about 3-5 km distant from the nearest villages. The largest neighboring city, Frankfurt am Main (population: ∼0.65 Million), is located about 30 km southeast of the mountain. The Taunus mountains are covered with relatively dense coniferous and deciduous trees. However, the area of the observatory, i.e., the summit of Kleiner Feldberg, is a clearing which is covered mainly with grass and low growth.

D.2 Sampling

Air from 2 m above the ground was cryogenically (liquid argon, -186℃) enriched using the sampler shown in *Figure D.2*. The sampler consists of five silanized glass loops (Duran 50, 30 cm × 6 mm I.D.) filled with silanized glasswool, two Teflon selection valves (Rheodyne), a mass flow controller

Figure D.1: An aerial picture of the Taunus Observatory. The circle indicates the
sampling location.

(MFC, 0-1000 ml/min, Bronk Horst, Holland) and a vacuum pump. Each
sample was collected at a flow rate of 200 ml min^{-1} for 5 min, corresponding
to a sample volume of 1.00 L. Five consecutive samples were collected for each
sampling period to determine the average mixing ratio of COS in the period.
One to three sets of samples were collected and analyzed per working day.
Sampling usually took place at 8:00, 10:00, 12:00 and 14:00 Central European
Time.

D.3   Analysis

Samples were analyzed for COS immediately after sampling, using the GC/FPD
system shown in *Figure D.3*. Before analyzing a sample, sulfur compounds
trapped in the loop were transferred into a silanized capillary glass loop (20
cm length, filled with 2 cm glasswool) immersed in liquid argon for further
focusing. This was done by warming the sample loop with water at room tem-
perature, and passing nitrogen (99.999%, Messer Griesheim) through both
loops. After a transfer time of about 5 min, the sulfur compounds were
injected into a $5' \times \frac{1}{8}''$ Teflon column packed with Carbopack B 100HT (Su-
pelco) by switching the 6-way valve (Rheodyne) to its injection position, and
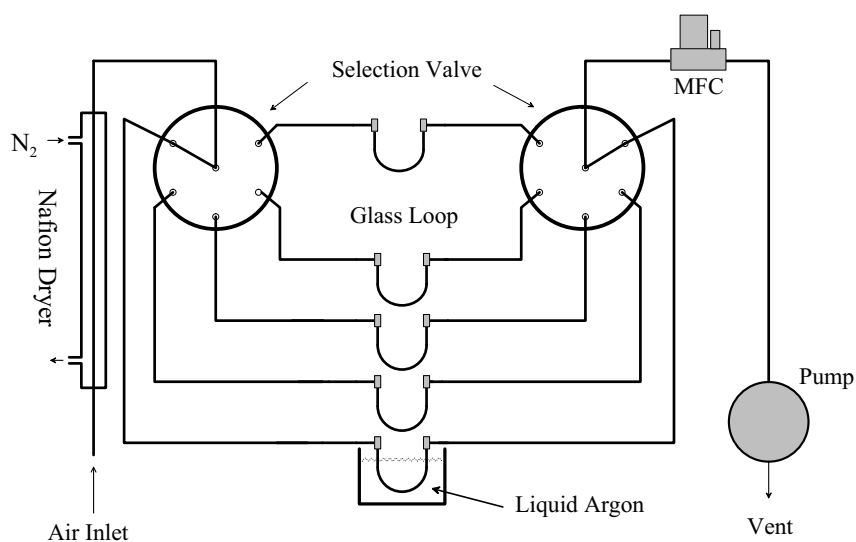
Figure D.2: Sampler for collecting atmospheric reduced sulfur gases.
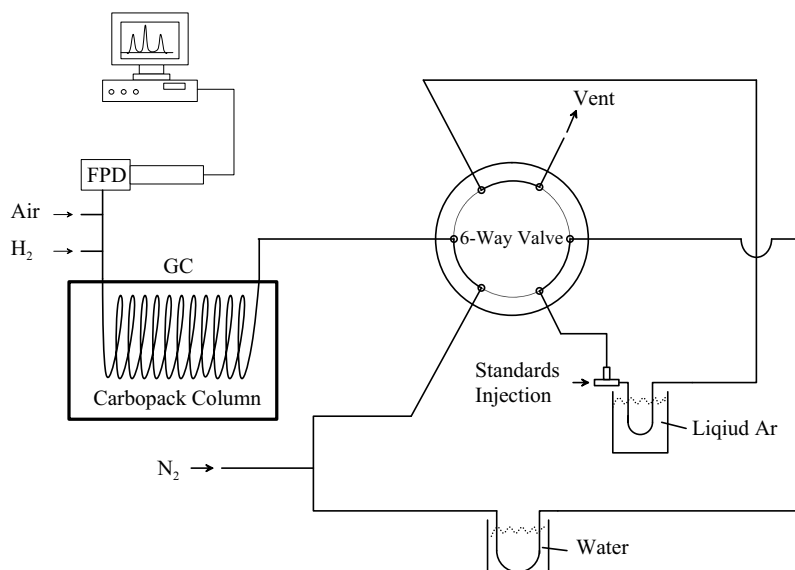
Figure D.3: GC/FPD system for analyzing sulfur gases in air samples collected using cryotraps.

warming at the same time the capillary glass loop with water. For optimal separation of the sulfur compounds the oven temperature of the GC (HP 5790A, Hewlett Packard) was held at 40°C for 2 min, and then heated to 80°C at the rate of 16°C min^{-1}. After separation, sulfur compounds were detected using a Tracor FPD. Chromatograms were acquired and processed by an E-Lab chromatography system (OMS-Technology) installed in a personal computer.

The GC/FPD system was calibrated daily by injecting standard gases from a permeation dilution device kept at 30.0±0.1°C. Permeation rates were determined gravimetrically about every half years. There was a rapid decrease of the permeation rate of the COS permeation tube between May 6 and October 29, 1998. This was not discovered until the end of October, 1998, leading to systematic errors in COS calibrations during this time period. Measurements during this period have been corrected using a method described in *Section D.4*. Even after correction, data from this period remain highly uncertain.

D.4   Correction of COS measurements at the Taunus Observatory between May 6 and October 29, 1998

Both COS and H$_2$S peaks are calibrated using standard gases from the permeation device. If the permeation rates of both gases are stable, the calibration curves should be:

$$\lg(M_{COS}) = a_{cos} + b_{cos}\lg(A_{COS}) \tag{D.1}$$

$$\lg(M_{H_2S}) = a_{H_2S} + b_{H_2S}\lg(A_{H_2S}), \tag{D.2}$$

where M_{COS} and M_{H_2S} are the injected masses of COS and H$_2$S, respectively, A_{COS} and A_{H_2S} are the peak areas of COS and H$_2$S, respectively, and a and b denote the intercepts and slopes of both calibration curves, respectively. Due to the decrease in the COS permeation rate, the calibration curve for COS changed to

$$\lg(M'_{COS}) = a'_{cos} + b'_{cos}\lg(A'_{COS}), \tag{D.3}$$

where M'_{COS} and A'_{COS} represent the changed mass and peak area for COS, respectively, and a'_{cos} and b'_{cos} the corresponding intercept and slope, respectively. The change in COS permeation rate was not discovered at that
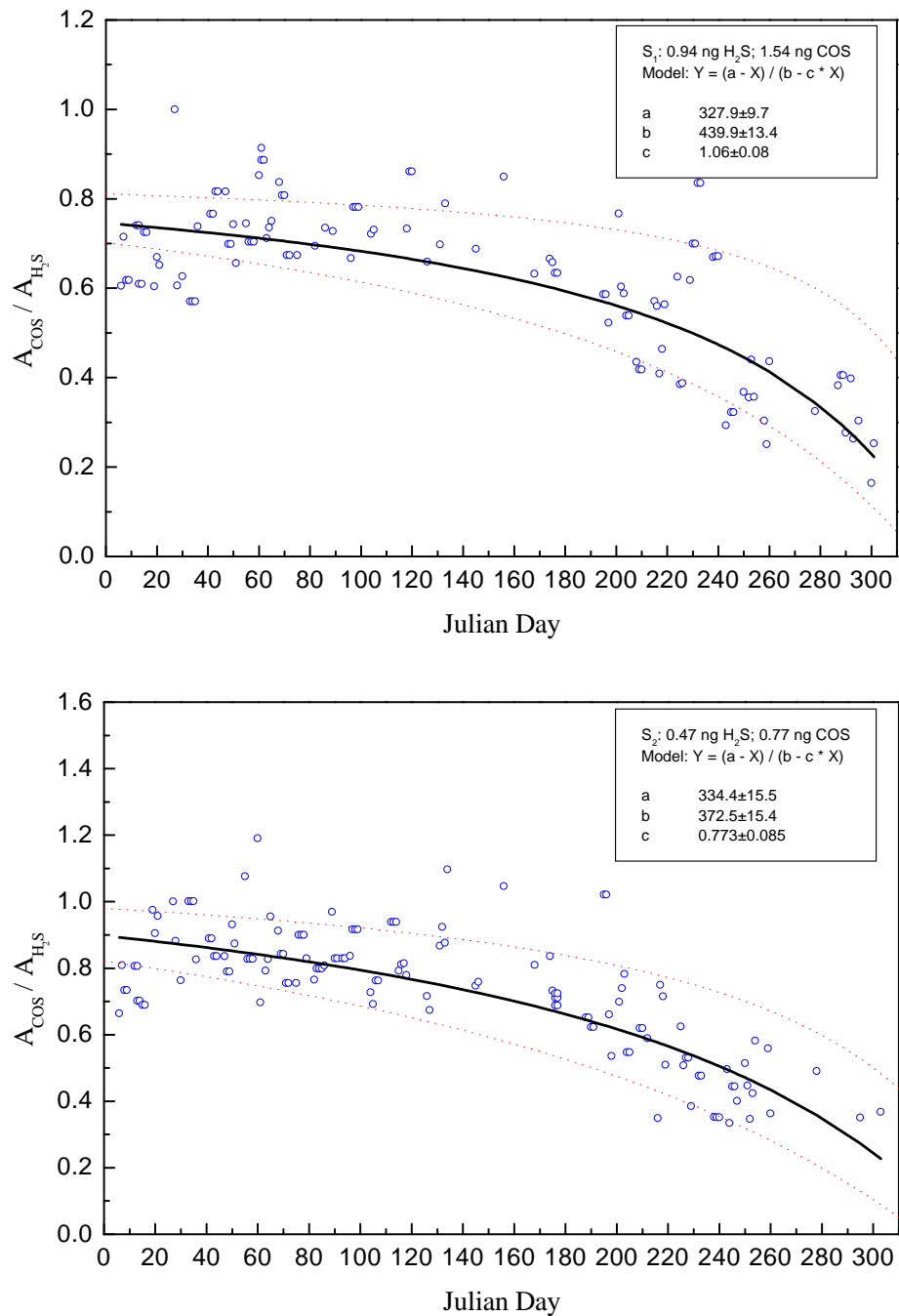
Figure D.4: Decline of the ratio $\frac{A_{COS}}{A_{H_2S}}$ of the standard samples S_1 (up) and S_2 (bottom) caused by the decrease in COS permeation rate between May and October, 1998. The solid lines represent nonlinear fits to the data points. The dotted lines show the 95% confidence belts of the fits.

time, the unchanged COS mass M_{COS} instead of M'_{COS} was used for calibrating COS peaks. As a result, a'_{cos} and b'_{cos} were both false.

The absolute values of the COS and H_2S peak areas may vary between calibrations because of the fluctuation in the sensitivity of the FPD. The ratio $\frac{A_{COS}}{A_{H_2S}}$ should be close to constant. However, $\frac{A_{COS}}{A_{H_2S}}$ declined after April, 1998, due to the decrease in the COS permeation rate, as shown in *Figure D.4*. The dependence of the ratio on time was obtained for the standards S_1 and S_2 by means of a nonlinear fit. The results are

$$\frac{A'_{COS}}{A_{H_2S}} = \frac{328 - t}{440 - 1.06t} \quad for \ S_1 \tag{D.4}$$

$$\frac{A'_{COS}}{A_{H_2S}} = \frac{328 - t}{440 - 1.06t} \quad for \ S_2, \tag{D.5}$$

where t is the number of days. At t=day 0, $A'_{COS} \to A_{COS}$ and

$$\frac{A_{COS}}{A_{H_2S}} = \frac{328}{440} = 0.745 \quad for \ S_1 \tag{D.6}$$

$$\frac{A_{COS}}{A_{H_2S}} = \frac{334}{373} = 0.895 \quad for \ S_2. \tag{D.7}$$

Combining *Equations D.4* and *D.6* gives

$$A_{COS} = A'_{COS}\frac{0.745(440 - 1.06t)}{328 - t} \quad for \ S_1. \tag{D.8}$$

Combining *Equations D.5* and *D.7* gives

$$A_{COS} = A'_{COS}\frac{0.895(373 - 0.773t)}{334 - t} \quad for \ S_2. \tag{D.9}$$

Equations D.8 and *D.9* were used for correcting the measurements between May 6 and 29 October, 1998. As a comparison, data before and after the correction are plotted in *Figure D.5*. It is difficult to judge the results of such a correction, because the true course of the COS mixing ratio is not known. The uncertainty in the corrected values could be quite large because of the large uncertainty in the fitted parameters in *Equations D.4* and *D.5*.
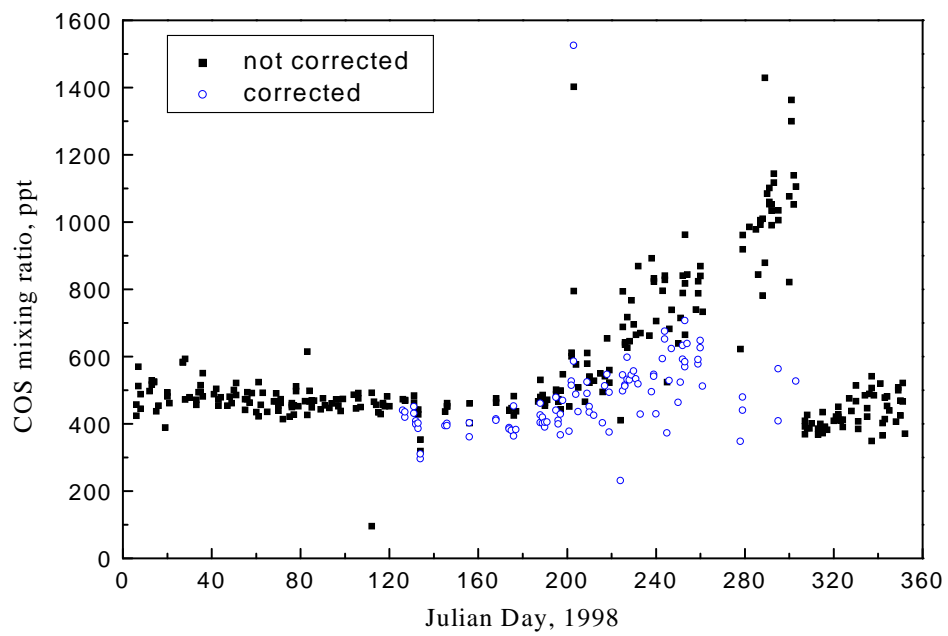
Figure D.5: Mixing ratios of atmospheric COS at the Taunus Observatory in 1998 before and after the corrections of the measurements between May 6 and 29 October, 1998.

List of Figures

List of Tables

List of Chemical Symbols

3-MPA	3-mercaptopropionic acid
CF_2Cl_2	dichlordifluormethane
$CFCl_3$	trichlorfluormthane
CH_3SH	methyl mercaptan (also MeSH)
CO	carbon monoxide
CO_2	carbon dioxide
COS	carbonyl sulfide
CS_2	carbon disulfide
CYS	cysteine
DMS	dimethyl sulfide
GSH	glutathione
H_2O	water
H_2S	hydrogen sulfide
H_2SO_4	sulfuric acid
HNO_3	nitric acid
HS	sulfhydryl radical
$Mg(ClO_4)_2$	magnesium perchlorate
N_2O	nitrous oxide
NH_3	ammonia
NO	nitric oxide
NO_2	nitrogen dioxide
O	atomic oxygen (ground state)
$O(^3P)$	atomic oxygen (ground state)
OH	hydroxyl radical
OH^-	hydroxide ion
RS	thiyl radical
S	atomic sulfur
SO	sulfur monoxide
SO_2	sulfur dioxide

List of Abbreviations

AMT	Atlantic Meridional Transect
ANT-XV/1	the 15th Antarctic Expedition / Section 1
ANT-XV/5	the 15th Antarctic Expedition / Section 5
a.s.l.	above sea level
CA	carbonic anhydrase
CDOM	chromophoric dissolved organic matter
CMDL	Climate Monitoring and Diagnostics Laboratory
CZCS	Coastal Zone Color Scanner
DAAC	Distributed Active Archive Center
DOM	dissolved organic matter
DWD	Deutscher Wetterdienst (Germany Weather Service)
EC	eddy correlation
EPC	electronic pneumatic control
ESA	European Space Agency
FBM	Frankfurt Biosphere Model
FFT	Fast Fourier Transform
FPD	flame photometric detector
GAW	Global Atmospheric Watch
GC	gas chromatograph
GEOSECS	Geochemical Ocean Sections Study
GPS	Global Positioning System
HA	humic acid
IFB	Institute for Bioclimatology
IHR	interhemispheric ratio
ITCZ	Intertropical Convergence Zone
MFC	mass flow controller
MLRA	multiple linear regression analysis
NASA	National Aeronautics and Space Administration
NIST	National Institute of Standards and Technology
NOAA	National Oceanic and Atmospheric Administration
NPP	net primary production

PAR	photosynthetically active radiation
PTFE	polytetrafluoroethylene
PVF	polyvinyl fluoride
REA	relaxed eddy accumulation
R/V	research vessel
SeaWiFs	Sea-viewing Wide Field-of-view Sensor
TTO	Transient Tracers in the Ocean
UV	ultraviolet

Bibliography

Adams, D. F., S. O. Farwell, M. R. Pack, and E. Robinson, Biogenic sulfur gas emissions from soils in eastern and southern United States, *J. Air Pollut. Control. Assoc.*, *31*, 1083–1089, 1981.

Aiken, J., D. G. Cummings, S. W. Gibb, N. W. Rees, R. Woodd-Walker, E. M. S. Woodward, J. Woolfenden, S. B. Hooker, J.-F. Berthon, C. D. Dempsey, D. J. Suggett, P. Wood, C. Donlon, N. Gonzalez-Benitez, I. Huskin, M. Quevedo, R. Barciela-Fernandez, C. de Vargas, and C. Mc-Kee, AMT-5 Cruise, NASA Report Tech. Memo. 1998-206892, Vol. 2, edited by S. B. Hooker and E. R. Firestone, *Technical Report 2*, NASA Goddard Space Flight Center, Greenbelt, Maryland, 1998.

Andreae, M. O., The ocean as a source of atmospheric sulfur compounds, in *The role of air-sea exchange in geochemical cycling*, edited by P. Buat-Ménard, pp. 331–362, D. Reidel, Dordrecht, 1986.

Andreae, M. O., Biomass burning: Its history, use, and distribution and its impact on environmental quality and global climate, in *Global biomass burning, Atmospheric, climatic, and biospheric implications*, edited by Joel S. Levine, pp. 1–21, MIT Press, Cambridge, MA, 1991.

Andreae, M. O. and P. J. Crutzen, Atmospheric aerosols: Biogeochemical sources and role in atmospheric chemistry, *Science*, *276*, 1052–1058, 1997.

Andreae, M. O. and R. J. Ferek, Photochemical production of carbonyl sulfide in seawater and its emission to the atmosphere, *Global Biogeochem. Cycles*, *6*, 175–183, 1992.

Aneja, V. P., J. H. Overton Jr., L. T. Cupitt, J. L. Durham, and W. E. Wilson, Carbon disulphide and carbonyl sulfide from biogenic sources and their contributions to the global sulfur cycle, *Nature*, *282*, 493–496, 1979.

Bandy, A. R., D. C. Thornton, D. L. Scott, M. Lalevic, E. E. Lewin, and A. R. Driedger, A time series for carbonyl sulfide in the northern hemisphere, *J. Atmos. Chem.*, *14*, 527–534, 1992.

Bange, H. W., S. Rapsomanikis, and M. O. Andreae, The Aegean Sea as a source of atmospheric nitrous oxide and methane, *Marine Chemistry*, *53*, 41–49, 1996.

Barnes, I., K. H. Becker, and I. Patroescu, The tropospheric oxidation of DMS: A new source of COS, *Geophys. Res. Lett.*, *21(22)*, 2389–2392, 1994.

Barnes, I. and D. J. Hofmann, Lidar measurements of stratospheric aerosol over Mauna Loa, *Geophys. Res. Lett.*, *24*, 1923–1926, 1997.

Bartell, U., U. Hofmann, B. Kreuzburg, M. O. Andreae, and J. Kesselmeier, COS and H_2S fluxes over a wet meadow in relation to photosynthetic activity: An analysis of measurements made on 6 September 1990, *Atmos. Environ.*, *27*, 1851–1864, 1993.

Bates, T. S., B. K. Lamb, A. Guenther, J. Dignon, and R. E. Stoiber, Sulfur emissions to the atmosphere from natural sources, *J. Atmos. Chem.*, *14*, 315–337, 1992.

Beier, N., Measuring fluxes of chemical components by eddy accumulation, in *Proc. 7th Symp. on Meteorological Observations and Instrumentation, New Orleans, LA, 13-18 January*, pp. 1–5, American Meteorological Society, Boston, MA, 1991.

Bekki, S. and J. A. Pyle, Two-dimensional assessment of the impact of aircraft sulphur emissions on the stratospheric sulphate aerosol layer, *J. Geophys. Res.*, *7(D14)*, 15,839–15,847, 1992.

Belviso, S., N. Mihalopoulos, and B. C. Nguyen, The supersaturation of COS in rain waters, *Atmos. Environ.*, *21(6)*, 1363–1367, 1987.

Belviso, S., B. C. Nguyen, and P. Allard, Estimate of carbonyl sulfide (OCS) volcanic source strength deduced from OCS/CO_2 ratios in volcanic gases, *Geophys. Res. Lett.*, *3*, 133–136, 1986.

Berresheim, H. and V. D. Vulcan, Vertical distributions of COS, CS_2, DMS and other sulfur compounds in a loblolly pine forest, *Atmos. Chem.*, *26A(11)*, 2031–2036, 1992.

Beverland, I. J., R. Milne, C. Biossard, D. H. ONeill, J. B. Moncrieff, and C. N. Hewitt, Measurement of carbon dioxide and hydrocarbon fluxes from a sitka spruce forest using micrometeorological techniques, *J. Geophys. Res.*, *101*, 22,807–22,815, 1996a.

Beverland, I. J., J. B. Moncrieff, D. H. Oneill, and K. J. Hargreaves R. Milne, Measurement of methane and carbon dioxide fluxes from peatland ecosystems by the conditional-sampling technique, *Q. J. R. Meteorol. Soc.*, *122*, 819–838, 1996b.

Bingemer, H. G., M. O. Andreae, T. W. Andreae, P. Artaxo, G. Helas, D. J. Jacob, N. Mihalopoulos, and B. C. Nguyen, Sulfur gases and aerosols in and above the equatorial African rain forest, *J. Geophys. Res.*, *97(D6)*, 6207–6217, 1992.

Bingemer, H. G., S. Bürgermeister, R. L. Zimmermann, and H.-W. Georgii, Atmospheric COS: Evidence for a contribution of anthropogenic sources?, *J. Geophys. Res.*, *95*, 20,617–20,622, 1990.

Blezinger, S., C. Wilhelm, and J. Kesselmeier, Enzymatic consumption of carbonyl sulfide (COS) by marine algae, *Biogeochem.*, *48(2)*, 185–197, 2000.

Brown, K. A. and J. N. B. Bell, Vegetation - the missing sink in the global cycle of COS, *Atmos. Environ.*, *20*, 537–540, 1986.

Buckley, D. J., R. L. Desjardins, J. L. M. Lalonde, and R. Brunke, A linearized, fast response gas sampling apparatus for eddy accumulation studies, *Comput. Electron. Agric.*, *2*, 243–250, 1988.

Businger, J. A. and S. P. Oncley, Flux measurement with conditional sampling, *J. Atmos. Ocean. Technol.*, *2*, 349–352, 1990.

Butler, J. H., J. W. Elkins, C. M. Brunson, K. B. Egan, T. M. Thompson, T. J. Conway, and B. D. Hall, Trace gases in and over the West Pacific and East Indian Oceans during the El Niño Southern Oscillation event of 1987, *Technical Report ERL ARL-16*, NOAA, Air Resource Lab, Silver Spring, Md., 1988.

Cadle, R. D., A comparison of volcanic and other fluxes of atmospheric trace gas constituents, *Rev. Geophys. Space Phys.*, *18*, 746–752, 1980.

Carroll, M. A., Measurements of COS and CS_2 in the free troposphere, *J. Geophys. Res.*, *90*, 10,483–10,486, 1985.

Carroll, M. A., L. E. Heidt, R. J. Cicerone, and R. G. Prinn, OCS, H_2S, and CS_2 fluxes from a salt water marsh, *J. Atmos. Chem.*, *4*, 375–395, 1986.

Castro, M. S. and J. N. Galloway, A comparison of sulfur-free and ambient air enclosure techniques for measuring the exchange of reduced sulfur gases between soils and the atmosphere, *J. Geophys. Res.*, *96*, 15,427–15,437, 1991.

Cellier, P. and Y. Brunet, Flux-gradient relationships above tall plant canopies, *Agric. For. Meteorol.*, *58*, 93–117, 1992.

Chameides, W. L., F. Fehsenfeld, M. O. Rodgers, C. Cardelino, J. Martinez, D. Parrish, W. Lonneman, D. R. Lawson, R. A. Rasmussen, P. Zimmerman, J. Greenberg, P. Middleton, and T. Wang, Ozone precursor relationships in the ambient atmosphere, *J. Geophys. Res.*, *97(D5)*, 6037–6055, 1992.

Chin, M., *An atmospheric studies of carbonyl sulfide and carbon disulfide and their relationship to stratospheric background sulfur aerosol*, Ph.D. thesis, Ga. Inst. of Technol., Atlanta, 1992.

Chin, M. and D. D. Davis, Global sources and sinks of OCS and CS_2 and their distributions, *Global Biogeochem. Cycles*, *7*, 321–337, 1993.

Chin, M. and D. D. Davis, A reanalysis of carbonyl sulfide as a source of stratospheric background sulfur aerosol, *J. Geophys. Res.*, *100(D5)*, 8993–9005, 1995.

Conrad, R. and K. Meuser, Soils contain more than one activity cosuming carbonyl sulfide, *Atmos. Environ.*, *34*, 3635–3639, 2000.

Conrad, R, W. Seiler, G. Bunse, and H. Giehl, Carbon monoxide in seawater (Atlantic Ocean), *J. Geophys. Res.*, *87*, 8839–8852, 1982.

Crutzen, P. J., The possible importance of CSO for the sulfate layer of the stratosphere, *Geophys. Res. Lett.*, *3*, 73–76, 1976.

Crutzen, P. J. and M. O. Andreae, Biomass burning in the tropics: Impact on atmospheric chemistry and biogeochemical cycles, *Science*, *250*, 1669–1678, 1990.

Crutzen, P. J., A. C. Delany, J. Greenberg, P. Haagenson, L. Heidt, R. Leub, W., Pollock, W. Seiler, A. Wartburg, and P. Zimmerman, Tropospheric chemical composition measurements in Brazil during the dry season, *J. Atmos. Chem.*, *2*, 33–256, 1985.

Crutzen, P. J., L. E. Heidt, J. P. Krasnec, W. H. Pollock, and W. Seiler, Biomass burning as a source of atmospheric gases CO, H_2, N_2O, NO, CH_3Cl and COS, *Nature*, *282*, 253–256, 1979.

De Bruyn, W. J., E. Swartz, J. H. Hu, J. A. Shorter, P. Davidovits, D. R. Worsnop, M. S. Zahniser, and C. E. Kolb, Henry's law solubilities and Setchenow Coefficients for biogenic reduced sulfur species obtained from gas-liquid uptake measurements, *J. Geophys. Res.*, *100*, 7245–7251, 1995.

De Mello, W. Z. and M. E. Hines, Application of static and dynamic enclosures for determining dimethyl sulfide and carbonyl sulfide exchange in sphagnum peatlands: Implications for the magnitude and direction of flux, *J. Geophys. Res.*, *99*, 14,601–14,607, 1994.

den Hartog, G. D. and H. H. Neumann, An empirical study on dry deposition of air pollutants to forests, Project description, *Technical Report AQRB-84-011-L*, AES, Canada, 1984.

Denmead, O. T. and E. F. Bradley, Flux-gradient relationships in a forest canopy, in *The Forest-Atmosphere Interaction*, edited by B. A. Hutchison and B. B. Hicks, pp. 421–442, D. Reidel Publishing Company, Dordrecht, Boston, Lancaster, 1985.

Desjardins, R. L., *A study of carbon dioxide and sensible heat fluxes using the eddy correlation technique*, Ph.D. thesis, Cornell University, 1972.

Dippel, J. and W. Jaeschke, A comparison between natural and anthropogenic emissions of the reduced sulfur compounds H_2S, COS, and CS_2 in a tropical industrialized region, *J. Atmos. Chem.*, *25*, 251–270, 1996.

Ellenberg, H., R. Mayer, and J. Schauermann, *Ökosystemforschung - Ergebnisse des Sollingprojektes 1966-1986*, Verlag Eugen Ulmer, Stuttgart, 1986.

Elliot, S., E. Lu, and F. S. Rowland, Rates and mechanisms of the hydrolysis of carbonyl sulfide in natural waters, *Environ. Sci. & Technol.*, *23*, 458–461, 1989.

Engel, A. and U. Schmidt, Vertical profile measurements of carbonylsulfide in the stratosphere, *Geophys. Res. Lett.*, *21*, 2219–2222, 1994.

Erickson, D. J., III, Variations in the global sea-air transfer velocity field of CO_2, *Global Biogeochem. Cycles*, *3*, 37–41, 1989.

Erickson, D. J., III, A stability dependent theory for air-sea gas exchange, *J. Geophys. Res.*, *98*, 8471–8488, 1993.

Erickson, D. J., III and B. E. Eaton, Global biogeochemical cycling estimates with CZCS satellite data and general circulation models, *Geophys. Res. Let.*, *20(8)*, 683–686, 1993.

Fall, R., D. L. Albritton, F. C. Fehnsenfeld, W. C. Kuster, and P. D. Goldan, Laboratory studies of some environmental variables controlling sulfur emissions from plants, *J. Atmos. Chem.*, *6*, 341–362, 1988.

Fan, S.-M., S. C. Wofsy, P. S. Bakwin, and D. J. Jacob, Micrometeorological measurements of CH_4 and CO_2 exchange between the atmosphere and subarctic tundra, *J. Geophys. Res.*, *97*, 16,627–16,643, 1992.

Ferek, R. J. and M. O. Andreae, The supersaturation of carbonyl sulfide in surface waters of the Pacific Ocean off Peru, *Geophys. Res. Lett.*, *10*, 393–396, 1983.

Ferek, R. J. and M. O. Andreae, Photochemical production of carbonyl sulphide in marine surface waters, *Nature*, *307*, 148–150, 1984.

Finnigan, J. J., Turbulent transport in flexible plant canopies, in *The Forest-Atmosphere Interaction*, edited by B. A. Hutchison and B. B. Hicks, pp. 443–480, D. Reidel Publishing Company, Dordrecht, Boston, Lancaster, 1985.

Flöck, O. R. and M. O. Andreae, Photochemical and non-photochemical formation and destruction of carbonyl sulfide and methyl mercaptan in ocean waters, *Mar. Chem.*, *54*, 11–26, 1996.

Flöck, O. R., M. O. Andreae, and M. Dräger, Environmentally relevant precursors of carbonyl sulfide in aquatic systems, *Mar. Chem.*, *59*, 71–85, 1997.

Freney, J. R., M. V. Ivanov, and H. Rodhe, The sulfur cycle, in *The major biogeochemical cycles and their interactions*, edited by B. Bolin and R. B. Cook, pp. 56–61, John Wiley & Sons, Chichester, 1983.

Freney, J. R. and C. H. Williams, The sulfur cycle in soil, in *The Global biogeochemical cycle*, edited by M. V. Ivanov and J. R. Freney, pp. 129–201, John Wiley & Sons, Chichester, 1983.

Fried, A. and B. Henry, Potential calibration errors in carbonyl sulfide permeation devices: Implications for atmospheric studies, *J. Geophys. Res.*, *103(D15)*, 18,895–18,906, 1998.

Fried, A., B. Henry, R. A. Ragazzi, M. Merrick, J. Stokes, T. Pyzdrowski, and R. Sams, Measurements of carbonyl sulfide in automotive emission and an assessment of its importance to the global sulfur cycle, *J. Geophys. Res.*, *97(D13)*, 14,621–14,634, 1992.

Fried, A., L. F. Klinger, and D. J. Erickson III, Atmospheric COS exchange in bog microcosms, *Geophys. Res. Lett.*, *20(2)*, 129–132, 1993.

Garrat, J. R., Flux profile relationships above tall vegetaion, *Q. J. R. Meteorol. Soc.*, *104*, 199–211, 1978.

Garrat, J. R., Surface influence upon vertical profiles in the atmospheric near-surface layer, *Q. J. R. Meteorol. Soc.*, *106*, 803–819, 1980.

Gash, J. H. C., A note on estimating the effect of a limit fetch on micrometeorological evaporation measurements, *Bound.-Layer Meteorol.*, *35*, 409–413, 1986.

Gettelman, A., The evaluation of aircraft emissions in the stratosphere, *Geophys. Res. Lett.*, *25(12)*, 2129–2132, 1998.

Giovanelli, J., Sulfur amino acids of plants: an overview, in *Methods in Enzymology*, edited by W.B. Jacoby and O.W. Griffith, volume 143, pp. 419–426, Academic Press, New York, 1987.

Goldan, P. D., R. Fall, W. C. Kuster, and F. C. Fehnsenfeld, Uptake of COS by growing vegetation: A major tropospheric sink, *J. Geophys. Res.*, *93*, 14,186–14,192, 1988.

Goldan, P. D., W. C. Kuster, D. L. Albritton, and F. C. Fehsenfeld, The measurement of natural sulfur emissions from soil and vegetation: Three sites in the Eastern United States revisited, *J. Atmos. Chem.*, *5*, 439–467, 1987.

Golombek, A. and R. G. Prinn, A global three-Dimensional model of the stratospheric sulfuric acid layer, *J. Atmos. Chem.*, *16*, 179–199, 1993.

Grainier, C. and G. Brasseur, Impact of heterogeneous chemistry on model predictions of ozone changes, *J. Geophys. Res.*, *97(D16)*, 18,015–18,033, 1992.

Gries, C., T. H. Nash III, and J. Kesselmeier, Exchange of reduced sulfur gases between lichens and the atmosphere, *Biogeochem.*, *6*, 25–39, 1994.

Griffith, D. W. T., N. B. Jones, and W. A. Matthews, Interhemispheric ratio and annual cycle of carbonyl sulphide (OCS) total column from ground-based solar FTIR spectra, *J. Geophys. Res.*, *103(D7)*, 8447–8454, 1998.

Guenther, A., W. Baugh, K. Davis, G. Hampton, P. Harley, L. Klinger, L. Vierling, P. Zimmerman, E. Allwine, S. Dilts, B. Lamb, H. Westberg, D. Baldocchi, C. Geron, and T. Pierce, Isoprene fluxes measured by enclosure, relaxed eddy accumulation, surface layer gradient, mixed layer gradient, and mixed layer mass balance techniques, *J. Geophys. Res.*, *101(D13)*, 18,555–18,567, 1996.

Hanst, P. L., L. L. Spiller, D. M. Watts, J. W. Spence, and M. F. Miller, Infrared measurement of fluorocarbons, carbon tetrachloride, carbonyl sulfide, and other atmospheric trace gases, *J. Air Pollut. Cont. Ass.*, *25(12)*, 1220–1226, 1975.

Harnisch, J, R. Borchers, and P. Fabian, COS, CS_2 and SO_2 in aluminium smelter exhaust, *Environ. Sci. & Pollut. Res.*, *2(4)*, 229–232, 1995a.

Harnisch, J., R. Borchers, P. Fabian, and K. Kourtidis, Aluminium production as a source of Atmospheric carbonyl sulfide (COS), *Environ. Sci. & Pollut. Res.*, *2(3)*, 161–162, 1995b.

Hartmann, D. L., Global Physical Climatology, in *International Geophysical Series*, edited by R. Dmowska and J. R. Holton, Vol. 56, Academic Press, Inc., New York, 1994.

Haunold, W., G. Ockelmann, and H.-W. Georgii, Neuartiger Gaschromatograph zur Messung von SO_2 und reduzierten schwefelgasen in Reinluftgebieten, *Staub-Reinhaltung der Luft*, *49*, 191–193, 1989.

Hicks, B. B. and R. T. McMillen, A simulation of the eddy accumulation method for measuring pollutant fluxes, *J. Clim. Appl. Meteor.*, *23*, 637–643, 1984.

Himmelblau, D. M., Diffusion of dissolved gases in liquids, *Chem. Rev.*, *64*, 527–550, 1964.

Hines, M. E. and M. C. Morrison, Emission of biogenic sulfur gases from Alaskan tundra, *J. Geophys. Res.*, *97(D15)*, 16,703–16,707, 1992.

Hofmann, D. J., Increase in the stratospheric background sulfuric acid aerosol mass in the past 10 years, *Science*, *248*, 996–1000, 1990.

Hofmann, D. J., Aircraft sulphur emissions, *Nature*, *349*, 659, 1991.

Hofmann, D. J., Atmospheric Carbon Dioxide - Current Understanding and Plans for Future Research: CMDL Testimony on Terrestrial Carbon Dioxide Uptake to US Senate Subcommittee, *Technical report*, NOAA Climate Monitoring and Diagnostics Laboratory, 2000.

Hofmann, D. J., J. M. Rosen, and J. M. Kiernan, Stratospheric aerosol measurements, IV, Global time variations of the aerosol burden and source consideration, *J. Atmos. Sci.*, *33*, 1782–1788, 1976.

Hofmann, U., *Vergleichende Untersuchungen zum Austausch von reduzierten Schwefelverbindungen zwischen Vegetation und Atmosphäre im Feldversuch und unter kontrollierten Bedingungen*, Ph.D. thesis, Universität Mainz, 1993.

Hofmann, U., R. Hofmann, and J. Kesselmeier, Field measurements of reduced sulfur compounds over wheat during a growing season, in *Precipitation scavenging and atmosphere-surface exchange. Volume 2: Atmosphere-Surface Exchange Processes*, edited by S. E. Schwartz and W. G. N. Slinn, pp. 967–977, Hemisphere, Washington, DC, 1992.

Hoge, F. E., M. E. Williams, R. N. Swift, J. K. Yungel, and A. Vodacek, Satellite retrieval of the absorbance coefficient of chromophoric dissolved organic matter in continental margins, *J. Geophys. Res.*, *100*, 24,847–24,854, 1995.

Huber, B., *Austausch flüchtiger Schwefelverbindungen in land- und forstwirtschaftlichen Ökosystemen*, Wissenschaftsverlag Maraun, Frankfurt, 1994.

Ibrom, A., C. Schuetz, T. Tworek, K. Morgenstern, A. Oltchev, M. Falk, J. Constaintin, and G. Gravenhorst, Eddy-correlation measurements of the fluxes of CO_2 and H_2O above a spruce stand, *Phy. and Chem. Earth*, *21*, 409–414, 1996.

Inn, E. C. Y., J. F. Vedder, and D. O'Hara, Measurement of stratospheric sulfur constituents, *Geophys. Res. Lett*, *8*, 5–8, 1981.

Inn, E. C. Y., J. F. Vedder, B. J. Tyson, and D. O'Hara, COS in the stratosphere, *Geophys. Res. Lett.*, *6(3)*, 191–193, 1979.

Jähne, B., K. O. Münnich, R. B. A. Dutzi, W. Huber, and P. Libner, On the parameters influencing air-water gas exchange, *J. Geophys. Res.*, *92*, 1937–1949, 1987.

Johnson, J. E., The lifetime of carbonyl sulfide in the troposphere, *Geophys. Res. Lett.*, *8*, 934–940, 1981.

Johnson, J. E., *The role of the oceans in the atmospheric cycle of carbonyl sulfide*, Ph.D. thesis, University of Washington, 1985.

Johnson, J. E., A. R. Bandy, D. C. Thornton, and T. S. Bates, Measurements of atmospheric carbonyl sulfide during the NASA Chemical Instrument Test and Evaluation Project: Implications for the global COS budget, *J. Geophys. Res.*, *98*, 23,443–23,448, 1993.

Johnson, J. E. and T. S. Bates, Atmospheric Measurements of carbonyl sulfide, dimethyl sulfide, carbon disulfide using ECD, *J. Geophys. Res.*, *98(D12)*, 23,411–23,421, 1993.

Johnson, J. E. and H. Harrison, Carbonyl sulfide concentrations in the surface waters and above the Pacific Ocean, *J. Geophys. Res.*, *91*, 7883–7888, 1986.

Kaimal, J. C., J. C. Wyngaard, Y. Izumi, and O. R. Cot, Spectral characteristics of surface-layer turbulence, *Quart. J. R. Met. Soc.*, *98*, 563–589, 1972.

Kesselmeier, J., F. X. Meixner, U. Hofmann, A.-L. Ajavon, S. Leimbach, and M. O. Andreae, Reduced sulfur compounds exchange between the atmosphere and tropical tree species in southern Cameroon, *Biogeochem.*, *23*, 23–45, 1993.

Kesselmeier, J. and L. Merk, Exchange of carbonyl sulfide (COS) between agricultural plants and the atmosphere: Studies on the deposition of COS to peas, corn and rapeseed, *Biogeochem.*, *23*, 47–59, 1993.

Kesselmeier, J., N. Teusch, and U. Kuhn, Controlling variables for the uptake of atmospheric carbonyl sulfide (COS) by soil, *J. Geophys. Res.*, *104(D9)*, 11,577–11,584, 1999.

Khalil, M. A. K. and R. A. Rasmussen, Global sources, lifetimes and mass balances of carbonyl sulfide (OCS) and carbon disulfide (CS_2) in the Earth's atmosphere, *Atmos. Environ.*, *8(9)*, 1805–1813, 1984.

Kindermann, J., G. Würth, and G. H. Kohlmaier, Interannual variation of carbon exchange fluxes in terrestrial ecosystems, *Global Biogeochem. Cycles*, *10*, 737–755, 1996.

Kjellström, E., A three-dimensional global model study of carbonyl sulfide in the troposphere and the lower stratosphere, *J. Atmos. Chem.*, *29*, 151–177, 1998.

Kluczewski, S. M., J. N. B. Bell, K. A. Brown, and M. J. Minski, The uptake of ^{35}S-carbonyl sulphide by plants and soils, in *Ecological aspects of radionuclide release, Special Publication of British Ecological Society III*, edited by P. J. Coughtrey, pp. 91–104, Blackwell Scientific Press, Oxford, 1983.

Kluczewski, S. M., K. A. Brown, and J. N. B. Bell, Deposition of [^{35}S]-carbonyl sulphide to vegetable crops, *Radiat. Prot. Dosim*, *11*, 173–177, 1985.

Kourtidis, K. A., R. Borchers, P. Fabian, and J. Harnisch, Carbonyl sulfide (COS) measurements in the Arctic polar vortex, *Geophys. Res. Lett.*, *22(4)*, 393–396, 1995.

Kramm, G., N. Beier, R. Dlugi, and H. Müller, Evaluation of conditional sampling methods, *Contr. Atmos. Phys.*, *72*, 2, 1999.

Kuhn, U., *Spurengasaustausch klimarelevanter reduzierter Schwefelverbindungen zwischen Biosphäre und Atmosphäre: COS Transfer der Flechten und anderer biotischer Kompartimente*, Ph.D. thesis, Universität Mainz, 1997.

Kuhn, U., C. Ammann, A. Wolf, F. X. Meixner, M. O. Andreae, and J. Kesselmeier, Carbonyl sulfide exchange on an ecosystem scale: Soil represents a dominant sink for atmospheric COS, *Atmos. Environ.*, *33(6)*, 995–1008, 1999.

Kuhn, U. and J. Kesselmeier, Lichens involved in the exchange of carbonyl sulfide between the biosphere and the atmosphere, in *The Proceedings of EUROTRAC Symposium '96*, edited by P. M. Borrell, P. Borrell, T. Cvitas, K. Kelly, and W. Seiler, pp. 189–196, Computational Mechanics Publications, Southampton, 1996.

Kuhn, U., A. Wolf, C. Gries, T. H. Nash III, and J. Kesselmeier, Field measurements on the exchange of carbonyl sulfide between lichens and the atmosphere, *Atmos. Environ.*, *34(28)*, 4867–4878, 2000.

Lacis, A., J. Hansen, and M. Sato, Climate forcing by stratospheric aerosols, *Geophys. Res. Lett.*, *19*, 1607–1610, 1992.

Lamb, B., H. Westberh, G. Allwine, L. Bamesberger, and A. Guenther, Measurement of biogenic sulfur emission from soil and vegetation: Application of dynamic enclosure methods with Natusch filter and GC/FPD analysis, *J. Atmos. Chem.*, *5*, 469–491, 1987.

Lancashire, P. D., H. Bleiholder, T. van den Boom, P. Langelddeke, R. Stauss, E. Weber, and A. Witzenberger, A uniform decimal code for growth stages of crops and weeds, *Annal of Applied Biology*, *119*, 561–601, 1991.

Laubach, J., M. Raschendorfer, H. Kreilein, and G. Gravenhorst, Determination of heat and water vapour fluxes above a spruce forest by eddy correlation, *Agric. For. Meteorol.*, *71*, 373–401, 1994.

Lazrus, A. L. and B. W. Gandrud, Stratospheric aerosol, *J. Geophys. Res.*, *79*, 3424–3431, 1974.

Lehmann, S. and R. Conrad, Characteristics of turnover of carbonyl sulfide in four different soils, *J. Atmos. Chem.*, *23*, 193–207, 1996.

Leifer, R., Project Airstream: COS measurements in the stratosphere and troposphere, *J. Geophys. Res.*, *94(D4)*, 5173–5181, 1989.

Lenschow, D. H. and M. R. Raupach, The attenuation of fluctuations in scalar concentrations through sampling tubes, *J. Geophys. Res.*, *96*, 15,259–15,268, 1991.

Leuning, R. and J. Moncrieff, Eddy-covariance CO_2 flux measurements using open- and closed-path CO_2 analysers: Corrections for analyser water vapour sensitivity and damping of fluctuations in air sampling tubes, *Bound.-Layer Meteor.*, *53*, 63–76, 1990.

Liss, P. S. and L. Merlivat, Air-sea gas exchange rates: Introduction and system, in *The role of air-sea exchange in geochemical cycling*, edited by P. Buat-Ménard, pp. 113–127, D. Reidel, Dordrecht, 1986.

Liss, P. S. and P. G. Slater, Flux of gases across the air-sea interface, *Nature*, *247*, 181–184, 1974.

Louisnard, N., G. Fergant, A. Girard, L. Gramont, O. Lado-Bordowsky, J. Laurent, S. Le Boiteux, and M. P. Lemaitre, Infrared absorption spectroscopy applied to stratospheric profiles of minor constituents, *J. Geophys. Res.*, *88*, 5365–5376, 1983.

Majewski, M., R. Desjardins, P. Rochette, E. Pattey, J. Selber, and D. Glotfelty, Field comparison of an eddy accumulation and an aerodynamic-gradient system for measuring pesticide volatilization fluxes, *Environ. Sci. & Technol.*, *27*, 121–128, 1993.

Maroulis, P. J., A. L. Torres, and A. R. Bandy, Atmospheric concentrations of carbonyl sulfide in the southwestern and eastern United States, *Geophys. Res. Lett.*, *4(11)*, 510–512, 1977.

Massman, W. J., The attenuation of concentration fluctuations in turbulent flow through a tube, *J. Geophys. Res.*, *98*, 15,269–15,273, 1991.

Matthews, E., Global litter production, pools, and turnover times: estimates from measurement data and regression models, *J. Geophys. Res.*, *102*, 18,771–18,800, 1997.

Melillo, J. M. and P. A. Steudler, The effect of nitrogen fertilization on the COS and CS_2 emissions from temperature forest soils, *J. Atmos. Chem.*, *9*, 411–417, 1989.

Mihalopoulos, N., B. Bonsang, B. C. Nguyen, M. Kanakidou, and S. Belviso, Field observations of COS deficit near the ground: Possible implication of vegetation, *Atmos. Environ.*, *23(10)*, 2159–2166, 1989.

Mihalopoulos, N., B. C. Nguyen, J. P. Putaud, and S. Belviso, The oceanic source of carbonyl sulfide (COS), *Atmos. Environ.*, *26*, 1383–1394, 1992.

Mihalopoulos, N., J. P. Putaud, B. C. Nguyen, and S. Belviso, Annual variation of atmospheric carbonyl sulfide in the marine atmosphere in the southern Indian Ocean, *J. Atmos. Chem.*, *13*, 73–82, 1991.

Miller, J. C. and J. N. Miller, *Statistics for analytical chemistry*, Ellis Horwood PTR Prentice Hall, New York, 3rd edition, 1993.

Monahan, E. C. and M. C. Spillane, The role of oceanic whitecaps in air-sea gas exchange, in *Gas Transfer at Water Surfaces*, edited by W. Brutsaert and G. H. Jirka, pp. 495–503, D. Reidel, Norwell, Mass., 1984.

Moncrieff, J. B., I. J. Beverland, D. H. Neill, and F. D. Cropley, Controls on trace gas exchange observed by a conditional sampling method, *Atmos. Environ.*, *32(19)*, 3265–3274, 1998.

Monin, A. S. and A. M. Obukhov, Basic laws of turbulent mixing in the surface layer of the atmosphere, *Tr. Geofiz. Inst. Akad. Nauk SSSR*, *151*, 163–187, 1954.

Morgenstern, K., *Fluß-Gradient-Beziehung für CO_2, H_2O und fühlbare Wärme über einem Fichtenbestand im Solling*, Diplomarbeit, Universität Göttingen, 1997.

Najjar, R. G., D. J. Erickson III, and S. Madronich, Modelling the air-sea fluxes of gases formed from the decomposition of dissolved organic matter: Carbonyl sulfide and carbon monoxide, in *Role of Nonliving Organic Matter in the Earth's Carbon Cycle*, edited by R. G. Zepp and C. Sonntag, pp. 107–132, John Wiley & Sons, New York, 1995.

Neumann, H. H., G. den Hartog, and L. F. Guise-Bagley, Evaluation of a digital-valve eddy accumulator using water vapour flux measurements and numerical simulations of its performance, *Atmos. Environ.*, *23(6)*, 1305–1313, 1989.

Nguyen, B. C., B. Bonsang, N. Mihalopoulos, and S. Belviso, Carbonyl sulfide emissions from African savannah burning, paper presented at Chapman Conference on Global Biomass Burning: Atmospheric, Climatic and Biospheric Implications, Williamsburg, Va., March 19-23, 1990.

Nguyen, B. C., N. Mihalopoulos, J. P. Putaud, and B. Bonsang, Carbonyl sulfide emission from biomass burning in tropics, *J. Atmos. Chem.*, *22*, 55–65, 1995.

Oncley, S. P., A. C. Delany, T. W. Horst, and P. P. Tans, Verification of flux measurement using relaxed eddy accumulation, *Atmos. Environ.*, *27*, 2417–2426, 1993.

Pattey, E., R. L. Desjardins, and R. Rochette, Accuracy of the relaxed eddy-accumulation technique, evaluated using CO_2 flux measurements, *Bound.-Layer Meteor.*, *66*, 341–355, 1993.

Pattey, E., R. L. Desjardins, H. Westberg, B. Lamb, and T. Zhu, Measurement of isoprene emissions over a black spruce stand using a tower-based relaxed eddy-accumulation system, *J. Appl. Meteorol.*, *38(7)*, 870–877, 1999.

Philip, J. R., The damping of a fluctuating concentration by continuous sampling through a tube, *Aust. J. Phys.*, *16*, 454–463, 1963.

Pos, W. H. and H. Berresheim, Automotive tire wear as a source for atmospheric OCS and CS_2, *Geophys. Res. Lett.*, *20*, 815–817, 1993.

Pos, W. H., D. D. Riemer, and R. G. Zika, Carbonyl sulfide (OCS) and carbon monoxide (CO) in natural waters: evidence of a coupled production pathway, *Marine Chemistry*, *62*, 89–101, 1998.

Protoschill-Krebs, G. and J. Kesselmeier, Enzymatic pathways for the consumption of carbonyl sulphide (COS) by higher plants, *Bot. Acta*, *105*, 206–212, 1992.

Protoschill-Krebs, G., C. Wilhelm, and J. Kesselmeier, Consumption of carbonyl sulphide by chlamydomonas reinhardtii with different activities of carbonic anhydrase (CA) induced by different CO_2 growing regimes, *Bot. Acta*, *108*, 445–448, 1995.

Protoschill-Krebs, G., C. Wilhelm, and J. Kesselmeier, Consumption of carbonyl sulphide (COS) by higher plants carbonic anhydrase (CA), *Atmos. Environ.*, *30*, 3151–3156, 1996.

Putaud, J. P. and B. C. Nguyen, Assessment of dimethylsulfide sea-air exchange rate, *J. Geophys. Res.*, *101*, 4403–4411, 1996.

Radford-Knoery, J. and G. A. Cutter, Determination of carbonyl sulfide and hydrogen sulfide species in natural waters using specialized collection procedures and gas chromatography with flame photometric detection, *Anal. Chem.*, *65*, 976–982, 1993.

Radford-Knoery, J. and G. A. Cutter, Biogeochemistry of dissolved hydrogen sulfide and carbonyl sulfide in the western North Atlantic Ocean, *Geochim. Cosmochim. Acta*, *58*, 5421–5431, 1994.

Rannik, U., On the surface layer similarity at a complex forest site, *Journal of Geophysical Research*, *103(D8)*, 8685–8697, 1998.

Rasmussen, R. A., M. A. K. Khalil, and S. D. Hoyt, The oceanic source of carbonyl sulfide (COS), *Atmos. Environ.*, *16*, 1591–1594, 1982.

Raupach, M. R., Anomalies in flux-gradient relationships over forest, *Bound.-Layer Meteor.*, *16*, 467–486, 1979.

Rennenberg, H., The significance of higher plants in the emission of sulfur compounds from terrestrial ecosystems, in *Trace Gas Emissions from Plants*, edited by Th. D. Sharkey, E. A. Holland, and H. A. Mooney, pp. 217–260, Academic Press, San Diego, 1991.

Rennenberg, H., P. Schröder, and B. Huber, Emission of reduced sulfur compounds from agricultural and forest ecosystems, in *EUROTRAC Annual Report 1990, Part 4, BIATEX*, pp. 156–162, Garmisch-Partenkirchen, 1991.

Rinsland, C. P., E. Mahieu, R. Zander, M. R. Gunson, R. J. Salawitch, A. Y. Chang, A. Goldman, M. C. Abrams, M. M. Abbas, M. J. Newchurch, and F. W. Irion, Trends of OCS, HCN, SF$_6$, CHClF$_2$ (HCFC-22) in the lower stratosphere from 1985 and 1994 atmospheric trace molecule spectroscopy experiment measurements near 30N latitude, *Geophys. Res. Let.*, *23(7)*, 2349–2352, 1996.

Rinsland, C. P., R. Zander, E. Mahieu, P. Demoulin, A. Goldman, D. H. Ehhalt, and J. Rudolph, Ground-based infrared measurements of carbonyl sulfide total column abundances: Long-term trends and variability, *J. Geophys. Res.*, *97*, 5995–6002, 1992.

Rodriguez, J. M., M. K. W. Ko, and N. D. Sze, Role of heterogeneous conversion of N$_2$O$_5$ on sulphate aerosols in global ozone loses, *Nature*, *352*, 134–137, 1991.

Rowland, P. S., The atmospheric and oceanic sinks for carbonyl sulfide, in *4th International Conference of the Commission on Atmospheric Chemistry and Global Pollution*, Abstract IV–6, Boulder, Colorado, 1979.

Sandalls, F. J. and S. A. Penkett, Measurements of carbonyl sulphide and carbon disulphide in the atmosphere, *Atmos. Environ.*, *11*, 197–199, 1977.

Schröder, P., Plants as sources of atmospheric sulfur, in *Sulfur nutrition and assimilation in higher plants: regulatory agricultural and environmental aspects*, edited by L. J. De Kok, I. Stulen, H. Rennenberg, C. Brunold, and W. E. Rauser, pp. 253–270, SPB Academic Publishing, The Hague, 1993.

Schuepp, P. H., M. Y. Leclerc, J. I. MacPherson, and R. L. Desjardins, Footprint prediction of scalar fluxes from analytical solutions of the diffusiion equation, *Bound.-Layer Meteorol.*, *50*, 355–373, 1990.

Schütz, C., *Eddy-Korrelationsmessungen von CO$_2$-Flüssen im Solling - Aufbau und Test eines Meßsystems*, Diplomarbeit, Universität Göttingen, 1996.

Sedlacek, W. A., E. J. Mroz, A. L. Lazrus, and B. W. Gandrud, A decade of stratospheric sulfate measurements compared with observations of volcanic eruptions, *J. Geophys. Res.*, *88*, 3741–3776, 1983.

Servant, J., The burden of sulphate layer of the stratosphere during volcanic "quiescent" periods, *Tellus*, *38(B)*, 74–76, 1986.

Sharma, M. M., Kinetics of reactions of carbonyl sulphide and carbon dioxide with amines and catalysis by brönsted bases of the hydrolysis of COS, *Trans. Faraday Soc.*, *61*, 681–688, 1965.

Siedler, G. and H. Peters, Properties of sea water, in *Landolt-Börnstein Numerical Data and Functional Relationships in Science and Technology*, edited by J. Sündermann, volume 3: Oceanography, pp. 233–264, Springer-Verlag, Berlin, 1986.

Simmons, J. S., L. Klemedtsson, H. Hultberg, and M. E. Hines, Consumption of atmospheric carbonyl sulfide by coniferous boreal forest soils, *J. Geophys. Res.*, *104(D9)*, 11,569–11,576, 1999.

Simpson, I. J., G. W. Thurtell, H. H. Neumann, G. den Hartog, and G. C. Edwards, The validity of similarity theory in the roughness sublayer above forests, *Bound.-Layer Meteor.*, *87(1)*, 69–99, 1998.

Solomon, S., R. W. Sanders, R. R. Garcia, and J. G. Keys, Increased chlorine dioxide over Antarctica caused by volcanic aerosols from Mount Pinatubo, *Nature*, *363*, 245–248, 1993.

Speer, R. E., K. A. Peterson, T. G. Ellestad, and J. L. Durham, Test of a prototype eddy accumulator for measuring atmospheric vertical fluxes of water vapor and particulate sulfate, *J. Geophys. Res.*, *90(D1)*, 2119–2122, 1985.

Staubes, R. and H.-W. Georgii, Biogenic sulfur compounds in seawater and the atmosphere of the Antarctic region, *Tellus*, *5B*, 27–137, 1993.

Staubes, R., H.-W. Georgii, and G. Ockelmann, Flux of COS, DMS, and CS$_2$ from various soils in Germany, *Tellus*, *41B*, 305–313, 1989.

Staubes-Diederich, R., *Verteilung von Dimethylsulfid, Carbonylsufid und Schwefelkohlenstoff in Ozean und mariner Atmosphäre*, Ph.D. thesis, Universität Frankfurt, 1992.

Steinbacher, M., *Untersuchungen zum Austausch von Carbonylsulfid (COS) über einem Waldökosystem*, Diplomarbeit, Universität Frankfurt, 2000.

Steudler, P. A. and B. J. Peterson, Contribution of gaseous sulfur from salt marshes to the global sulfur cycle, *Nature*, *311*, 455–457, 1984.

Steudler, P. A. and B. J. Peterson, Annual cycle of gaseous sulfur emissions from a New England spartina alterniflora marsh, *Atmos. Environ.*, *19(9)*, 1411–1416, 1985.

Stull, R. B., *An Introduction to Boundary Layer Meteorology*, Kluwer Academic Publishers, Dordrecht, 1988.

Sze, N. D. and M. K. W. Ko, CS_2 and COS in the stratospheric sulphur budget, *Nature*, *280*, 308–310, 1979.

Talbot, R. W., J. E. Dibb, K. I. Klemm, J. D. Bradshaw, S. T. Sandholm, D. R. Blake, G. W. Sachse, J. Collins, B. G. Heikes, G. L. Gregory, B. E. Anderson, H. B. Singh, D. C. Thornton, and J. T. Merrill, Chemical characteristics of continental outflow from Asia to the troposphere over the western Pacific Ocean during September-October 1991: Results from PEM-West A, *J. Geophys. Res.*, *101(D1)*, 1713–1725, 1996.

Tanaka, T. N. and S. Aoki, Seasonal and meridional variations of atmospheric carbon dioxide in the lower troposphere of the northern and southern hemispheres, *Tellus*, *39B*, 29–41, 1987.

Tans, P., T. Conway, and T. Nakazawa, Latitudinal distribution of the sources and sinks of atmospheric carbon dioxide derived from surface observations and an atmospheric transport model, *J. Geophys. Res.*, *94*, 5151–5172, 1989.

Taylor, G. E. Jr., S. B. Jr. McLaughlin, D. S. Shriner, and W. J. Slevidge, The flux sulfur-containing gases to vegetation, *Atmos. Environ.*, *17*, 789–796, 1983.

Thom, B. S., J. B. Stewart, H. R. Oliver, and J. H. C. Gash, Comparison of aerodynamic and energy budget estimates of fluxes over a pine forest, *Q. J. R. Meteorol. Soc.*, *101*, 93–105, 1975.

Thornton, D. C., A. R. Bandy, and B. W. Blomquist, Impact of anthropogenic and biogenic sources and sinks on carbonyl sulfide in north Pacific troposphere, *J. Geophys. Res.*, *101(D1)*, 1873–1881, 1996.

Toon, O. B. and J. B. Pollack, Stratospheric aerosols and climate, in *The Stratospheric Aerosol Layer*, edited by R. C. Whitten, volume New York, pp. 121–146, Springer-Verlag, 1982.

Torres, A. L., P. J. Maroulis, A. B. Goldberg, and A. R. Bandy, Atmospheric COS measurements on project GAMETAG, *J. Geophys. Res.*, *85*, 7357–7360, 1980.

Trenberth, K. E., W. G. Large, and J. G. Olson, The effective drag coefficient for evaluating wind stress over the oceans, *J. Clim.*, *2*, 1507–1516, 1989.

Turco, R. P., R. C. Whitten, and O. B. Toon, Stratospheric aerosols: Observation and theory, *Rev. Geophys.*, *20*, 233–279, 1982.

Turco, R. P., R. C. Whitten, O. B. Toon, J. B. Pollack, and P. Hamill, COS, stratospheric aerosol and climate, *Nature*, *283*, 283–285, 1980.

Turner, S. M. and P. S. Liss, Measurements of various sulphur gases in a coastal marine environment, *J. Atmos. Chem.*, *2*, 223–232, 1985.

Tworek, T., *Messungen von Wasserdampf- und CO_2-flüssen über und in einem Fichtenbestand*, Diplomarbeit, Universität Göttingen, 1996.

Uher, G., *Photochemische Produktion von Carbonyl Sulfid (COS) im Oberflächenwasser der Ozeane: Prozeßstudien und ein empirisches Modell*, Ph.D. thesis, University of Mainz, 1994.

Uher, G. and M. O. Andreae, The diel cycle of carbonyl sulfide in marine surface waters: Field study results and a simple model, *Aquatic Geochem.*, *2*, 313–344, 1997a.

Uher, G. and M. O. Andreae, Photochemical production of COS in North Sea water: A process study, *Limnology and Oceanography*, *42(3)*, 28–38, 1997b.

Ulshöfer, V. S. and M. O. Andreae, Carbonyl sulfide (COS) in the surface ocean and the atmospheric COS budget, *Aquatic Geochemistry*, *3*, 283–303, 1998.

Ulshöfer, V. S., O. R. Flöck, G. Uher, and M. O. Andreae, Photochemical production and air-sea exchange of carbonyl sulfide in the eastern Mediterranean Sea, *Mar. Chem.*, *53*, 25–39, 1996.

Ulshöfer, V. S., G. Uher, and M. O. Andreae, Evidence for a winter sink of atmospheric carbonyl sulfide in the northeast Atlantic Ocean, *Geophys. Res. Lett.*, *22*, 2601–2604, 1995.

Velmeke, F., *Versuche zur Korrelation von Photosynthese mit dem Austausch flüchtiger Schwefel-Verbindungen zwischen Bäumen and Atmospäre*, Diplomarbeit, Universität Mainz, 1993.

Wanninkhof, R., Relationship between wind speed and gas exchange over the ocean, *J. Geophys. Res.*, *97*, 7373–7382, 1992.

Watts, S. F., The mass budgets of carbonyl sulfide, dimethyl sulfide, carbon disulfide and hydrogen sulfide, *Atmos. Environ.*, *34*, 761–779, 2000.

Weast, R. C., *CRC Handbook of chemistry and physics*, CRC Press, Cleveland, Ohio, USA, 60th edition, 1979.

Weisenstein, D. K., G. K. Yue, M. K. W. Ko, N. D. Sze, J. M. Rodriguez, and C. J. Scott, A two-dimensional model for sulfur species and aerosols, *J. Geophys. Res.*, *102(D11)*, 13,019–13,035, 1997.

Weiss, P. S., J. E. Johnson, R. H. Gammon, and T. S. Bates, Reevaluation of the open ocean source of carbonyl sulfide to the atmosphere, *J. Geophys. Res.*, *100(D11)*, 23,083–23,092, 1995.

Wilson, J. D. and G. E. Swaters, The source area influencing a measurement in the planetary boundary layer: The "footprint" and the "distribution of contact distance", *Bound.-Layer Meteor.*, *55*, 25–46, 1991.

Wyngaard, J. C. and C.-H. Moeng, Parameterizing turbulent diffusion through the joint probability density, *Bound.-Layer Meteor.*, *60*, 1–13, 1992.

Zepp, R. G. and M. O. Andreae, Factors affecting the photochemical production of carbonyl sulfide in sea water, *Geophys. Res. Lett.*, *21*, 2813–2816, 1994.

Acknowledgements

This dissertation would not have been achieved without the support and help of many individuals and institutions.

I wish to thank my advisor, Prof. Dr. Ulrich Schmidt for giving me this interesting topic, and for his guidance and support during the period in his group.

I am grateful to Prof. Dr. Meinrat O. Andreae for his readiness as the second expert to give his opinion on this dissertation, and for permitting me to use one of the seawater equilibrators of his department.

I am greatly indebted to Dr. Heinz G. Bingemer for his guidance, encouragement and advice, for permitting me to use his valuable unpublished data from COS measurements at the Taunus Observatory, and for numerous discussions and help which were not limited to my academic life.

I am very thankful to my colleague, Graeme Handisides for improving the manuscript of this dissertation and for much friendly help in the last years.

I would like to thank all the other colleagues who have helped me. Martin Steinbacher deserves my hearty thanks for accompanying me during the campaigns in 1999 in the Solling forest, for his support measurements of the air-soil exchange of COS and CS_2, and for all other help. Thomas Wetter accompanied and helped me during one of the field experiments in the Solling forest. I thank him for his support. I am grateful to Oliver Riediger for his masterly support in the computer and network technology.

Several outside scientists deserve my best thanks. I received indispensable supports during the measurements in the Solling forest from the Institute for Bioclimatology (IFB), University of Göttigen. I wish to thank Prof. Dr. Gode Gravenhorst, director of IFB for permitting me to measure at the forest site. Especially, I would like to thank Drs. Andreas Ibrom and Kai Morgenstern for many discussions, for their technical and logistical support, and for providing me unconditionally with their meteorological data and CO_2 and H_2O fluxes. Dr. Ulrich Bartell accompanied me during my first Atlantic cruise and participated in the measurements. The CDOM absorbance data I used in this dissertation were provided by Dr. A. James Kettle, who made

Curriculum Vitae

Name:	Xiaobin Xu
Date of Birth:	October 9, 1960
Birthplace:	Jintan, Province Jiangsu, China
Nationality:	Chinese
Family Status:	Married, one child

Academic Qualifications:

July, 1984:	Bachelor of Science
July, 1987:	Master of Science

Education:

1967-1973:	Primary school in Jintan
1973-1977:	Middle school in Jintan
1980-1984:	Bachelor's course at Peking University
	Main subject: Chemistry
1984-1987:	Master's course at Peking University
	Main subject: Environmental chemistry
	Thesis title: Study on Atmospheric H_2O_2

Working Experience:

1977-1980:	Farming in Jintan
1987-1991:	Research assistant at the Institute of Atmospheric Chemistry, Chinese Academy of Meteorological Sciences
1991-1992:	Researcher (as scholarship holder) at the Institute for Meteorology and Geophysics, J.W. Goethe University Frankfurt am Main
1993-1996:	Research scientist at the Institute of Atmospheric Chemistry, Chinese Academy of Meteorological Sciences
1996-2001:	Scientific coworker at the Institute for Meteorology and Geophysics, J.W. Goethe University Frankfurt am Main